THESIS FOR THE DEGREE OF DOCTOR OF PHILOSOPHY

# Development of an efficient solver for detailed kinetics in reactive flows

Andrea Matrisciano

Department of Mechanics and Maritime Sciences
CHALMERS UNIVERSITY OF TECHNOLOGY
Gothenburg, Sweden 2021

Development of an efficient solver for
detailed kinetics in reactive flows
ANDREA MATRISCIANO
ISBN 978-91-7905-476-2



Doktorsavhandlingar vid Chalmers tekniska högskola
Ny serie nr 4943
ISSN 0346-718X

Department of Mechanics and Maritime Sciences
Division of Combustion and Propulsion Systems
Chalmers University of Technology
SE-412 96 Gothenburg
Sweden
Telephone + 46 (0)31-772 1000

Printed by Chalmers Reproservice
Gothenburg, Sweden 2021

To my dear friend Harry

# Abstract

The use of chemical kinetic mechanisms in CAE tools for reactive flow simulations is of high importance for studying and predicting pollutant formation. However, usage of complex reaction schemes is accompanied by high computational cost in both 1D and 3-D CFD frameworks. The combustion research community has addressed such challenge via two main approaches: 1) tailor made mechanism reduction strategies; 2) pre-tabulation of the chemistry process and look-up during run-time. The present work covers both topics, although much of the methodology development and validation efforts focused on tabulation.

In the first phase of the PhD work, an isomer lumping strategy based on thermodynamic data was developed and applied to a detailed three component reaction mechanism for n-decane, alpha-methylnaphthalene and methyl decanoate comprising 807 species and 7807 reactions. A total of 74 isomer groups were identified within the oxidation of n-decane and methyl decanoate via the assessment of the Gibbs free energy of the isomers. The lumping procedure led to a mechanism of 463 species and 7600 reactions, which was compared against the detailed version over several reactor conditions and over a broad range of temperature, pressure and equivalence ratio. In all cases, excellent agreement between the predictions obtained using the lumped and the detailed mechanism has been observed with an overall absolute error below 12%.

In the second phase of the PhD work, a tabulated chemistry approach was developed, implemented and validated against an on-the-fly chemistry solver across different simulation frameworks. As a first attempt, a flamelet-based tabulation method for soot source terms was coupled to the stochastic reactor model and tested against a well stirred reactor-based approach under Diesel engine conditions. The main purpose was to assess and quantify benefits of tabulation within the 0-D SRM framework with respect to soot formation only. Subsequently, a latent enthalpy ($h_{298}$) based approach was developed and implemented within the SRM model to predict both combustion and emission formation. This approach was widely validated against the detailed on-the-fly solver solutions under 0-D reactor conditions as well as Diesel engine conditions for a wide range of operating points. Good agreement was found between the two solvers and a remarkable speed-up was obtained in terms of computational costs of the simulation. As a last step, the same tabulated chemistry solver was coupled to a commercial CFD software via user defined functions and performances were assessed against the built-in on-the fly chemistry solver under Diesel engine sector simulations. The tabulated chemistry solver proved to be within an acceptable level of accuracy for engineering studies and showed a consistent speed-up in comparison to the online chemistry solver.

Across all the investigated frameworks, the developed tabulated chemistry solver was found to be a valid solution to speed-up simulation time without compromising accuracy of the solution for combustion and emissions predictions for engine applications. In fact, the much-reduced CPU times allowed the SRM to be included in broader engine development campaigns where multi-objective optimization methods where efficiently used to explore new engine designs.

**Keywords**: Detailed chemistry, Chemical lumping, Tabulated chemistry, Progress Variable, Stochastic Reactor Model

# Contents

# List of Publications

This thesis is based on the following publications, referred to by their Roman numerals:

**I. An *a priori* Thermodynamic Data Analysis based Chemical Lumping Method for the Reduction of Large and Multi-component Chemical Kinetic Mechanisms.**

**Matrisciano A.**, Seidel L., Mauss F.
Submitted to International Journal of Chemical Kinetics

**II. Soot Source Term Tabulation Strategy for Diesel Engine Simulations with SRM.**

**Matrisciano A.**, Borg A., Perlman C., Lehtiniemi H., Pasternak M., Mauss F.
SAE Technical Paper 2015-24-2400, 2015, doi:10.4271/2015-24-2400.

**III. Development of a Computationally Efficient Progress Variable Approach for a Direct Injection Stochastic Reactor Model.**

**Matrisciano A.**, Franken T., Perlman C., Borg A., Lehtiniemi H., Mauss F.
SAE Technical Paper 2017-01-0512, 2017, doi:10.4271/2017-01-0512.

**IV. A Computationally Efficient Progress Variable Approach for In-Cylinder Combustion and Emissions Simulations.**

**Matrisciano A.**, Netzer C., Werner A., Borg A., Seidel L., Mauss F.
SAE Technical Paper 2019-24-0011, 2019, doi:10.4271/2019-24-0011.

**V. Development of a Computationally Efficient Tabulated Chemistry Solver for Internal Combustion Engines Optimization using Stochastic Reactor Models.**

**Matrisciano A.**, Franken T., Gonzales Mestre L.C., Borg A., Mauss F.
Applied Sciences, 10 (24) 8979, 2020, doi:10.3390/app10248979.

# Other Relevant Publications

1. **Systematic Reduction of Detailed Chemical Reaction Mechanisms for Engine Applications.**

   Seidel L., Netzer C., **Matrisciano A.**, Klauer C., Pasternak M., Mauss F.
   Journal of Engineering for Gas Turbines and Power 139 (9), 2017, doi:10.1115/1.4036093.

2. **Diesel Engine Performance Mapping using a Parametrized Mixing Time Model.**

   Pasternak M., **Matrisciano A.**, Klauer C., Mauss F.
   International Journal of Engine Research, 19 (2) 202-213, 2018, doi:10.1177/1468087417718115

3. **Multi-Objective Optimization of Water Injection in Spark-Ignition Engines using the Stochastic Reactor Model with Tabulated Chemistry.**

   Franken T., Netzer C., **Matrisciano A.**, Pasternak M., Seidel L., Borg A., Lehtiniemi H., Mauss F., Kulzer A.C.
   International Journal of Engine Research, 20 (10) 1089-1100, 2019, doi:10.1177/1468087419857602

4. **Prediction of Thermal Stratification in an Engine-Like Geometry using a Zero-Dimensional Stochastic Reactor Model.**

   Franken T., Klauer C., **Matrisciano A.**, Kienberg M., Mauss F.
   International Journal of Engine Research, Special Issue, 2019, doi:10.1177/1468087418824217

5. **A process for an Efficient Heat Release Prediction at the Concepts Screening Stage of Gasoline Engine Development.**

   Rota C., Morgan R., Mustafa K., Osborne R., **Matrisciano A.**
   International Journal of Engine Research, 2020, doi:10.1177/1468087420947317

6. **Analysis of the Water Addition Efficiency on Knock Suppression for Different Octane Ratings.**

   Franken T., Seidel L., **Matrisciano A.**, Mauss F., Kulzer A.C., Schuerg F.
   SAE Technical Paper 2020-01-0551, 2020, doi:10.4271/2020-01-0551

7. **Multi-Objective Optimization of Fuel Consumption and $NO_x$ Emissions with Reliability Analysis Using a Stochastic Reactor Model**

   Franken T., Duggan A., **Matrisciano A.**, Lehtiniemi H., Borg A., Mauss F.
   SAE Technical Paper 2019-01-1173, 2019, doi:10.4271/2019-01-1173

8. **Advanced Predictive Diesel Combustion Simulation using Turbulence Model and Stochastic Reactor Model.**

   Franken T., **Matrisciano A.**, Sommerhoff A., Willems W., Lehtiniemi H., Borg A., Netzer C., Mauss F.
   SAE Technical Paper 2017-01-0516, 2017, doi:10.4271/2017-01-0516

9. **Influence of Nozzle Eccentricity on Spray Structures in Marine Diesel Sprays.**

   Nagy I.G., **Matrisciano A.**, Lehtiniemi H., Mauss F., Schmid A.
   SAE Technical Paper 2017-24-0031, 2017, doi: 10.4271/2017-24-0031

10. **On the Performance of Biodiesel Blends-Experimental Data and Simulations Using a Stochastic Fuel Test Bench.**

    **Matrisciano A.**, Pasternak M., Wang X., Antoshkiv O., Mauss F., Berg P.
    SAE Technical Paper 2014-01-1115, 2014, doi:10.4271/2014-01-1115

# Nomenclature

## Greek Symbols

| | | |
|---|---|---|
| $\epsilon$ | Dissipation of turbulent kinetic energy | $m^2/s^3$ |
| $\phi$ | Equivalence Ratio | - |
| $\boldsymbol{\phi}(t)$ | Joint vector of the local scalar variables | - |
| $\lambda$ | Lambda | - |
| $\rho$ | Density | $kg/m^3$ |
| $\tau_{t,mix}$ | Turbulent mixing time | s |
| $\tau_{mix}$ | Scalar mixing time | s |
| $\omega_i$ | Chemistry source/sink term for species $i$ | 1/s |
| $\psi$ | Realization of the random variables | - |

## Latin Symbols

| | | |
|---|---|---|
| $A_r$ | Pre-exponential factor of reaction $r$ | 1/s |
| $C$ | Reaction progress variable | - |
| $\dot{C}$ | Reaction progress variable source term ($dC/dt$) | 1/s |
| $C_\tau$ | Mixing time constant | - |
| $c_p$ | Specific heat capacity at constant pressure | J/kgK |
| $E_{a,r}$ | Activation energy of reaction $r$ | J/mol |
| $h_{298}$ | Latent enthalpy | J/kg |
| $h_{298,u}$ | Latent enthalpy of the unburned state | J/kg |
| $h_{298,max}$ | Latent enthalpy of the maximum heat release state | J/kg |
| $h_g$ | Heat transfer coefficient | $W/m^2K$ |
| $h_i$ | Specific enthalpy of species $i$ | J/kg |
| $k$ | Turbulent kinetic energy | J/kg |
| $K$ | Mean kinetic energy | J/kg |
| $K_{eq}$ | Chemical equilibrium constant | - |
| $k_{b,r}$ , $k_{f,r}$ | Backward ($b$), forward ($f$) reaction rate of reaction $r$ | $mol/m^3s$ |
| $\tilde{k}_x$ | Combined reaction rate involving lumped species $L_x$ | $mol/m^3s$ |
| $l$ | Integral length scale | m |
| $\dot{m}_f$ | Fuel mass flow rate | kg/s |
| $N_R$ | Number of reactions in the reaction scheme | - |
| $N_S$ | Number of chemical species in the reaction scheme | - |
| $p$ | Pressure | Pa |

| | | |
|---|---|---|
| $R$ | Universal gas constant | J/mol |
| $s_l$ | Laminar flame speed | m/s |
| $s_t$ | Turbulent flame speed | m/s |
| $T$ | Temperature | K |
| $T_{ad}$ | Adiabatic flame temperature | K |
| $T_u$ | Temperature at the unburnt state | K |
| $T_W$ | Cylinder wall temperature | K |
| $u'$ | Velocity fluctuation | m/s |
| $V$ | Mean in-cylinder volume | $m^3$ |
| $W_i$ | Molar mass of species $i$ | g/mol |
| $Y_i$ | Mass fraction of species $i$ | - |

## Abbreviations

| | |
|---|---|
| 0-D | Zero-Dimensional |
| 3-D | Three-Dimensional |
| AMN / 1-MN | Alpha Methylnaphthalene, $C_{11}H_{10}$ |
| aTDC | After Top Dead Centre |
| BEV | Battery Electric Vehicle |
| bTDC | Before Top Dead Centre |
| BTU | Brandenburg Technical University Cottbus-Senftenberg |
| CAE | Computer Aided Engineering |
| CAD | Crank Angle Degree |
| CFD | Computational Fluid Dynamics |
| CI | Compression Ignition |
| CO | Carbon Monoxide |
| $CO_2$ | Carbon Dioxide |
| CPV | Combustion Progress Variable |
| DI | Direct Injection |
| ECFM-3Z | Extended Coherent Flame Model 3 Zones |
| EGR | Exhaust Gas Recirculation |
| EOI | End of Injection |
| ETRF | Ethanol Toluene Reference Fuel |
| FPI | Flame Prolongation |
| GHG | Green House Gases |
| HCCI | Homogeneous Charge Compression Ignition |
| HEV | Hybrid Electric Vehicle |
| ICE | Internal Combustion Engine |
| ICEV | Internal Combustion Engine Vehicles |
| IFP-EN | French Institute of Petroleum |
| ILDM | Intrinsic Low-Dimensional Manifold |
| ISAT | In Situ Adaptive Tabulation |
| KLSA | Knock Limit Spark Advance |
| LCA | Life Cycle Assessment |

| | |
|---|---|
| LES | Large Eddy Simulation |
| LHV | Lower Heating Value |
| MD | Methyl Decanoate, $C_{11}H_{22}O_2$ |
| NEDC | New European Driving Cycle |
| $NO_x$ | Nitrogen Oxides |
| NTC | Negative Temperature Coefficient |
| OEM | Original Equipment Manufacturer |
| PAH | Polycyclic Aromatic Hydrocarbons |
| PaSR | Partially Stirred Reactor |
| P-HEV | Plug-in Hybrid Electric Vehicle |
| PM | Particulate Matter |
| PRF | Primary Reference Fuel |
| QSSA | Quasi-Steady State Approximation |
| RANS | Reynolds Averaged Navier Stokes |
| RDE | Real Driving Emissions |
| RoHR | Rate of Heat Release |
| SAGE | Acronym of the detailed chemistry solver built-in the commercial CFD software CONVERGE |
| SI | Spark Ignition |
| SOI | Start of Injection |
| SRM | Stochastic Reactor Model |
| TCI | Turbulence Chemistry Interaction |
| TKI | Tabulated Kinetics of Ignition |
| TDC | Top Dead Centre |
| TRF | Toluene Reference Fuel |
| UDF | User Defined Function |
| uHC | Unburned Hydrocarbons |
| WLTP | Worldwide harmonized Light vehicle Test Procedure |
| WSR | Well Stirred Reactor |

# Chapter 1

# Introduction

The ever-stringent regulations on criteria pollutants, such as nitrogen oxides or particulate matter, and greenhouse gas emissions have been the key drivers for research and development of propulsion systems for the automotive industry in the past decades. On the one hand side, the well-known correlation between global warming and increase of GHG emissions from combustion of fossil fuels [1] has led legislators around the world to simstematically reduce the fleet average $CO_2$ emissions. In Figure 1.1 an overview of $CO_2$ targets, both past and projected, across the major developed countries is presented.

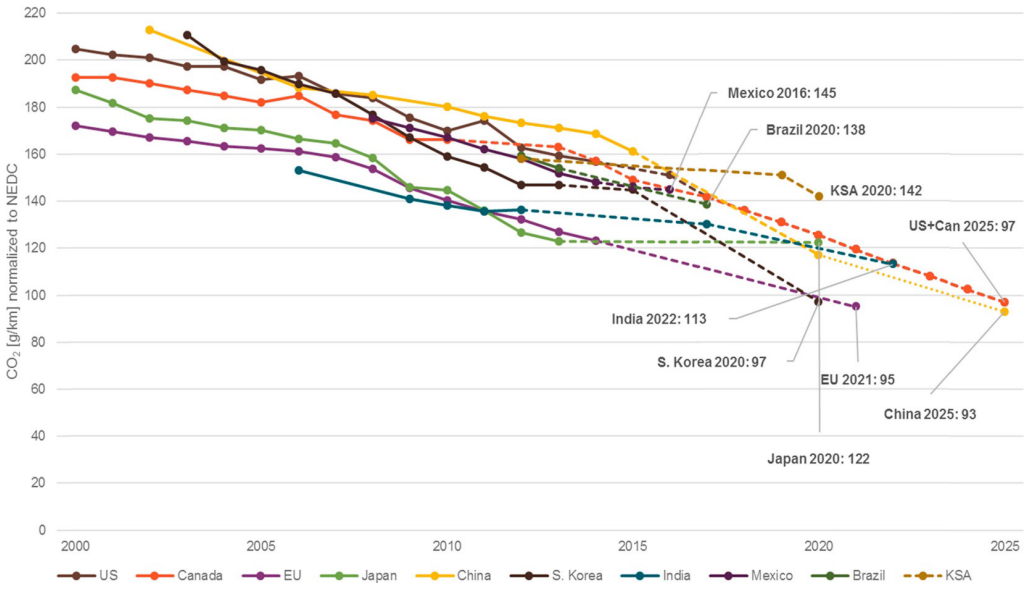


**Figure 1.1.** Historical evolution of $CO_2$ targets (normalized to NEDC-equivalents) in different countries [2].

On the other hand, the 2015 Diesel emission scandal [3], together with other factors, has strongly affected the regulations on allowed PM and $NO_x$ levels as well as the official procedures used to certify the actual emissions of a given vehicle (i.e., shift from

NEDC to WLTP cycle). A schematic overview of European criteria pollutant regulations and their evolution over the past decades is presented in Figure 1.2.

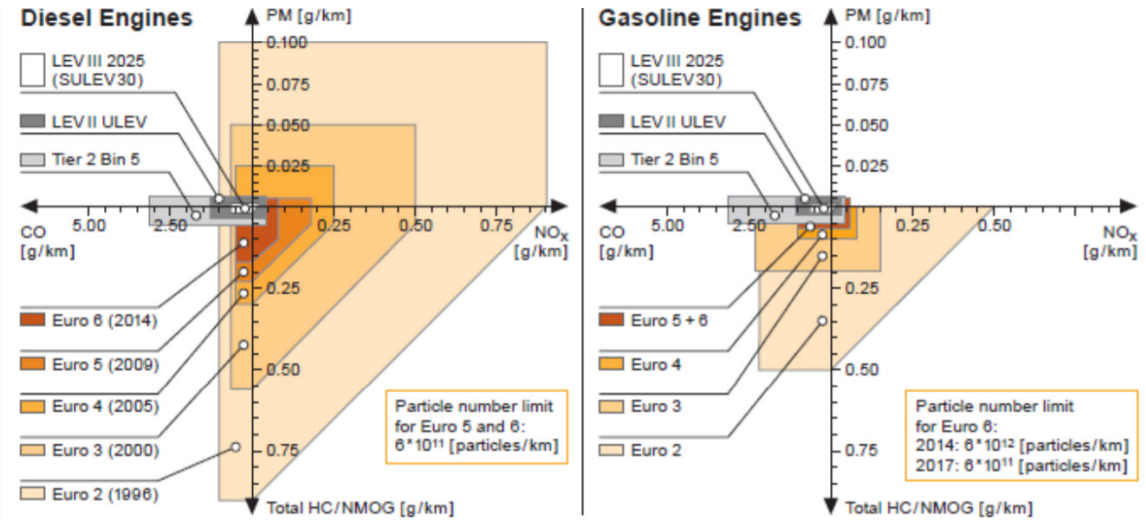


**Figure 1.2.** Historical evolution of European emission limits for Diesel and gasoline engines and some US references [4].

At the time of writing this thesis, all the mentioned regulations consider both pollutant and GHG emissions on a tank-to-wheel basis. Such convention, together with the challenging targets set for fleet average $CO_2$, has led to a technology shift clearly focused on electrification. The automotive sector is hence living a very complex era where new powertrain solutions (i.e., purpose-built battery electric vehicles) are being developed alongside hybridized internal combustion engine vehicles that feature various degrees of electrification. Among the many consequences of having a significant shift towards electric/electrified vehicles, electricity providers as well as governments are facing the non-trivial challenge of upgrading and-or building new power grids as well as charging infrastructures. All these aspects together have inevitably created a heated, and sometime controversial, debate on pros and cons of the different propulsion technologies based on life-cycle assessment of emissions rather than tank-to-wheel only [5].

While both scientific and legislator communities are far from reaching consensus on what should or would be the optimal path for future powertrains, numerous reports and review articles (i.e., [6, 7, 8, 9]) tend to agree on the fact that internal combustion engines will keep playing an important role in mobility, freight, transport and mobile machinery sectors for at least the next two decades.

## 1.1. Motivation

Despite the ongoing debate on future shares of powertrain solutions, the internal combustion engine has arguably still a crucial role within the mobility sector. As of the data from 2019 [10], the market penetration of electric vehicles (intended as both P-HEVs and BEVs) has been 3.46% of the newly registered vehicles in Europe.

Considering also that the average vehicle age across European countries is approximately 11.5 years [11], it can be concluded that it is still more than relevant to continue developing internal combustion engines as a propulsion technology for the decade to come.

The increasing levels of hybridization represent an excellent chance to increase the overall powertrain efficiency. The additional power from the electric motor can in fact act as an enabler for new engine technologies (i.e., modern spark-ignited engines with pre-chamber) and improve the low efficiency areas in the engine map. Apart from the light-duty sector, there are many applications where, given the current status of battery and fuel cell technologies, the ICE is still considered the propulsion system of choice from the engineering as well as cost and practicality standpoints. These applications are for instance: the heavy- and medium duty, maritime and off-road vehicle sectors.

With respect to the engineering development of the ICE, the diversity and complexity of the phenomena to be considered, to correctly evaluate both fuel and engine characteristics, challenge the engine development process as well as its integration with exhaust after treatment systems. In modern engine development practices, experiments and simulations are going hand in hand. The use of numerical models can extend the knowledge of experimental investigations by making details such as local flow, spray formation and chemistry more understandable.

With respect to the combustion process, modern CAE tools allow the incorporation of detailed chemical reaction mechanisms to describe fuel oxidation and emission formation. A general trend noticeable across many OEMs nowadays is to progressively reduce the amount of experimentally driven campaigns, since they require expensive equipment in comparison to virtual test benches [12], design of experiments and numerical optimizations [13]. 3-D Computational Fluid Dynamics analyses offer the greatest level of detail for predicting physical processes such as the turbulent flow field and the spray evolution and mixture preparation. Employing combustion models based on reaction mechanisms allow on top to predict emissions formation.

Future demands for 3-D CFD modelling require more and more fuel chemistry effect investigations, the generation of engine performance maps and the application within optimization algorithms for design exploration. However, employment of high spatial and temporal discretization, and depending on the turbulence modeling approach (i.e., RANS or LES) and the size of the reaction mechanisms, 3-D CFD may become too computationally expensive. Further, with continuous progress in chemical reaction mechanism development, surrogate fuel models tend to contain more and more important reaction pathways as well as an increasing number of species [14]. To overcome such limits, on the one hand mechanism reduction techniques, such as the chemistry guided reduction technique with its extension to engine conditions [15], are applied. On the other hand, the mechanisms are maintained in their full detail, but their solution is separated from the solution of the physics. Those concepts are called tabulated chemistry approaches since the chemistry is solved prior to the 0-D or the 3-D CFD simulation and stored in look-up tables. During run-time, the combustion chemistry solver step is then reduced to a cell/zone local table look-up step where source terms are retrieved to reconstruct the chemical state. This approach avoids not only the computation of the chemistry solution on-the-fly but may also reduce

considerably the number of transported scalars. Both factors lead to a significant reduction of the computational time needed to perform the simulation. Thanks to these advantages tabulated chemistry-based methods have received a lot of attention by the combustion chemistry community in the past decades.

## 1.2. Objectives and Thesis Structure

The present work received funding from a Marie-Curie FP7 action (ECCO-MATE, grant agreement number 607214 [16]) and was organized such that both mechanism reduction techniques as well as tabulation methods are investigated. Given the requirements of the action providing funding, it was decided to direct most of the efforts towards the development of a robust multi-framework method for chemistry tabulation/look-up rather than pursue advanced mechanism reduction techniques. In the last phase of the PhD work, additional funding was received via the FFI project (Fuel flexible engine platform 2, grant agreement number P39368-2-F-Flex2 [17]).

In the first eight months of the PhD study, a collaboration was established with the chair of thermodynamics and thermal process engineering at BTU Cottbus-Senftenberg, Germany. The main objective of this activity was to investigate the potential and limitations of isomer lumping techniques when applied to large multi-component kinetic schemes. As a result of this collaboration, an isomer lumping technique was developed based on a Gibbs free energy driven analysis and it is reported in the appended paper I. Such methodology was later also included in the best practice steps for mechanism reduction of LOGE's chemistry guided reduction technique [15].

In the subsequent years, a close collaboration with the development and application teams of LOGE AB [18] was established to investigate different tabulation/progress variable approaches for both auto-ignition and soot/$NO_x$ emissions. In the second appended paper II, a flamelet-based soot source term tabulation technique was coupled with the Stochastic Reactor Model (SRM) framework and soot results were compared to a well stirred reactor-based (WSR) on-the-fly chemistry solution. This work represented the first step towards a much larger development work focused on including tabulation within the main autoignition solver step of the SRM rather than for emissions prediction only.

Hence, within the scope of paper III, the full code infrastructure of the SRM was updated to accommodate a tabulated chemistry-based solver across all sub-models (i.e., the fuel injection, heat transfer, turbulent mixing etc.). The newly developed method (noted as CPV - Combustion Progress Variable) was then compared against the on-the-fly chemistry solver-based SRM solution and assessed with respect to engine performance as well as computational times. This activity was in fact aligned with the main objective of the overall PhD work. Remarkable speed-ups were noted, while keeping an acceptable loss of accuracy in combustion prediction, across all investigated engine operating conditions. The newly implemented tabulated chemistry framework was later included as one of the standard models in the technological offerings from LOGE and applied in several other co-authored works (i.e., [13, 19]). The CPV method in the SRM has then been thoroughly validated under compression and spark ignition

engine conditions in paper V. This work featured several methodology improvements and speed-ups compared to the implementation used in paper III.

In conjunction with the efforts for the 0-D SRM implementation, the coupling of the CPV solver with the commercial CFD software CONVERGE 2.4 [20] was developed and tested. In paper IV a comparison between the tabulated and the built-in on-the-fly chemistry solver (SAGE) is presented for different Diesel engine conditions assuming sector meshes in a 3-D CFD RANS framework. As done for the 0-D framework, the objective of this work was to assess pros and cons of applying the CPV model in 3-D CFD in terms of combustion and emissions predictions as well as run-times. In this framework noticeable speed-ups were obtained, and the model proved to be a feasible solution to consider especially for multi-objective 3-D CFD optimization campaigns that would normally require an unaffordable run-time with traditional on-the-fly combustion chemistry solvers.

This thesis is organized into seven chapters. The present chapter gives an overview of the challenges faced by powertrain development engineers as well as the motivation of the present work. Chapter 2 provides a concise overview on the basics of chemical reaction kinetics and discusses the isomer lumping technique developed during the first year of the PhD studies. Chapter 3 gives a comprehensive literature review on progress variable-based techniques as well as a fundamental description and verification of the tabulated chemistry solver (CPV) developed in this thesis. In Chapter 4 a broad description of the 0-D SRM modeling framework and its sub-models is given, together with a brief overview on how the developed solver was coupled to the commercial CFD code used in this thesis. Chapter 5 and Chapter 6 discuss the engine simulation campaigns performed to validate the developed CPV solver in 0-D SRM and 3-D CFD frameworks, respectively. Chapter 7 presents a summary of the thesis as well as a brief discussion on possible future improvements.

## Chapter 2

# Detailed Chemistry in Reactive Flows

Independently on the spatial dimensions considered in a reactive flow simulation, a methodology that describes the transition from reactants to products of the scalars defined in the computational domain must be implemented. Whether it is an internal combustion engine, a gas turbine or a laboratory flame, an accurate simulation of the fuel oxidation process is often among the dominant aspects to be considered by the combustion modeler. This chapter aims to give a concise overview on the challenges connected to the usage of detailed reaction mechanisms as well as a description of the mechanism reduction strategy developed in the present work.

## 2.1. Global Schemes

The simplest approach to model combustion chemistry is to consider a so-called global reaction mechanism, also noted in literature as one-step or multi-step reaction scheme. The un-reacted fuel species usually goes directly to fully burned products at a given rate. These schemes typically feature not more than a couple of dozens of species and reactions in total and rely on two main assumptions [21]:

- Quasi-steady state approximation (QSSA): some intermediate species or radicals are assumed to have reached an equilibrium state. These species do not evolve anymore, their mass fractions are constant and their overall reaction rates are negligible (production rate is equal to the consumption rate).
- Partial equilibrium: some elementary reactions of the chemical scheme are assumed to have reached equilibrium.

The reaction rates for each of the global step are usually derived from detailed schemes and optimized for the application of choice. Depending on the complexity and the operating range of the target application (i.e., a laboratory burner or a gas turbine) the rates are either optimized by hand or with the help of optimization algorithms. Such procedures rely on a set of appropriately chosen experimental data.

Given their very compact size (in terms of number of species) and relatively low complexity of their final formulation, global chemical schemes are an attractive solution for numerous industrial applications. An example of this category of methods, often

found in commercial CFD codes as a built-in option, is the Shell model [22]. This approach features a fitting procedure [23] that was shown to deliver good auto-ignition predictions for gasoline and Diesel fuels [24]. Global schemes however, present clear limitations in terms of predictive capabilities if the chemical schemes are used outside the conditions for which the reaction rates were fitted. Furthermore, in case the investigation focuses on the prediction of intermediate products and-or towards understanding of pollutants formation (i.e., $NO_x$ and soot), usage of global mechanisms may yield to poor results.

## 2.2. Detailed Chemical Kinetic Schemes

In most of the combustion processes, there are very seldom reactions in which the original reactants interact with each other in a single step, at the molecular level, and produce the final products. For example, the representation of stoichiometric combustion of methane shown in (2.1) is a gross simplification [25].

$$CH_4 + 2O_2 \rightarrow CO_2 + 2H_2O \tag{2.1}$$

There are, in fact, many intermediate elementary steps with intermediate species involved before the final formation of carbon dioxide and water. Products may also consist of many more species than just $CO_2$ and $H_2O$. Furthermore, depending on the fuel, chemical reactions can happen at very different time scales. Hence a correct representation of how fast or slow a certain species is formed or consumed is crucial.

A chemical reaction can be described as [21]:

$$A + B + C \xrightarrow{k} D + E + F \tag{2.2}$$

where the capital letters denote the different species involved in the reaction. The forward and backward reactions, describing the consumption and formation of species $A$ can be expressed as in (2.3) and (2.4), respectively:

$$\frac{d[A]}{dt} = -k_{f,r}\,[A]^a\,[B]^b\,[C]^c \tag{2.3}$$

$$\frac{d[A]}{dt} = k_{b,r}\,[D]^d\,[E]^e\,[F]^f \tag{2.4}$$

The superscripts $a$, $b$, $c$, … are reaction orders with respect to species $A$, $B$, $C$, ..., $k$ is the rate coefficient and the subscripts $f$ and $b$ denote the forward and backward rate of reaction $r$. The rate coefficients of chemical reactions depend strongly on temperature and such dependency is highly non-linear. Generally, the reaction rates $k_r$ in detailed chemical schemes are described using the modified Arrhenius law:

$$k_r = A_r\, T^{n_r}\, exp\left(-\frac{E_{a,r}}{RT}\right) \tag{2.5}$$

The pre-exponential factor $A_r$ is related to the physical properties of the reaction $r$, such as: molecular sizes, angular effects, and average molecular speeds. The $n_r$ exponent, controls the dependency of the specific reaction on temperature, and $E_{a,r}$ is the energy needed to break up the molecular bonds (usually noted in literature as activation energy). $R$ and $T$ are the universal gas constant and temperature, respectively. In essence, a detailed scheme contains a comprehensive description of the fuel decomposition reactions and the successive breakdown of large molecules into small hydrocarbon fragments by means of Arrhenius laws (as in equation (2.5)).

In the past decades, and especially after the 2000s, a wide range of studies have been published on the combustion chemistry of liquid fuels, such as alkanes, cycloalkanes, aromatics, alcohols, and esters. A selection of studies that led to the compilation of a detailed scheme, has been proposed by Law et al. [14] (recently extended by Yuan et al. [26]) and is presented in Figure 2.1.

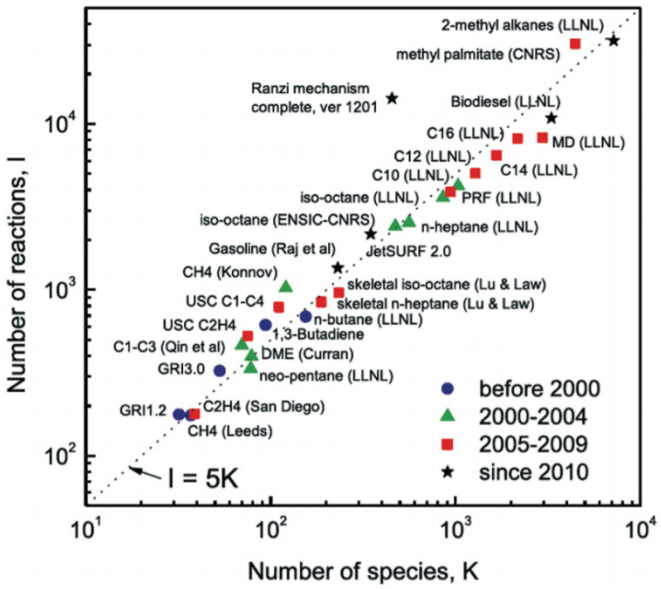


**Figure 2.1.** Correlation between number of reactions and number of species for various published kinetic models of hydrocarbons and bio-derived fuels. Figure initially proposed by Law et al. in [14] and recently extended by Yuan et al. in [26].

On the one hand, it can be noted that remarkable efforts have been made towards the understanding and modeling of the combustion of small and large hydrocarbons (i.e., $C_{16}H_{34}$). On the other hand, it can be concluded that the size of such kinetic models (intended as number of species and reactions) increases dramatically with the number of carbon atoms in the fuel molecule. This implies that, despite the high level of chemical information included, mechanisms having many hundreds (or even thousands)

of species are very often not applicable for numerical simulations of practical combustion devices.

Ideally, a so-called detailed scheme (as opposed to a global scheme) is designed to be able to describe the oxidation and reactivity (i.e., ignition delay, speciation, laminar flame speed) of the given fuel molecule for a broad range of initial conditions (temperature, pressure, equivalence ratio) [14]. However, as discussed in detail by Law [14], Yuan [26], Wang [27] and co-workers, it is not trivial to assess how comprehensive a detailed mechanism is, nor whether it is chemically rigorous. Many of the detailed mechanisms assessed in [14, 27] have been found to deliver good predictions against experimental data only within the target conditions taken into account during mechanism development. Among other reasons, this is due, on the one hand, to the lack of profound knowledge on how to obtain accurate rate constants (see Klippenstein [28]). On the other hand, due to the lack of experimental data covering conditions closer to the typical operating ranges of combustion systems. Hence, at the time being the development process of detailed chemical kinetic schemes faces two major challenges [26]:

1. How to make kinetic models more chemically rigorous.
2. How to make kinetic models applicable in engineering simulation frameworks.

The first challenge has been among the main driving forces leading, on the one hand, to substantial progress, especially in the last decade, in combustion diagnostic techniques, so to provide wider datasets for model validation. On the other hand, theoretical chemistry models (i.e., *ab initio* calculations [28]) have been broadly addressed in recent studies so to improve chemical rigorousness of kinetic models.

The second challenge relies on advancements in computational power, but also on the development of accurate model reduction techniques. In essence, the present thesis aims to tackle this challenge through the development of an isomer lumping technique (discussed in the following paragraphs) and a tabulation method for auto-ignition and emission prediction (discussed in Chapter 3).

## 2.3. Generation and Reduction of Detailed Schemes

With the exception of very small fuels (i.e., hydrogen [29]), detailed kinetic schemes of large molecules, such as *n*-heptane, would require an unfeasible computational cost if applied to combustion system simulations (i.e., a 3-D CFD Diesel engine sector case). It is therefore quite common that, once the detailed version of the mechanism has been developed, a reduction procedure is applied right after so to have a more usable scheme.

Commercial fuels (i.e., gasoline) are complex blends of hundreds of hydrocarbons belonging to different chemical categories such as: linear, branched, or cyclic alkanes, aromatics, esters etc. Having a kinetic scheme that includes all the components would be extremely challenging. The most common approach consists in defining a surrogate blend containing a handful of main fuel components where, ideally, each one captures the effects of a different chemical category [30]. Especially for ICE simulations, *n*-heptane and *iso*-octane are usually noted in literature as primary reference fuels as their

blend can represent the main properties of gasoline and Diesel fuels. In the past two decades numerous mechanisms have been developed by several groups for these two fuels following different strategies. The development of these models is a combined effort that relies on quantum chemistry calculations, empirical models, and an iterative validation against large datasets of experimental data.

While many schemes are developed mostly by hand, Curran and co-workers [31, 32] proposed in the early 2000s a detailed methodology leading to the compilation of an *n*-heptane [31] and an *iso*-octane [32] mechanisms. The method identifies 25 main reaction classes, covering both low and high temperature chemistry, and outlines a set of rules to define the rate constants in a semi-automatic way. The method proposed by Curran [31, 32], together with others, laid the ground work for many recent studies, which led to the development of established algorithms capable of generating chemical kinetic models in an semi-automated way (i.e. [33, 34]). A comprehensive review on state-of-the-art best practices, advances and future challenges in mechanism generation is given by van de Vijver and co-workers [35].

As noted for the mechanism generation field, mechanism reduction is also a fertile ground, and it has received remarkable attention by the combustion community. Development of reliable and systematic reduction methods that require minimum user input is necessary, due to the size of detailed kinetic schemes once they are generated (see Figure 2.1). Mechanism reduction techniques can be divided in three macro-categories: skeletal reduction, time-scale analysis, and chemical lumping [14]. Two aspects are common to these three categories and must be defined prior the reduction:

1. The target application range for the reduced scheme, by means of operating conditions (i.e., pressure, temperature, equivalence ratio sweeps).
2. The error control strategy for the mechanism feature of interest (i.e., ignition delay, flame speed). This is crucial to ensure that the accuracy of the reduced scheme is preserved throughout the reduction process.

The skeletal reduction strategy aims to automatically identify and explicitly remove species and reactions from the mechanism that have a negligible contribution to the physical conditions of interest. In skeletal reduction, species elimination is typically more involved than reaction elimination due to the complex species couplings. The resulting mechanisms, usually referred as skeletal due to their much-reduced final size, are then suitable for other techniques introducing model assumptions to further reduce the computational time. These techniques are mostly based on time scale analyses, such as quasi-steady state approximation, intrinsic low-dimensional manifolds (ILDM) [36] or computational singular perturbation (CSP) [37]. In the present work, chemical lumping was investigated, hence a more detailed description will be given in the following paragraphs.

## 2.4. Chemical Lumping

This method consists of combining species with similar properties and reaction pathways such that the number of species and reactions is substantially reduced. In

(2.6), a four reactions mechanism is presented in a schematic form (as proposed by Pepiot et al. [38]) where reactants $A_x$ form two isomers $L_x$, which then go to the products $P_x$ via the reactions $R_x$.

$$\begin{aligned}
&(R_1)\ A_1 \xrightarrow{k_1} L_1 \quad \omega_1 = k_1\left[A_1\right] \\
&(R_2)\ A_2 \xrightarrow{k_2} L_2 \quad \omega_2 = k_2\left[A_2\right] \\
&(R_3)\ L_1 \xrightarrow{k_3} P_1 \quad \omega_3 = k_3\left[L_1\right] \\
&(R_4)\ L_2 \xrightarrow{k_4} P_2 \quad \omega_4 = k_4\left[L_2\right]
\end{aligned} \tag{2.6}$$

The chemical lumping technique, also noted in literature as horizontal lumping, consists in combining isomers $L_x$ into one representative species $L$. The reaction rates $k_x$ of the reactions involving species $L_x$ are also combined into a new $\tilde{k}_x$. This procedure can be schematically formulated as in (2.7).

$$\begin{aligned}
&[L] = \left[L_1\right] + \left[L_2\right] \\
&\tilde{k}_3 = k_3 \frac{\left[L_1\right]}{[L]} \quad ; \quad \tilde{k}_4 = k_4 \frac{\left[L_2\right]}{[L]}
\end{aligned} \tag{2.7}$$

The resulting lumped mechanism (˜) can be then updated as reported in (2.8)

$$\begin{aligned}
&\left(\tilde{R}_1\right)\ A_1 \xrightarrow{\tilde{k}_1} \mathrm{L} \quad \widetilde{\omega}_1 = \tilde{k}_1\left[A_1\right] \\
&\left(\tilde{R}_2\right)\ A_2 \xrightarrow{\tilde{k}_2} L \quad \widetilde{\omega}_2 = \tilde{k}_2\left[A_2\right] \\
&\left(\tilde{R}_3\right)\ \mathrm{L} \xrightarrow{\tilde{k}_3} P_1 \quad \widetilde{\omega}_3 = \tilde{k}_3[\mathrm{L}] \\
&\left(\tilde{R}_4\right)\ L \xrightarrow{\tilde{k}_4} P_2 \quad \widetilde{\omega}_4 = \tilde{k}_4[L]
\end{aligned} \tag{2.8}$$

Typically, mechanisms of large hydrocarbons (i.e., *n*-decane, $C_{10}H_{22}$) involve large number of isomers that have similar thermal and transport properties, which in turn facilitates the application of horizontal lumping. As reported by Lu et al. [14], lumping has a high potential to keep the comprehensiveness of the source mechanism because it is based on the molecular properties of the species, which are valid over a broad range of conditions. Chemical lumping is usually adopted either as a modelling tool or as a reduction technique. In most of application though, lumping is employed as tool to reduce the computational time needed to solve detailed chemical models.

A significant effort was done to establish a mathematical strategy to lump a system of ordinary differential equations (ODEs) [39]. As reported by Lu et al. [14] the main aspects to be considered are:

1. The appropriate choice of the species to lump.
2. An accurate evaluation of the quantitative contribution of each isomer species to its lump group.

Several approaches that use numerical simplifying assumptions can be found in literature. For methane combustion, Huang et al. [40] proposed to choose the lump groups by introducing numerical criteria based on pre-calculated local concentration and rates of formation obtained using the detailed mechanism. For molecules larger than methane, where more chemically meaningful assumptions are needed rather than mere numerical considerations, the general trend for the choice of the lump group is to identify species having the same functional group and different distribution of radical or oxygenated sites on the molecule; isomers as such. For the estimation of the relative contribution of the isomers within the lump group several approaches have been published in the past. Such strategies are based on a variety of methods, from empirical correlations obtained through: pre-calculated reactor experiments [41, 42], quasi steady-state approximation on the detailed mechanism [43] as well as on statistical information derived from calculation performed using the detailed mechanism [38].

Another approach to estimate the relative contribution of the isomers within the lump group is to rely on a general set of a priori conditions, which are imposed on the detailed mechanism [44]. The method proposed in this thesis belongs to this category.

It is based on the findings from Ahmed et al. [45] and it has been refined, extended to a broader set of conditions and applied to oxygenated fuels. In the following paragraphs a short overview of the chemical kinetic scheme adopted will be given together with a detailed explanation of the proposed lumping methodology. The quality of the results obtained using the derived lumped mechanism is also partially presented. For the full set of the method validation results, please refer to paper I.

### 2.4.1. Chemical Kinetic Model for Diesel and Biodiesel Blends

The detailed reaction mechanism used to validate the lumping method is an *n*-decane, *α*-methylnaphthalene and methyl decanoate scheme with 807 species and 7807 reactions. The choice of the main surrogate fuels was done so that the chemical properties of pure Diesel and Rapeseed Methyl Esther (RME) could be matched. Cetane number and lower heating value of the widespread European commercial fuels listed in Table 2.1 have been considered, among other properties, as main targets to be matched by the modelled surrogate fuel mixtures. One of the surrogate fuel models typically considered to simulate commercial Diesel is a blend of *n*-decane and *α*-methylnaphthalene respectively in 70% and 30% on a volume base. Such mixture has been chosen according to average European Diesel composition in terms of *n*-alkanes and aromatic contents and it has been presented in several papers [46, 47, 48, 13]. To simulate RME behavior instead, a methyl decanoate (MD) reaction mechanism was

considered. Many chemical kinetic studies in the last years proposed methyl decanoate as the most suitable surrogate fuel for biodiesels such as RME [49, 50].

**Table 2.1.** Typical commercial European fuels properties.

| Property | Method | Diesel | RME |
|---|---|---|---|
| Density at 15 °C (kg/m³) | DIN EN 12185 | 839.2 | 883.3 |
| Kinematic Viscosity (mm²/s) | DIN EN 3104 | 3.03 | 4.46 |
| Cetane number (-) | DIN EN 15195 | 51.6 | 55.6 |
| Lower heating value (MJ/kg) | DIN EN 590 | 42.55 | 38.23 |

The generation of the chemical reaction mechanism was performed using the procedure described in [33] and [34]. In the first step, the detailed mechanisms for *n*-decane and methyl decanoate were generated. The C1 to C6 chemistry was taken from Seidel et al [51]. A wide range of reactor simulations were performed to validate the performance of the single component kinetic and, thereafter, the combined model was validated [47]. The thermodynamic data of the *n*-decane mechanism were taken from Westbrook et al [49]. The thermodynamic data for species within the methyl decanoate mechanism are taken from [50]. The transport data are taken from the LOGEfuel database [18]. As a final step, the *n*-decane - methyl decanoate mechanism was compiled with a sub-mechanism for $\alpha$-methylnaphthalene.

### 2.4.2. *A priori* Thermodynamic Based Lumping

Although all the methodologies cited in paragraph 2.4 can be identified as systematic and comprehensive lumping transformations, they all rely on an extensive set of simulated data using the detailed scheme. The method presented in this thesis relies on an *a priori* analysis of the thermo data of the isomers instead. The motivation is to maintain the applicability of the lumping approach to automatic mechanism generators and keep it independent from the detailed mechanism performance under relatively restrictive benchmark reactor conditions.

As a first step, the Gibbs free energies of all species of each isomer class were assessed and compared to each other. The main constrain used to decide whether to include each isomer in the lumped pseudo-species is the absolute difference in Gibbs free energy. In other words, isomers which showed very small differences (less than 1kJ) in Gibbs free energy were selected to be part of the lump group under the assumption that they would present equal concentrations. To verify until what extend this assumption can be considered valid, several constant volume reactor calculations were performed, and concentrations of the isomers were analyzed. A representative outcome of the outlined thermo data analysis and its verification is shown in Figure 2.2 for *n*-decane and methyl decanoate isomers of reaction class 1. See Curran et al. [31] for more details on the reaction classes and their definitions.

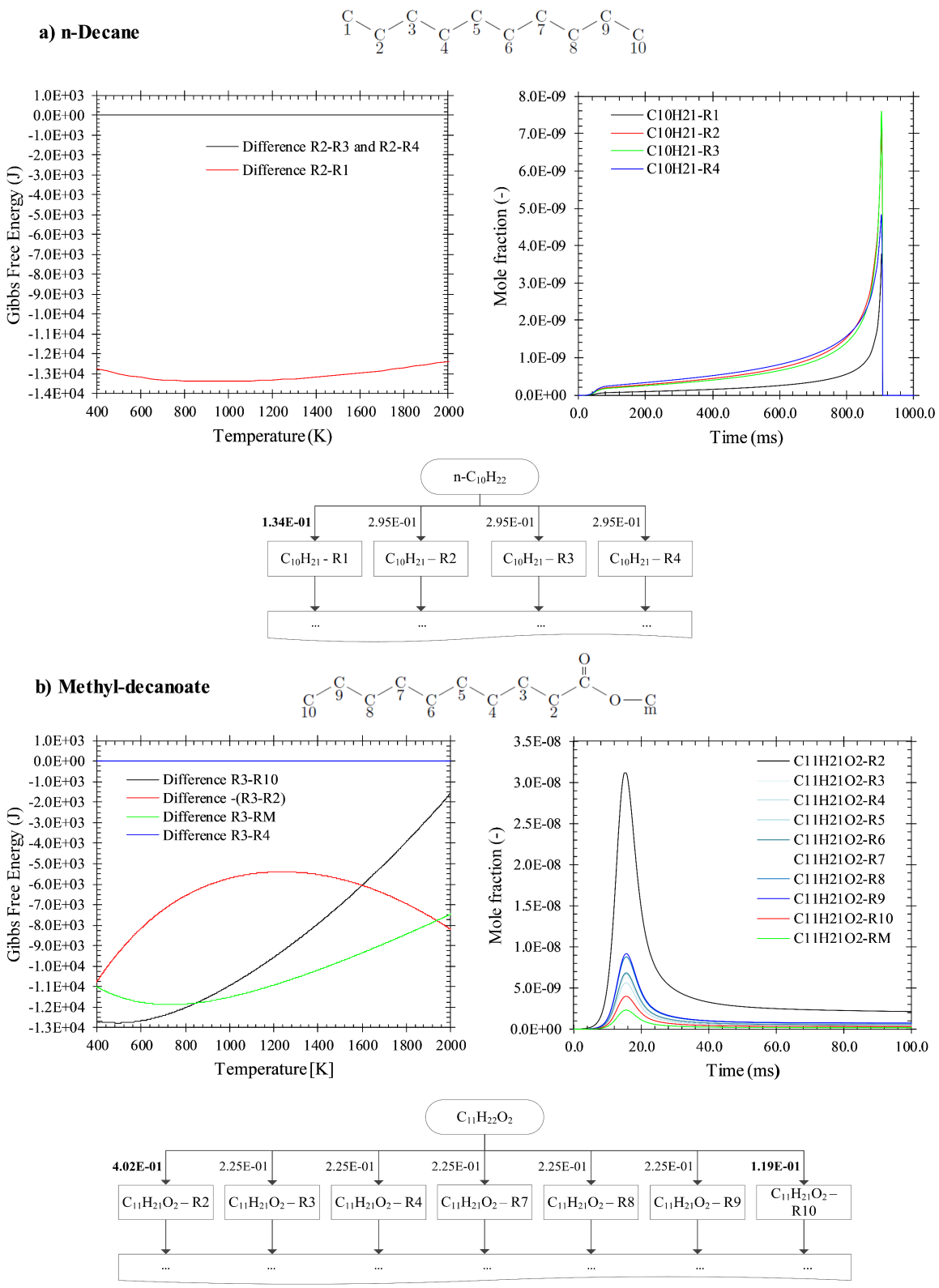


**Figure 2.2.** Schematic verification of the strategy adopted to choose the isomers to include in the lumped groups for **a)** *n*-decane and **b)** methyl decanoate. Left-side charts: absolute Gibbs free energy differences between isomers of reaction class 1; right-side charts: class 1 isomers mole fractions profiles; bottom scheme: flow analysis obtained with 0-D constant volume reactors at T = 800 K, p = 1 bar, $\phi$ = 1.0.

For both *n*-decane and methyl decanoate, the Gibbs free energy analysis (left side chart) for radical species formed during the unimolecular fuel decomposition reaction (noted in [31] as reaction class 1) and isomers concentration obtained under 0-D homogeneous constant volume reactor conditions at 800 K, 1 bar and stoichiometric conditions (right side chart) are presented. A schematic flow analysis with net carbon fluxes of the isomers for the mentioned reactor conditions is also shown.

With respect to the *n*-decane molecule scheme presented in the top part of Figure 2.2 a), a so-called primary position is defined when the given chemical reaction, i.e., class 1, produces an isomer having radical site on the C atom marked with the number 1. Consequently, a secondary position is defined when the formed isomers have radical site on the C atoms marked with 2, 3, 4 and 5 in Figure 2.2 a).

In agreement with the assumptions made by Ahmed and co-workers [45] for n-heptane mechanism lumping, considerable differences in Gibbs free energy were noticed between isomers having radical site in a primary position and those in secondary. Such dependency analysis schematically summarized in Figure 2.2, was conducted for isomers species in classes 1, 11, 12, 13 and 18 for all species with 5 carbon atoms or more. The overall trend for *n*-decane and methyl decanoate revealed that isomers with either the radical site or the functional group at a primary site show visibly lower concentrations compared to radicals with functions or radical site at the secondary position (see right side charts in Figure 2.2). Hence, two types of lumped species were introduced to describe the oxidation process. The species are labelled with the prefix *LP*- for primary and *LS*- for secondary species with respect to the positions of the radical site or the functional group. With respect to methyl decanoate analysis only, it is important to underline the following findings: for all isomer classes assessed, the Gibbs free energy of the species having radical site in position 2 and at the carbonyl group differs overall by 3-4 order of magnitudes with respect to isomers having radical site in primary or secondary position. This agrees with the strong differences in concentrations observed when simulating the mechanism under 0-D constant volume reactor conditions (see right-side chart in Figure 2.2 (b)). Isomers having radical site in position 2 and m were therefore excluded from the lumped pseudo-species.

As an additional *a priori* assumption, a special exception was done for reaction class 12 where QOOH is formed by peroxyl radical isomerization via a 5, 6, 7 or 8 membered rings. The new order is based on the number of C atoms between the radical position and the OOH group (which is directly correlated to the ring size of the transition state when QOOH is formed) after the first internal H atom abstraction replacing all $C_xH_yOOH$ isomers in the detailed scheme. A more detailed discussion on this aspect is reported in paper I.

The mechanism size after reduction consisted of 463 species and 7600 reactions. Once the isomers to be included in the group were chosen, a linear lumping approach [44] was applied. All selected isomers lumped to one species are assumed to have equal concentrations. The resulting rate coefficients are weighted by the rates for the lumped isomers and the numbers of reactants and products in the reaction equation. An exemplary derivation of the chemical source term obtained after the lumping process is outlined in paper I.

### 2.4.3. Lumping Method Validation using Constant Volume Reactors

Modelling of auto ignition was carried out assuming constant volume and homogeneous adiabatic conditions. The predicted ignition delay was determined by the evaluation of the maximum temperature gradient. To comprehensively verify the effect of the lumping procedure on the mechanism performance, single fuel calculations were performed and a mixture including all three components was tested as well. The motivation behind the choice of the mixture (0.71 *n*-decane, 0.23 $\alpha$-methylnaphthalene and 0.06 methyl decanoate by mole fraction) was on the one hand done based on the current legislation for European Diesel in terms of aromatic/biodiesel content allowed. On the other hand, to monitor potential influences of the lumping on the fuel-fuel interactions. Hence a blend, which will be labelled as -EU Diesel model- in the following figures, was widely studied. In Figure 2.3, comparisons of the ignition delay time predictions obtained using detailed and lumped mechanisms are presented for all the investigated gas compositions.

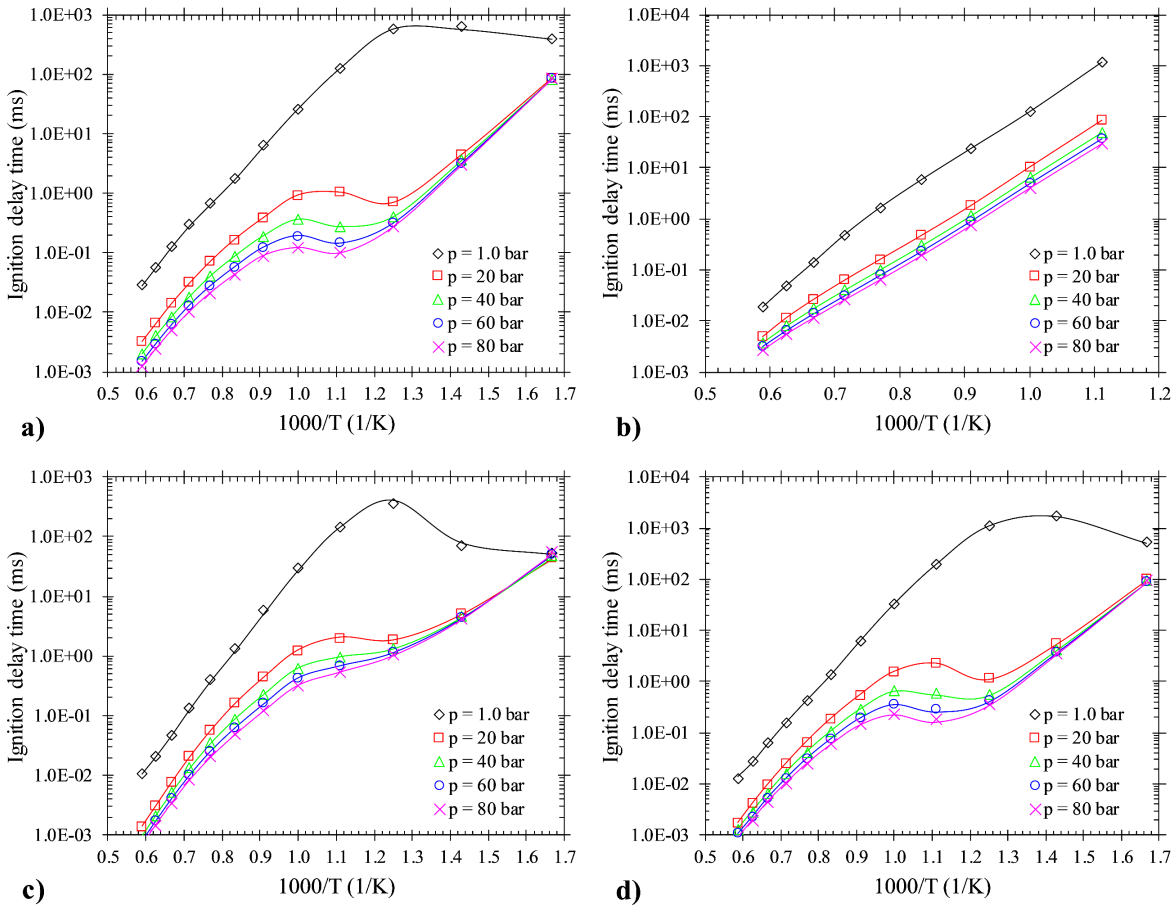


**Figure 2.3.** Simulated ignition delay times at $\phi = 1.0$ for detailed mechanism (symbols) and lumped mechanism (dashed line). **a)** Pure *n*-decane; **b)** pure $\alpha$-methylnaphthalene; **c)** pure methyl decanoate; **d)** EU Diesel model: 0.71 *n*-decane, 0.23 $\alpha$-methylnaphthalene, 0.06 methyl decanoate in mole fractions.

The predicted ignition delay was determined by the evaluation of the maximum temperature gradient. It is indeed noticeable that very good agreement was found between detailed and lumped mechanism predictions at stoichiometric conditions.

However, as logarithmic plots may be misleading in estimating error levels, Figure 2.4 shows the percentages of the absolute ignition delay time predictions differences between detailed and lumped mechanism on a linear scale for various pressure and equivalence ratios. Each chart row in Figure 2.4 was obtained with a different fuel labelled as a), b) and c), or fuel mixture d). In order to cover most of the typical light-duty Diesel engine combustion regimes, errors were assessed for initial pressures varying between 1 and 120 bar, and equivalence ratios between 0.5 and 2.0. It is noteworthy to mention that in Figure 2.4 negative error means under prediction of the ignition delay, with reference to the detailed mechanism simulation results, and vice versa.

Good agreement was found for all the conditions with an overall average error within 10%. The proposed lumping strategy showed good results also for *n*-decane and methyl decanoate as single fuel components. Especially in the NTC region, the lumped mechanism showed negligible deviations from the predictions with the detailed mechanism. With respect to Figure 2.4 b), no errors were noticed when pure $\alpha$-methylnaphthalene was simulated. Such results were indeed expected as the lumping procedure did not involve any species belonging to the aromatic oxidation pathways. As previously mentioned, such test was of high importance to verify whether the lumping of a multi-component mixture influenced the other fuels or not.

As for the methyl decanoate part instead (Figure 2.4 c)) higher deviations (absolute maximum = 21% at T = 800 K, and $\phi = 2.0$) were found at 1 bar. For this matter, a deeper investigation was carried out, to explore the validity of the assumptions made on the calculation of the lumped species rate-coefficients (see paper I for more details). As compactly shown in Figure 2.5, several 0-D constant volume reactor calculations were performed between 1 and 4 bar at rich conditions ($\phi = 2.0$) in order to compare predicted concentration of isomers between lumped and detailed mechanism. Isomer species profiles have been compared at 800 K since it was the condition where the lumped mechanism showed the lowest accuracy (as per Figure 2.4 c)). Figure 2.5 c) d) show that concentration profiles of the single isomers at 0.5 bar differ much more than those at 4 bar initial pressure. Since the proposed methodology relies on the assumption of equal concentration of the lumped species and therefore on equally distributed rates, higher deviations are expected compared to the detailed mechanism. In addition, the non-symmetry of the methyl decanoate molecule might also play a significant role and explain why such behavior has not been noticed for *n*-decane.

To check also whether the lumping strategy influenced the fuel-fuel interactions, the previously mentioned EU Diesel model was tested (see Figure 2.4 d)). Overall, the lumping approach did not show to affect the mechanism performance over the full range of operating conditions assessed for the three component blend.

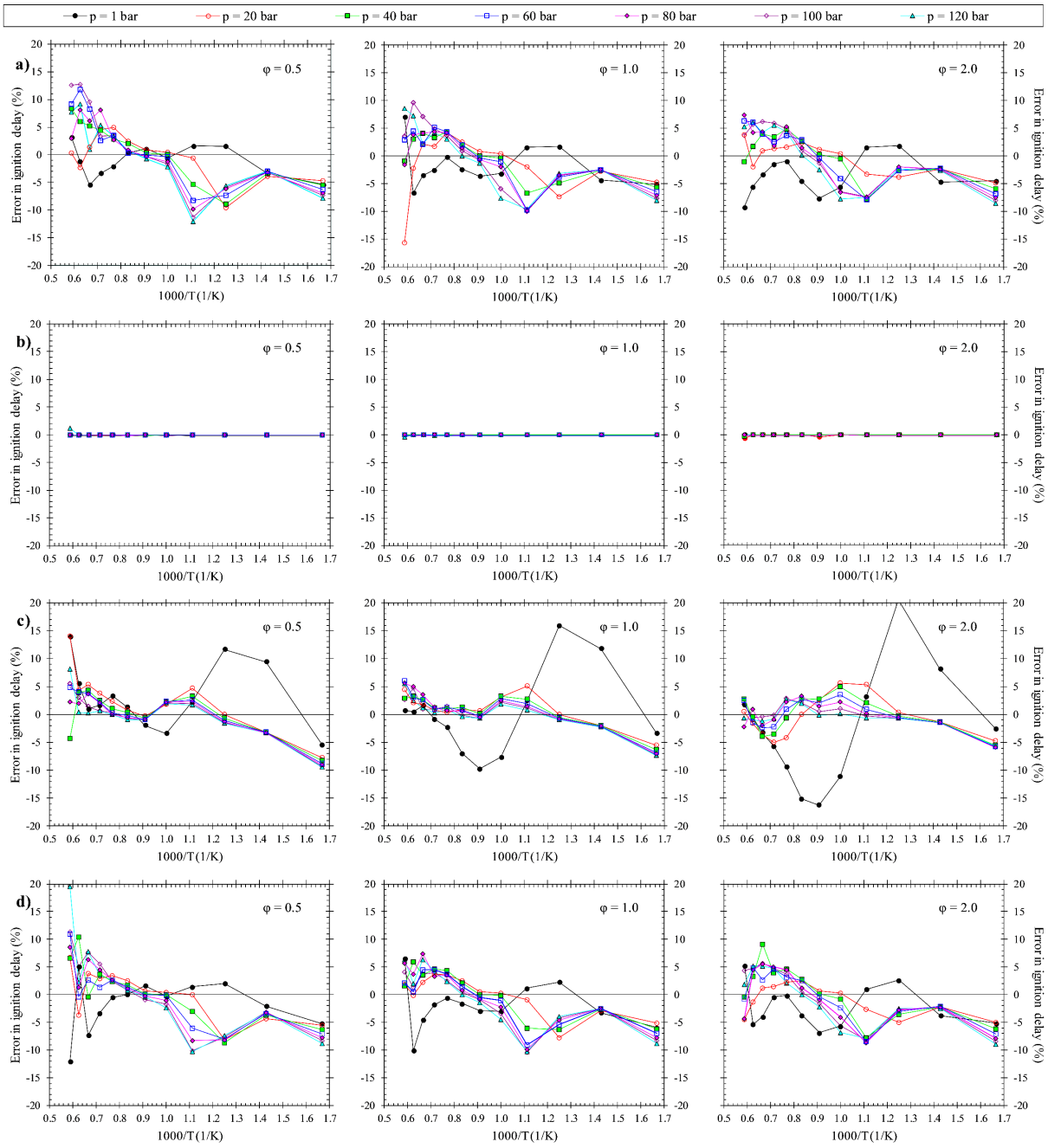


**Figure 2.4.** Absolut ignition delay time predictions' differences in percentage between detailed and lumped mechanism on linear scale for 1.0 to 120 bar initial pressure and 0.5 to 2.0 equivalence ratio. **a)** Pure *n*-decane; **b)** pure $\alpha$-methylnaphthalene; **c)** pure methyl decanoate; **d)** EU Diesel model: 0.71 *n*-decane, 0.23 $\alpha$-methylnaphthalene, 0.06 methyl decanoate in mole fractions.

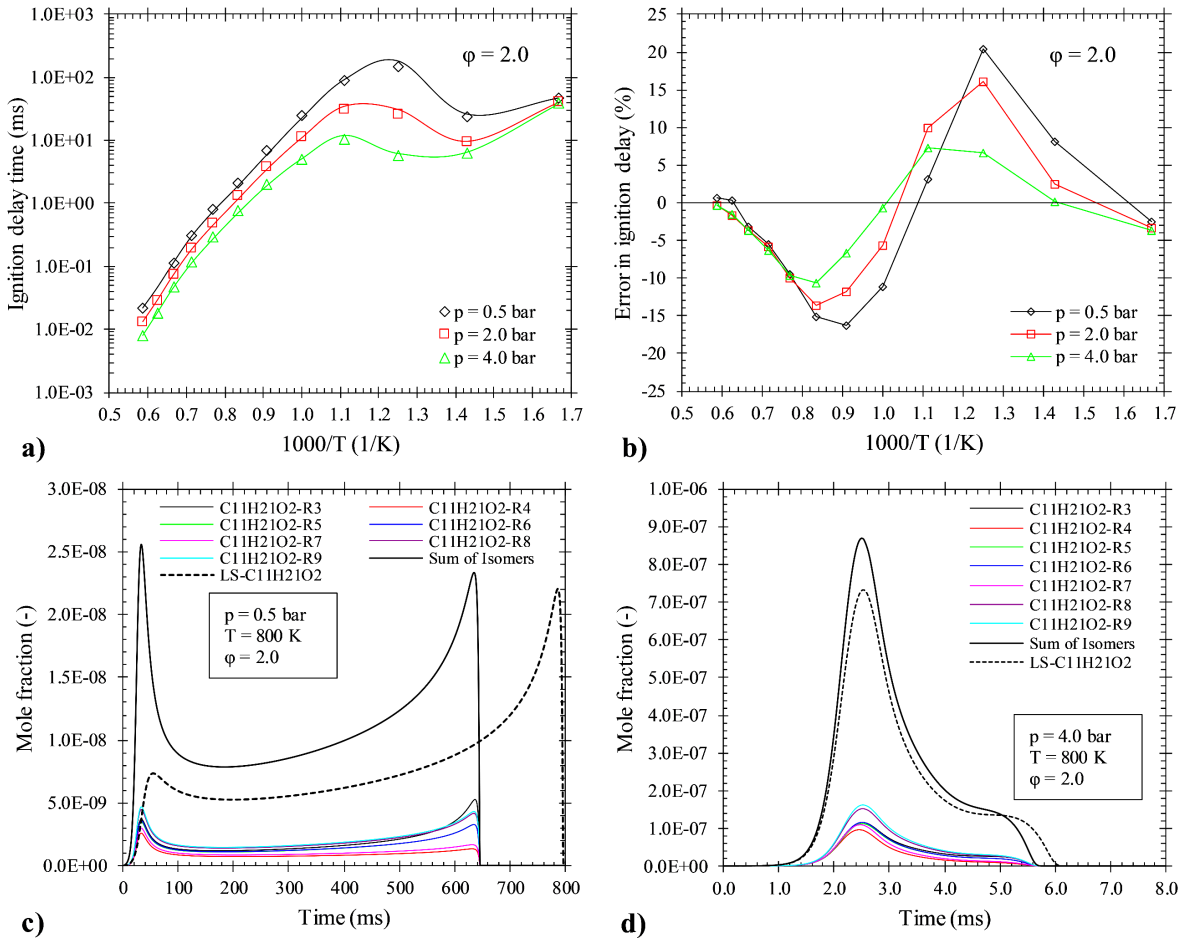


**Figure 2.5.** Investigation on lumped methyl decanoate mechanism pressure dependency. **a)** Ignition delay times of pure methyl decanoate/air at $\phi = 2.0$ for detailed mechanism (symbols) and lumped mechanism (dashed line); **b)** absolute ignition delay time prediction differences in percentage between detailed and lumped mechanism at $\phi = 2.0$ and 1, 2, and 4 bar initial pressure; **c) d)** comparison of predicted concentrations with detailed and lumped mechanism at T = 800K, $\phi = 2.0$, initial pressure is 1 bar in **c)** and 4 bar in **d)**.

A sensitivity analysis at 750 and 950 K, in a similar manner as applied to the *n*-heptane mechanism from Curran et al. [31], for both the detailed and the lumped mechanism was performed. The main focus was on low-medium temperature kinetics of the aforementioned EU Diesel model. Therefore, reactions belonging to classes 2 to 25 of the *n*-decane chemistry have been assumed to be of major importance for the reactivity at low and medium temperature. The forward rate coefficients of these reactions have been multiplied by a factor of two and the relative change in the ignition delay times has been compared. Thus, negative sensitivity coefficient means that the overall rate of fuel oxidation is enhanced by the examined reaction. The sensitivity coefficients were calculated at two different mixture conditions ($\phi = 1.0$ and 2.0) and two different pressures (p = 13 and 50 bar). All investigated sensitivities at the mentioned conditions are shown in Figure 2.6.

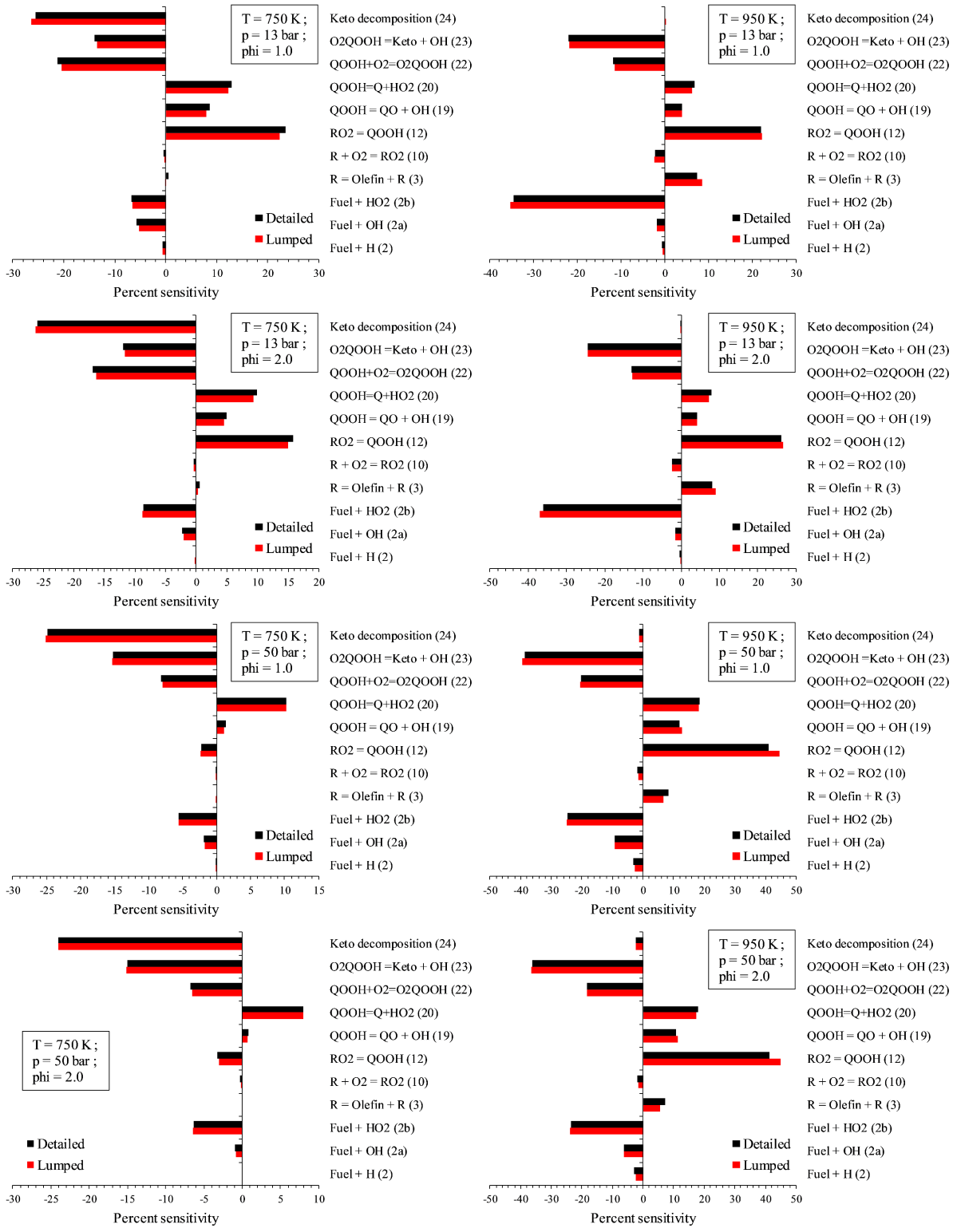


**Figure 2.6.** Sensitivity coefficients for ignition delay of the EU Diesel mixture (0.71 *n*-decane, 0.23 $\alpha$-methylnaphthalene, 0.06 methyl decanoate in mole fractions).

Very similar levels of sensitivity were found for all the considered reactions. The comparison of the sensitivities of the low-medium temperature reaction classes [31] (see numbers reported in curved brackets on the y axis of the charts in Figure 2.6) for the

detailed and lumped mechanism is a direct test on how the reactivity of the kinetic scheme is affected by the reorganization of the reaction mechanism. Only negligible deviations were found, demonstrating that not only the overall reactivity but also the class reactivities are maintained after the reduction process. The consequence of these findings is that the structure of the reorganized mechanism is not influenced by the kinetic assumptions for reaction rates.

Similar levels of accuracy between detailed and lumped mechanism predictions were obtained also in terms laminar flame speeds and speciation profiles, as well as under heavy-duty Diesel engine simulation using a 0-D SRM. See paper I for more details.

## 2.5. Summary

In the first eight months of the PhD work, a chemical lumping method based on an *a priori* thermodynamic data analysis was developed, as a result of a collaboration with the chair of thermodynamics at BTU Cottbus-Senftenberg, in Germany. The lumping method was applied to the reduction of a large three component reaction mechanism (807 species and 7807 reactions, see paragraph 2.4.1) where each isomer group was replaced with one single representative lumped pseudo species. The selection of the species to lump was performed based on the Gibbs free energy levels of each isomers class (assuming reaction classes as in [31]). The formulation of the rate coefficients of the lumped pseudo species was performed under the assumption of equal repartition. The methodology eventually led to the identification of 74 isomer groups and, consequently, a reduction of 418 species. The mechanism size after reduction consisted of 463 species and 7600 reactions.

Predictive capabilities of the reduced mechanism were compared to the results obtained with the detailed scheme under several reactor conditions (in both 0-D and 1-D frameworks). The lumping methodology revealed to be acceptable for the reduction of *n*-decane and methyl decanoate chemistry, with respect to accuracy loss. Even in the very sensitive NTC region, typical of low temperature ignition of large alkane and oxygenated fuel molecules, the lumped mechanism solutions showed to never deviate beyond 12%, on average, from the solutions of the detailed mechanism.

Furthermore, the resulting lumped mechanism gives an advantageous starting point for additional model reduction techniques, such as skeletal reduction methods. Since the main oxidation pathways are kept intact, though largely condensed, an easier evaluation of -important- from -unimportant- species is allowed. In addition, the presented lumping methodology is formulated so that it is of general applicability, and hence suitable to be implemented in automatic mechanism generators for large alkanes and oxygenated fuels.

In essence, one of the main goals of this activity was to formulate a reduction methodology as independent as possible from simulation results obtained using the detailed scheme. This is a significant aspect, when considering the development of automated mechanism generation tools since the reduction steps may be performed right after the generation. Gathering large datasets of simulation results with a scheme featuring several hundreds of species may be a very time consuming process even when

only 0-D simulation frameworks are considered. Hence, an *a priori* based methodology may be an attractive solution to speed up not only the final simulation time, but also the mechanism generation process itself. The present method was also incorporated in a broader mechanism reduction framework developed at LOGE GmbH and has been applied to various mechanisms as discussed in detail in the PhD thesis from Seidel [51].

After completion of the mechanism reduction work, a new phase of the PhD work was initiated in collaboration with the software development team at LOGE AB [52] in Lund, Sweden. The main focus of this second phase was shifted from mechanism reduction to chemistry tabulation method development. Hence, in the following chapters, broad attention will be given to tabulation aspects only.

# Chapter 3

# Tabulation Method and Verification using Homogeneous Reactors

The main focus of this thesis is the development of a computationally efficient chemistry tabulation strategy for autoignition and emission formation. As discussed in the previous chapter, this is an active area of research and remarkable efforts have been made in this field in the past decade. This chapter aims to: give an overview on the main categories of tabulation methods published with a discussion on their pros and cons; introduce the method formulated and developed in the present work; present the first fundamental validation campaign performed under 0-D homogeneous reactor conditions.

## 3.1. Background and Previous Works

As widely discussed by Pope in [53], the terminology *tabulated chemistry* is currently used in literature (as well as in the present thesis) to refer to two fundamentally different methods. On the one hand, the In Situ Adaptive Tabulation (ISAT) method relies on a thermo-chemical database which is constructed during the reactive flow simulation. While this method aims to reduce the computational time needed for the calculation of the chemical reaction rates, it is not a model reduction method since the given reaction mechanism is used in its full definition. On the other hand, a so-called *structured pre-tabulation* method is defined if it is based on the two following steps [53]:

1. The thermo-chemical database, or a globally generated manifold, is constructed by using a given detailed, reduced or skeletal mechanism prior to the reactive flow computation.
2. The generated thermo-chemical database is coupled to the reactive flow governing equations via a reduced set of variables.

For each numerical iteration, the reactive flow solver computes the flow field properties as well as the coordinates needed to perform the table look-up. Typically, the thermo-chemical look-up table coordinates are much less than the number of species involved

in the initially used chemical mechanism. Hence, this kind of tabulated chemistry approach constitutes a model reduction methodology. The tabulation method developed in this thesis, belongs to the latter category (defined earlier as *structured pre-tabulation* [53]).

The appropriate choice and the definition of the table look-up coordinates, as well as the strategy used to construct, and access the thermo-chemical table during run-time is influenced by many factors such as: the chosen model for turbulent combustion (i.e., flamelet, well stirred reactor), the turbulence modeling framework (i.e., RANS, LES) and the physical problem (i.e., a laboratory flame, an ICE at various speed and load points). As discussed by Fiorina et al. [54], there is no universal set of coordinates capable of capturing the impact of kinetics, molecular diffusion and heat losses on the flame structure. A preliminary classification of the methods proposed in the literature can be made based on whether a mathematical or a physical analysis is used to define the look-up coordinates. The Intrinsic Low-Dimensional Manifold (ILDM) initially proposed by Mass and Pope [36], and its later extension (FPI) by Giquel et al. [55] to improve performance under cool flame conditions, have been among the most impactful mathematical methods proposed. The dynamic behavior of the nonlinear response of the chemical system is identified by examining the eigenvalues and eigenvectors of the system of equations. Fast time scales are cut-off based on a given time threshold which influences the number of coordinates (and hence transported scalars) needed to derive the chemical state of the full reactive system.

Flamelet models on the other hand, are based on physical (rather than mathematical) considerations. With respect to non-premixed combustion, Peters [56] proposed that the flame structure can be assumed to be locally one-dimensional and is dependent on time and the coordinate normal to the flame front. The flamelet equations are solved in mixture fraction ($Z$) space where turbulence-chemistry interaction (TCI) effects are considered via the scalar dissipation rate of the mixture fraction. The flamelet assumption is particularly suitable for tabulation method definition since the thermo-chemical state of the combustion process can be described locally by only a small number of control parameters. Furthermore, many engineering applications, i.e., gas turbines, fall into the flamelet regime, where the chemistry is fast, and reactions take place in thin layers. For the mentioned reasons, many research groups across the globe have proposed numerous successful studies for premixed, partially premixed and non-premixed combustion in the past decade [57-64]. Complex phenomena such as soot formation under engine conditions have been successfully predicted using flamelet library-based soot source terms [65-68]. Among the many improvements proposed in recent years, noticeable efforts have been made also towards more efficient memory management strategies so that storage and compute requirements for either the code or the look-up table are reduced [69, 70].

With reference to internal combustion engine simulations, applications of the well stirred reactor approach (see paragraph 4.2.1), as opposed to flamelet-based methods, have systematically increased in recent years. Although the WSR has some important shortcomings, such as the lack of turbulence chemistry-interaction effects, the ease of use, together with the availability of several reduced multi-component schemes, has

arguably led most automotive OEMs towards using the WSR as the combustion model of choice for engine research and development activities. The tabulation method developed in this thesis is based on the WSR concept. Hence, in this chapter broader focus is given to this category of tabulation techniques.

The use of homogenous 0-D reactors for auto-ignition tabulation has been widely explored in literature over the last years with different levels of complexity. In [71], only the ignition delay time is stored in the table. This information, once retrieved from using cell local temperature, pressure, equivalence ratio and EGR, is employed within the well-known Livengood-Wu integral [72] for knock prediction in SI engines. Such method, however, only allows to estimate the instant of the auto-ignition event with no information on the heat release rate nor its magnitude. A similar but more advanced approach has been proposed by Lafossas et al. [73], where the estimation of the autoignition is done via a passive transported precursor scalar whose formulation relies on an empirical correlation dependent on fuel octane number, pressure and temperature.

The models mentioned so far lack the description of a crucial part in the auto-ignition of hydrocarbons, this is to say the low temperature combustion (also addressed in literature as the negative temperature coefficient region). To tackle such problem, Pires da Cruz et al. [74] proposed a method where both the high and low temperature ignition delay times are stored in the table. Validation was done under 0-D reactor conditions (assuming constant pressure/volume) as well as under diesel engine conditions in 3-D CFD. An improved version of such model was later proposed by Colin et al. [75] where a progress variable-based approach was used rather than a simple tabulation of the ignition delays. In this configuration, an additional tabulation dimension is introduced as the pre-tabulation is done for different values of the progress variable, which varies between $C = 0$ (being unburned mixture) and $C = 1$(being fully burned mixture). Further, during run-time the progress variable source term $\dot{C}$ is retrieved for each cell/zone and it is used to reconstruct the mixture state on the given oxidation trajectory. Later improvements of such method proposed by Knop et al. [76], also incorporated a turbulence chemistry interaction term during the tabulation stage so that TCI effects could be accounted for in 3-D CFD reactive flow simulations within the ECFM framework. The model (named Tabulated Kinetics of Ignition - TKI in [76]) has been applied to predict the ignition process of Diesel Homogeneous Charge Compression Ignition (HCCI) engines and is currently implemented in various commercial CFD codes.

With respect to 0-D/1-D frameworks, the number of applications of tabulated chemistry-based methods is rather limited. Its implementation, however, is potentially very useful as it allows to preserve the details of the original complex kinetics, with a minimal impact on the computing time. In addition, tabulation and 0-D/1-D modeling coupling broadens the range of feasible system simulation studies such as a cylinder-to-cylinder knock estimation or emission trends prediction during transient engine operating conditions (i.e., WLTP cycles). Within the SI engine simulation framework, Bougrine et al. [77] proposed a two-zone 0-D model (referenced as One-Dimensional Coherent Flame Model Tabulated Chemistry (CFM1D-TC)) where the chemical part

of the combustion process was tabulated using laminar 1-D premixed flame solutions. In addition, a time-scale model was formulated to better represent the relaxation towards equilibrium of CO and NO species with the help of homogeneous reactor calculations. Mosbach et al. [78] proposed a storage/retrieval technique for HCCI combustion in which various quantities such as ignition timing, cumulative heat release, CO, $CO_2$ emissions etc., were tabulated as function of engine geometry, equivalence ratio, octane number and intake temperature using an HCCI-SRM. Their technique was based on tabulating the evolution of the engine cycle and does therefore not allow use of the same table for different engines or different engine operating points. Leicher et al. [79] proposed a table look-up approach based on mixture fraction and reaction entropy as progress variable. Their methodology was implemented in a SRM and tested under constant pressure reactor conditions. Dulbecco et al. [80] proposed a tabulated multi-zone combustion model for HCCI Diesel combustion, tracking the combustion chemistry with eight species. Bozza et al. [81] implemented the previously mentioned TKI approach [76] within a 0-D/1-D phenomenological combustion model for better knock prediction in spark ignited engines compared to the traditionally used Livengood-Wu [72] approach. Validation under both 0-D reactors and knocking SI engine simulation at stoichiometric conditions showed promising results when compared to the on-the-fly chemistry solution.

## 3.2. Progress Variable Definition

Independently on whether the tabulation strategy is based on a flamelet or a homogeneous reactor paradigm, the definition of the progress variable is arguably the core of any table-based method. The progress variable (often noted in this thesis also as reaction progress or as $C$) is by definition the parameter with which the chemical trajectory, between unburned and burned sate, is parametrized. Given the non-linearity of the combustion chemistry process with temperature, the formulation of a comprehensive reaction progress variable is not trivial. Fuel specific regimes, such as NTC regions, can highly affects the accuracy and effectiveness of a given progress variable definition. Furthermore, depending on whether the target analysis presents a premixed or a diffusion flame regime, the progress variable definition may vary.

In the past decade, these aspects have been studied extensively and a relatively broad range of reaction progress definitions have been proposed. As discussed in detail by Ihme [82], Vervisch [83], Hasse [84] and co-workers, the guiding principles behind the formulation of a progress variable are:

1. The definition of $C$ should result in a transport equation that can be conveniently solved in a combustion simulation.
2. The scalars defining $C$ should all evolve on comparable timescales.
3. All parameters that define the manifold should be independent on one another.
4. The set of parameters from which the manifold is formed should uniquely characterize each point in the thermochemical state space.

5. The progress variable should result in a monotonic function $C(t)$ for all initial conditions in order to have a non-singular mapping.

In [82], [83] and [84] the authors propose solid optimization-based procedures to construct the progress variable under the assumption of it being a combination of a given number ($N$) of reactive scalars as in the following expression.

$$C = \sum_{i=1}^{N} \alpha_i Y_i \tag{3.1}$$

In equation (3.1), $\alpha_i$ and $Y_i$ are the weighting factor and the species mass fraction of species $i$, respectively. The most common definitions found in literature feature a linear combination of reactants and products. In the following equations some selected examples are reported.

Pierce et al. [60] $$C = Y_{CO_2} + Y_{H_2O} \tag{3.2}$$

Fiorina et al. [61] $$C = Y_{CO} + Y_{CO_2} \tag{3.3}$$

Poinsot et al. [85] $$C = Y_{CO} + Y_{CO_2} - Y_{O_2} \tag{3.4}$$

de Goey et al. [86] $$C = 22.7\, Y_{CO_2} - 31.3\, Y_{O_2} \tag{3.5}$$

Pitsch et al. [87] $$C = Y_{CO_2} + Y_{H_2O} + Y_{CO} + Y_{H_2} \tag{3.6}$$

de Goey et al. [88] $$C = \frac{Y_{CO_2}}{w_{CO_2}} + \frac{Y_{H_2O}}{w_{H_2O}} + 0.6\frac{Y_{CH_4}}{w_{CH_4}} - 0.4\frac{Y_{H_2}}{w_{H_2}} \tag{3.7}$$

In equations (3.2) and (3.3), the progress variable is defined as a linear combination of final combustion products and all the five guiding principles, listed earlier in the text are fulfilled. These are in fact among the most commonly used $C$ definitions in literature and have been implemented in numerous codes, thanks to their simplicity and universal validity for hydrocarbon combustion. However, progress variable definitions as in (3.2) and (3.3) fail to correctly represent cool flame auto-ignition, which is a crucial regime especially for Diesel combustion simulations. When using highly reduced schemes, which often do not present a detailed representation of the low temperature chemistry, a CO-$CO_2$ based progress variable definition, may still approximate well the combustion progress. When used in combination with detailed schemes, poor representation of the low temperature ignition may become evident instead.

In an attempt to better represent the cool flame auto-ignition, more elaborate progress variable definitions have been proposed. In [85] Poinsot and co-workers included oxygen in the reaction progress definition (3.4) due to the relatively regular consumption of oxygen during combustion. de Goey et al. [86] also proposed a $CO_2$-$O_2$ based definition with a set of optimized weighting factors, which depend on the target application (i.e., a premixed, non-premixed flame). Ihme and Pitsch [87] proposed to include also $H_2$ on top of CO, $CO_2$ and $H_2O$ (equation (3.6)) so to have a generally applicable formulation that could represent in detail low and high temperature ignition events. However, this definition may or may not deliver an accurate representation of the combustion trajectory depending on the initial conditions. Hence, an automated procedure for the optimization of the weighting factors for species ($\alpha_i$, all set to 1.0 in equation (3.6)) is usually necessary prior to the application of the tabulation method on the target application. Details on the formulation and results of such optimization procedures can be found in [82], [83] and [84].

In equation (3.7) de Goey and co-workers proposed a more elaborate progress variable definition featuring a weighting strategy based on both empirical factors ($\alpha_i$ set to 0.6 and 0.4 for the fuel species) and the molecular mass ($w_i$) of the respective species. This definition was proposed to study preferential diffusion effects in lean premixed methane-hydrogen-air flame kernels in a DNS framework with very good results.

While all the definitions presented so far are valid solutions to establish a predictive tabulation approach, performance and accuracy of the method depend strongly on the formulation of the weighting factors for each species mass fraction involved in the $C$ equation. Furthermore, depending on the target application (i.e., a premixed or a diffusion flame), as well as on the hydrocarbon considered, the same definition may lead to different performance.

An alternative concept, with respect to the species-based definition as in equation (3.1), has been proposed by Colin and co-workers [76] where temperature is the only quantity used. This definition, in its normalized form $C(t)$, reads as follows:

$$C(t) = \frac{T - T_{ini}}{T_{equ} - T_{ini}} \tag{3.8}$$

In (3.8), $T$ is the evolving temperature, $T_{ini}$ and $T_{equ}$ are the initial temperature and equilibrium temperature, respectively. All temperatures are extracted from previously computed homogeneous reactor detailed chemistry calculations at constant-pressure. Compared to the progress variable definitions based on species, the temperature-based one has the remarkable advantage of being applicable to potentially any fuel without the need of empirical optimization of weighting factors ($\alpha_i$ see equation (3.1)). Another important advantage of such method is the fact that it can also capture the cool flame auto-ignition process. Thanks to these features, and its simplicity, this method is widely adopted in ICE combustion simulations at the industrial level. It has therefore been implemented in several commercial CFD codes as part of the well-known ECFM-TKI tabulation approach. However, as also discussed by

the authors in [76], the major drawback of using temperature as progress variable is the formulation of the transport equation for $C$ in the computational domain. For reaction progress definitions based on equation (3.1), transport equations, as well as source terms, are of straight forward formulation since reactive scalars are conserved quantities. Temperature on the other hand, is not a conserved quantity and hence the formulation of the reaction progress, as well as potential source terms from spray, are not easy to formulate. To overcome this problem, Colin and co-authors [76] proposed an additional progress variable definition valid only within the CFD computations (while during the tabulation step the definition in (3.8) remains).

$$\tilde{C}(t) = 1 - \frac{\tilde{Y}_F}{\tilde{Y}_{F,0}} \tag{3.9}$$

In (3.9) $\tilde{Y}_F$ and $\tilde{Y}_{F,0}$ are the evolving fuel mass fraction and the initial fuel mass fraction, respectively. The underlying assumption behind this solution, is the fact that the heat release law from the complex chemistry solution (parametrized using temperature) can be recovered via the instantaneously burnt fuel mass. Hence, as stated by the authors in [76], the combustion is interpreted as a global single-step reaction, which progress is defined by the tabulated reaction rate.

Although this method has been successfully validated in numerous studies, it requires imposing an inconsistency between the progress variable definition used during the tabulation and the run-time retrieval processes (see equations (3.8) and (3.9)).

In the present work, the progress variable definition proposed in [58] is adopted instead. To parametrize the reaction progress, latent enthalpy (enthalpy of formation at standard state, $h_{298}$) is used to define the reaction progress variable $C$ as reported below (3.10), together with its normalized form $C(t)$ (3.11).

$$C = h_{298} = \sum_{i=1}^{N_{Species}} h_{298,i}\, Y_i \tag{3.10}$$

$$C(t) = \frac{h_{298} - h_{298,u}}{h_{298,max} - h_{298,u}} \tag{3.11}$$

In equation (3.11), $h_{298}$ is the latent enthalpy calculated at 298 K summed over all species ($N_{Species}$) of the given mechanism, subscript $u$ denotes unburned state, and $max$ denotes the most reacted state, which is assumed to be where the maximum cumulated chemical heat is released. As discussed in [58] this progress variable can be used to track both low and high temperature reactions and hence also the cool flame heat release. Figure 3.1 shows the typical evolution of $h_{298}$ together with temperature for a homogeneous 0-D constant pressure reactor calculation. Initial pressure and

temperature are 10 bar and 750 K, respectively, while the reacting gas is a stoichiometric mixture of *n*-$C_7H_{16}$ and air (chemical kinetic scheme taken from [89]). It can be seen that the $h_{298}$ follows the combustion chemistry trajectory through both the low and high temperature ignition regime, in full consistency with temperature. As mentioned for the temperature-based $C$ definition, the latent enthalpy-based definition is also easy to implement and is fully independent on the fuel molecule or the target application.

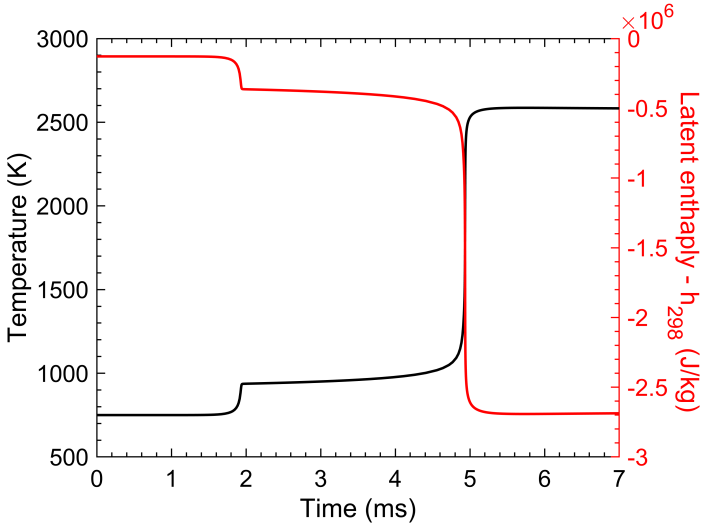


**Figure 3.1.** Temperature (black) and latent enthalpy at 298 K (red) as function of time for a constant pressure reactor calculation at 10 bar and 750 K for a stochiometric *n*-heptane/air mixture.

The main reason for which the $C$ definition in (3.11) was preferred over the temperature-based one (3.8), is the fact that latent enthalpy is a conserved scalar and hence the formulations of a transport equation, as well as a spray source term are rather easy. This allows then to have full consistency between the progress variable definitions during the tabulation process and the look-up/retrieval process occurring at run-time.

Nevertheless, it is important to note that also the $h_{298}$ based definition presents a major drawback when applied to fuel rich mixtures (i.e., $\phi > 3.0$). As listed earlier in the text, one necessary characteristic of the normalized progress variable is its monotonicity between unburned ($C(t) = 0$) and burned ($C(t) = 1.0$) conditions. Under lean and stoichiometric conditions, the maximum chemical heat release point (noted in equation (3.11) as $h_{298,max}$) coincides with equilibrium conditions. However, for fuel rich conditions as well as for phases with endothermic reactions under high pressure or high EGR conditions, the mixture relaxes towards equilibrium after reaching the maximum heat released point and the monotonicity of $C(t)$ is not fulfilled. Hence, during the tabulation process a cut-off is implemented so that $C(t) = 1.0$ may not always be the equilibrium condition. After extensive testing, which will be discussed in the next chapters, this assumption was considered acceptable for engine applications

in both 0-D SRM and 3-D CFD frameworks. Due to the usually high turbulence levels, locally rich cells tend to be quickly mixed towards either stoichiometry or lean mixture state. This compensates for the intrinsic inaccuracy of the progress variable definition in (3.11).

The method developed in this thesis has been given the acronym CPV, which stands for Combustion Progress Variable. Throughout the thesis, and in most of the graphs in the next chapters, the tabulated chemistry solver results will be labelled as CPV.

## 3.3. Auto-ignition and Emissions Source Terms Tabulation

The CPV model relies on a tabulation grid built as function of Exhaust Gas Recirculation ($EGR$), pressure ($p$), unburned temperature ($T_u$) and equivalence ratio ($\phi$). Detailed chemistry simulations are performed for the chosen fuel molecule, or a mixture of multiple fuels, assuming 0-D adiabatic constant pressure reactors. In the present work, the tabulation process was performed using the software LOGEtable [18]. Initial mixture unburned temperature ($T_u$), pressure ($p$), equivalence ratio ($\phi$) and $EGR$ are the input variables of the look-up table, as well as the normalized reaction progress $C(t)$. Table grid points were optimized so to cover the widest possible range of thermodynamic conditions that can be expected to be found in conventional direct injected engines, while trying to keep the final table size within an acceptable file size (below 2GB space on disk). The final table grid consists of 205 200 points, which are distributed across the tabulation parameter as outlined in Table 3.1.

**Table 3.1.** Tabulation grid obtained after the grid optimization campaign.

| Parameter | Lower bound | Upper bound | Number of points |
|---|---|---|---|
| Unburned Temperature (K) | 300 | 1400 | 76 |
| Pressure (bar) | 1.0 | 200.0 | 18 |
| Equivalence Ratio (-) | 0.05 | 6.0 | 30 |
| EGR mass fraction (-) | 0.0 | 0.4 | 5 |

The progress variable source terms ($dC/dt$) are stored together with the mixture molar mass, the thermodynamic polynomial coefficients and any chemical species that the user decides to monitor. In the present work, the following species have been included in the tabulation process so that major emissions and standard engine performance analyses could be easily visualized: Fuel species, $O_2$, $N_2$, $CO_2$, $H_2O$, CO, $H_2$, $C_2H_2$, $C_2H_4$ and the lumped unburned hydrocarbons species (uHC). The uHC lumped species in this thesis consist of the sum of the mass or mole fractions of all species containing at least one carbon and one hydrogen atom. In total, a table with the grid/output settings described above resulted in a size on disk of approximately 1.5 GB.

All the mechanisms used in this thesis included a detailed kinetic soot model as well as thermal NO model. Soot and NO formation are rather slow processes and require a

separate source term treatment to be correctly reconstructed during run-time. A separate source term tabulation strategy was developed and included in the present tabulation method. Details will be presented in the following paragraphs only with respect to the soot source terms strategy. The NO source term tabulation is not described herein to comply with confidentiality agreements established with LOGE.

### 3.3.1. Soot Source Terms

The detailed kinetic soot model as introduced in [90] is applied in each homogeneous reactor calculation grid point. The pathways of the PAH growth are modelled based on the mechanism from [91] and [90], with the updates from [47]. These kinetic pathways include the formation of the first benzene ring and small PAH species up to four aromatic rings. The growth of larger PAH molecules is described using a fast polymerization model [90]. The kinetic soot model contains a detailed description of the chemical and physical phenomena leading to soot growth and oxidation. For readability, the model is herein described in a rather concise form. A thorough description can be found in [90]. Further discussion and application of the soot model can also be found in [92, 93, 94, 95].

For the modelling of the soot particle size distribution function (PSDF) the method of moments with interpolative closure is used [96, 97]. This method is based on the statistical moments, since it is known that any mathematical function can be described by these moments. The moments of the soot PSDF are defined as:

$$M_r = \sum_{i=1}^{\infty} i^r N_i \tag{3.12}$$

where $M_r$ is the $r^{th}$ soot moment, $i$ is the size class counter, and $N_i$ is the number density of soot particles belonging to size class $i$. Following equation (3.12), the soot moment $M_0$ is the total number density. Soot moment $M_1$ yields the soot mass and can therefore be used to calculate the soot mass fraction or the soot volume fraction. It was found in previous works that the use of these two moments (0 and 1 only) is sufficient [90], higher order moments can be neglected. The source term of the soot moments $\dot{M}_r$ is given by the sum of the source terms of the different sub-processes considered: particle inception ($PI$), condensation ($Cond$), coagulation ($Coag$), surface growth ($SG$), fragmentation ($Fr$) and oxidation ($Ox$):

$$\frac{dM_r^*}{dt} = \dot{M}_{r,PI} + \dot{M}_{r,Cond} + \dot{M}_{r,Coag} + \dot{M}_{r,SG} + \dot{M}_{r,Fr} + \dot{M}_{r,Ox} \tag{3.13}$$

Particle inception or nucleation describes the formation of the first soot particle formed via coagulation of two-dimensional PAH molecules. Though this is still an active area of fundamental research, it is considered that during the particle inception the planar PAH molecules evolve into a three-dimensional soot particle held together by

Van der Waals forces. In the model, PAH with more than four aromatic rings are allowed to combine and form a soot particle nucleus and incept as proposed in [98]. Condensation describes the process of particle mass growth from the gas phase by the coagulation of PAHs to the particle surface. In the tabulation process of the soot source terms, it was decided to not pre-condition the rates on any pre-assumed soot concentration. Therefore, the condensation source cannot be calculated, and PAH is assumed to participate in particle inception only ($\dot{M}_{r,Cond} = 0$ in equation (3.13)). During run-time, steady state between condensation and particle inception is assumed. This enables to calculate total amount of PAH using the stored particle inception rate $NUC_{PAH}$ defined as follows:

$$NUC_{PAH} = (\alpha\, C\langle i\rangle^{\frac{1}{6}})\, {}^{P}M_0^2 + (C_f M_{2/3}\langle i\rangle^{-1/3})\, {}^{P}M_0 \tag{3.14}$$

From this rate the number density of PAH ($^{P}M_0$) and subsequently the particle inception and condensation source terms can be calculated. The source term for particle inception can be calculated from the collision frequency $C_f$, the total number density of the PAH size distribution function $^{P}M_0$ and the mean number of $C_2$ groups of the PAH $\langle i\rangle$.

$$\dot{M}_{r,PI} = \frac{1}{2}\alpha NUC_{PAH} C_f (2\langle i\rangle)^r\, \langle i\rangle^{1/6}\, {}^{P}M_0^2 \tag{3.15}$$

where $\alpha = 4\sqrt{2}$. According to the findings in [99], $\langle i\rangle = 12$ is chosen for the stored sources in the look-up table, which results in 24 carbon atoms (12 $C_2$ groups). Further it is assumed that two colliding PAH are of the same size.

When soot particles collide, they can either form larger spherical particles or form agglomerates. These processes are called coagulation. Coagulation does not contribute to soot mass formation or consumption but affects the soot surface available for surface reactions. Following [100], the agglomerate structure is considered by assuming a constant fractal dimension for soot $D_f = 1.8$. Beside the growth of the particles by condensation of PAHs, the hot reactive surface of the soot particles can also receive smaller gas-phase hydrocarbons. This process is called surface growth and has a strong impact on the final soot mass. Acetylene ($C_2H_2$) was found to be the major contributor to surface growth [101]. In the applied kinetic model, surface growth reactions are modeled through the hydrogen abstraction acetylene addition (HACA) mechanism [96], extended by a separate ring closure (HACARC) [90].

Oxidizer from the gas phase reduce the soot mass. In the model, oxidation reaction by OH and $O_2$ are considered. The interactions with the gas phase are described by the rates of surface growth and oxidation considering the fraction of surfaces sites $\alpha$ of the soot particle surface. For more details and discussions on reaction rate constants ($f_{3a}$, $k_{1a,b}$, $k_{1b,b}$ etc.) presented in equations (3.18), (3.19) and (3.20) please refer to [90].

$$\dot{M}_{r,SG} = SOOT_{SG} \sum_{k=0}^{r-1} \binom{r}{k} {}^{S}M_{k+2/3}\, \Delta m^{r-k} \tag{3.16}$$

$$\dot{M}_{r,Ox} = SOOT_{Ox} \sum_{k=0}^{r-1} \binom{r}{k} {}^{S}M_{k+2/3}\, \Delta m^{r-k} \tag{3.17}$$

$$SOOT_{SG} = \alpha\, k_{3a,f} \left[C_2H_2\right] f_{3a}\, A \tag{3.18}$$

$$SOOT_{Ox} = \alpha\, (k_{4a} \left[O_2\right] A + k_5 [OH]) \tag{3.19}$$

$$A = \frac{k_{1a,f}[H] + k_{1b,f}[H] + k_5[OH]}{k_{1a,b}\left[H_2\right] + k_{1b,b}\left[H_2O\right] + k_2[H] + k_{3a,f}\left[C_2H_2\right] f_{3,a} + k_4[O_2]} \tag{3.20}$$

$\Delta m$ is the change of mass in one reaction step. It holds $\Delta m = 1$ for surface growth and $\Delta m = -1$ for oxidation. In order to facilitate modeling of the soot surface growth feed-back for the tabulated approach, the gas phase formation and consumption rates of $C_2H_2$ are stored in the look-up table. At high temperatures, the bond between $C_2H_2$ and the soot surface can be broken. The $C_2H_2$ abstraction is called fragmentation and can be modelled by:

$$\dot{M}_{r,Fr} = SOOT_{Fr} \sum_{k=0}^{r-1} \binom{r}{k} {}^{S}M_{k+\theta/3}\, \Delta m^{r-k} \tag{3.21}$$

$$SOOT_{Fr} = \alpha k_{10,b} \tag{3.22}$$

As soot oxidation, this process leads to a reduction of the soot mass, therefore $\Delta m = -1$. To allow for model calibration, a set of scaling factors can be given by the user and will be multiplied by the tabulated source terms for nucleation ($NUC_{PAH}$), surface growth ($SOOT_{SG}$), fragmentation ($SOOT_{Fr}$), oxidation by $O_2$ and oxidation by OH ($SOOT_{Ox}$).

### 3.3.2. NO Source Terms

The underlying mechanism used to calculate thermal NO is based on the Zeldovich formulation [102, 103]:

$$\begin{aligned} O + N_2 &\leftrightarrow NO + N \\ N + O_2 &\leftrightarrow NO + O \\ N + OH &\leftrightarrow NO + H \end{aligned} \tag{3.23}$$

A similar strategy as the one presented for soot is established during the tabulation as well as the look-up/retrieval stage to reconstruct the instantaneous NO mass fractions. Details of this sub-model are not presented for confidentiality reasons.

## 3.4. Interpolation Error Assessment

Before applying the methodology to engine simulations, the interpolation strategy for the source term retrieval was tested using homogeneous reactors. For all the points included in the tabulation grid, temperature evolution from the online chemistry solver constant pressure calculation were compared to the respective solution retrieved from the table using linear interpolation. The error between online and tabulated solution was then quantified based on the mean squared difference of the vector composed by the errors at 5, 10, 50 and 90 percent of energy released location (noted as $E_{5\%}$, $E_{10\%}$, $E_{50\%}$ and $E_{90\%}$ in Figure 3.2) at all given reactor points.

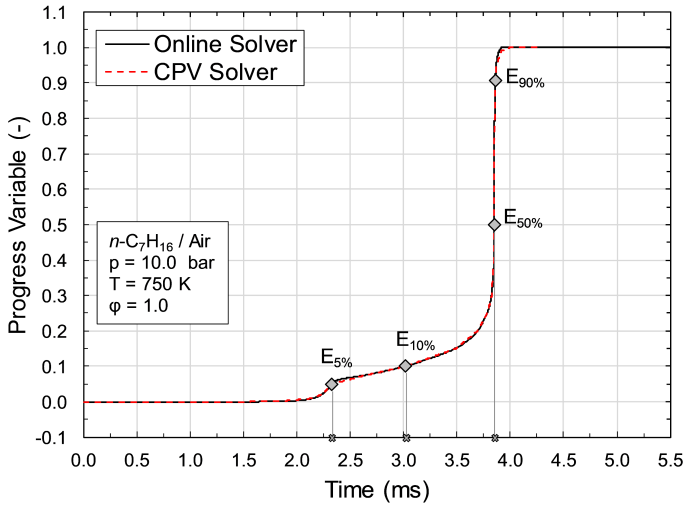


**Figure 3.2.** Online and tabulated chemistry solutions for the progress variable (based on equation (3.11)) evolution of a stoichiometric *n*-heptane/air mixture at 10 bar and 750 K.

The global interpolation error was then defined based on the average error of the location of the $E_{5\%}$, $E_{10\%}$, $E_{50\%}$ and $E_{90\%}$ points. In equations (3.24) and (3.25), where $i = 5, 10, 50, 90$ and $N_{errors} = 4$ the exact definitions of the interpolation errors are given.

$$\epsilon_i = \frac{E_{i,Tabulated} - E_{i,Online}}{E_{i,Online}} \bullet 100 \tag{3.24}$$

$$\bar{\epsilon} = \sum_{i=1}^{N_{errors}} \epsilon_i \Big/ N_{errors} \tag{3.25}$$

In Figure 3.3 and Figure 3.4 exemplary results of the error quantification campaign are presented in pixel plot format assuming the error definition in equation (3.24) for conditions at 1 and 35 bar pressure, respectively. In Figure 3.5 the averaged interpolation errors, as per the definition in equation (3.25), are shown.

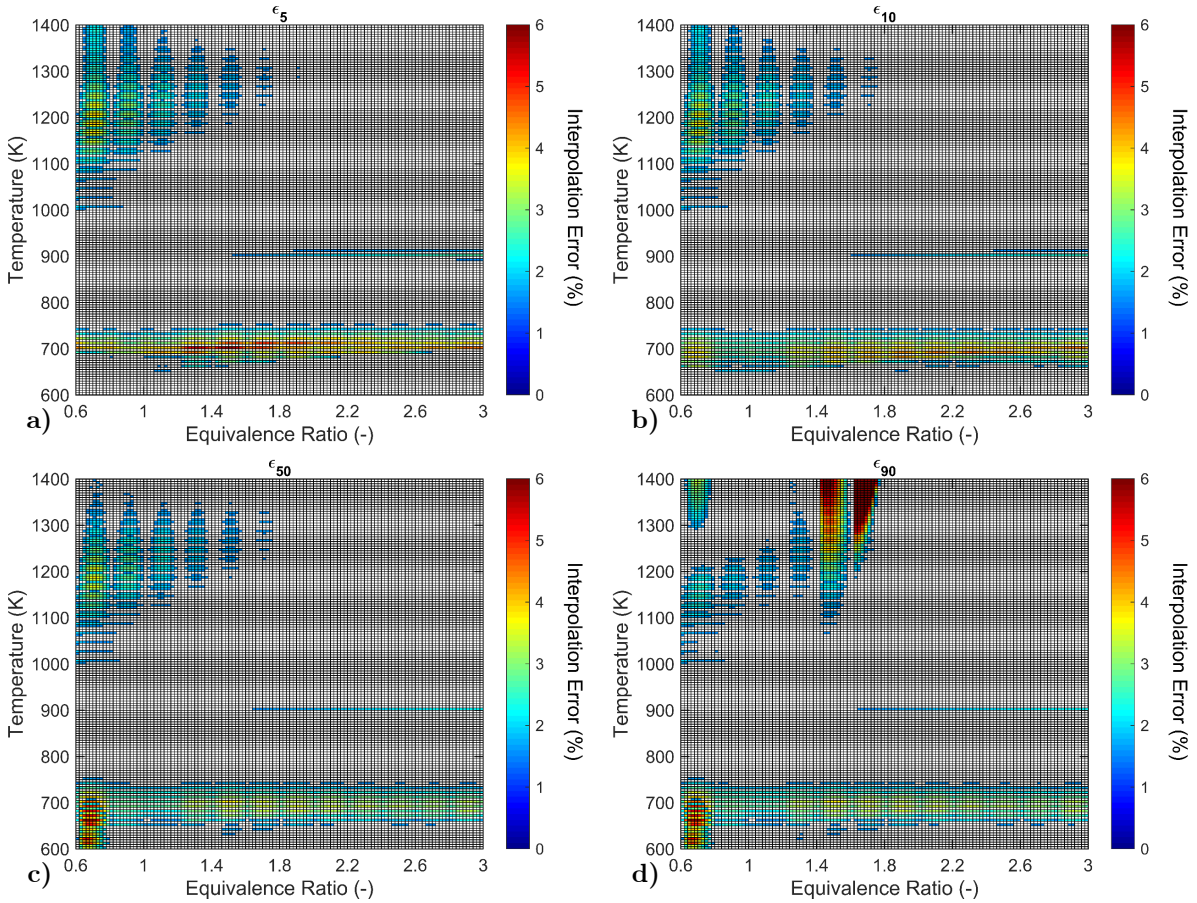


**Figure 3.3.** Interpolation error maps calculated as noted in equation(3.24) **a)** at 5%, **b)** at 10%, **c)** at 50% and **d)** at 90% of the energy released during a constant pressure reactor calculation at 1 bar initial pressure and 0% EGR using *n*-heptane as fuel.

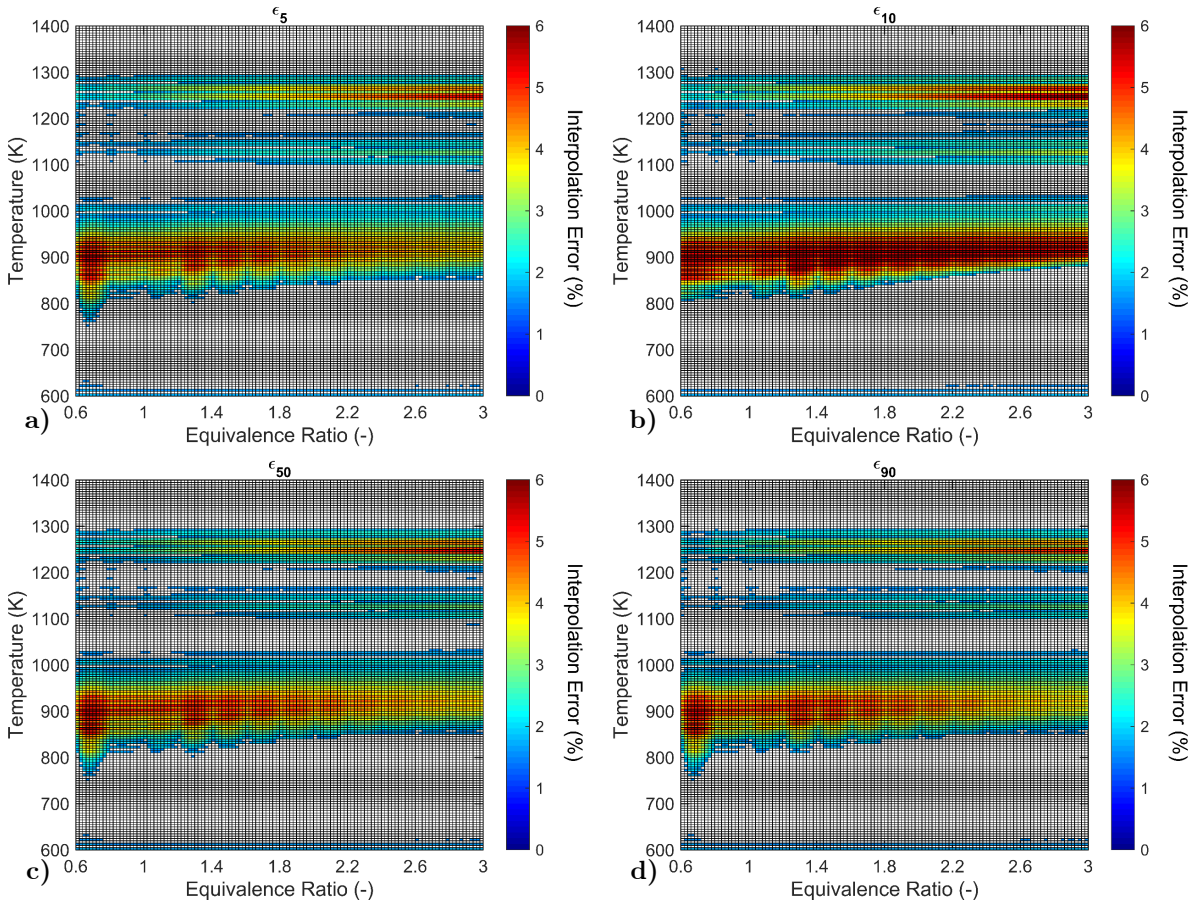


**Figure 3.4.** Interpolation error maps calculated as noted in equation (3.24) **a)** at 5%, **b)** at 10%, **c)** at 50% and **d)** at 90% of the energy released during a constant pressure reactor calculation at 35 bar initial pressure and 0% EGR using *n*-heptane as fuel.

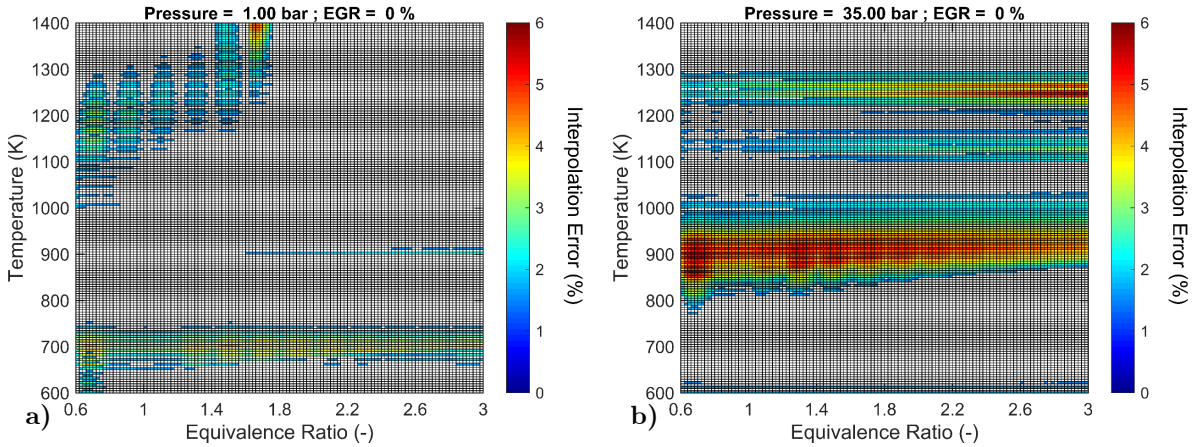


**Figure 3.5.** Averaged interpolation error maps calculated as noted in equation (3.25) **a)** at 1 bar and **b)** at 35 bar initial pressure assuming a constant pressure reactor calculation with 0% EGR using *n*-heptane as fuel.

The interpolation errors were assessed for a large set of operating conditions covering lean to rich ($\phi = 0.6 - 3.0$) conditions as well as from low to high unburned temperatures ($T = 600 - 1400\,K$) under constant pressure reactor conditions. *n*-Heptane was used as fuel molecule and the mechanism developed by Zeuch et al. [89] was employed. The main goal of this campaign was to quantify the accuracy of the interpolation routine under the simplest reactor conditions, so to have a higher confidence in results assessment during the subsequent engine simulation campaign. In the SRM and 3-D CFD simulation frameworks numerous sub-models are coming into play and hence error compensation-propagation effects may arise. For a more effective error visualization as well as to better highlight the exact areas where interpolation errors are noticeable, pixel contours were conditionally formatted so that every case having an error below 0.5% is displayed in white. All cases presenting an error above 0.5% will have contours consistent with the RGB color bar instead.

For the whole range of computed conditions, the solution retrieved from the table is never exceeding a 6% discrepancy on a single point basis, while the overall average error is approximately 1.5%. As expected, interpolation errors are more visible in the NTC regions, which is the most challenging area to parametrize when progress variable methods are concerned [63, 76].

While a tighter tabulation grid in temperature space could have delivered even lower errors, the present level of accuracy was considered acceptable. This decision was based on the one hand, on the globally low errors but also on method usability considerations. A tighter table grid results in a larger file size on disk, which in turn affects the random access memory (RAM) requirement for the engine simulations during run-time. Hence, the present configuration was considered to be an acceptable trade-off.

# Chapter 4

# Models for Internal Combustion Engine Simulations

In the present work various engine simulation campaigns have been performed under different modelling frameworks, ranging from 0-D to RANS 3-D CFD. This chapter aims to give a brief description of the different models, sub-models and algorithms adopted.

## 4.1. The Stochastic Reactor Model

The SRM considers the gas inside the cylinder as an ensemble of notional particles that can mix with each other and exchange heat with the cylinder walls. Each particle has a chemical composition, temperature, and mass; that is, each particle represents a point in phase-space for species mass fraction and temperature. A schematic visualization of the concept, along with an exemplary distribution of the property of the particles (i.e., enthalpy or gas composition) is shown in Figure 4.1.

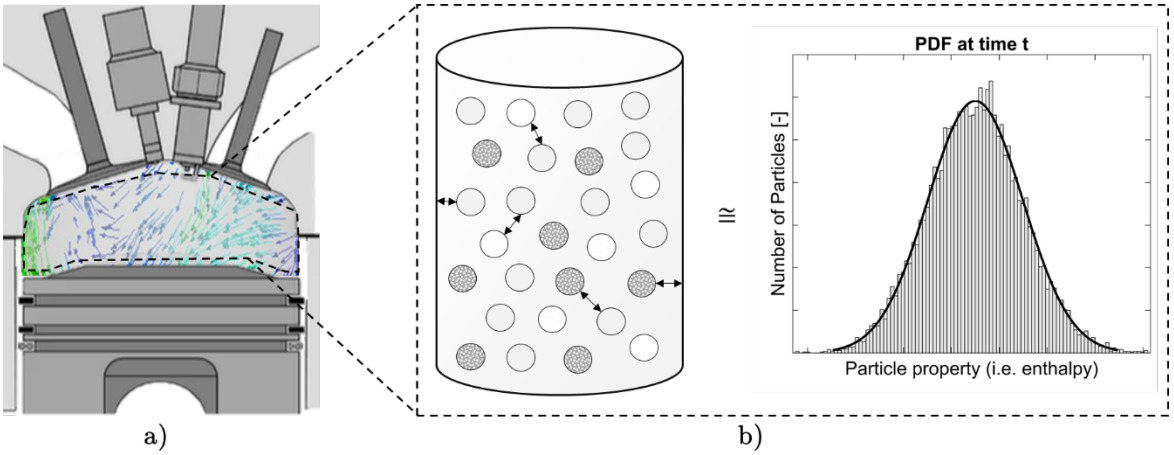


**Figure 4.1.** Schematic visualization of the SRM concept; **a)** engine physical space; **b)** 0-D particles in the SRM computational space and an exemplary distribution of particle properties at a given time-step $t$.

The temperature $T(t)$ and species concentrations $Y_i(t)$ are treated as random variables that can vary within the cylinder and determine the composition of the gas mixture using probability density functions. The in-cylinder mixture is thus represented by a PDF in phase space and the particles constitute the realization of this distribution. In practice all stochastic particles in the SRM represent a portion of the in-cylinder mass and rather than a PDF, a mass density function (MDF) is used; the MDF can be considered as a mass-based discretization of the PDF. The solution for the mass fractions and temperature is obtained from the transport equation for the MDF. These data are further used to calculate other engine quantities, such as pressure and heat release rate. The joint vector $\boldsymbol{\phi}(t)$ of the local scalar variables is defined as:

$$\boldsymbol{\phi}(t) = \left(Y_1, \ldots, Y_{N_s}, T; t\right) \equiv \left(\phi_1, \ldots \phi_{N_s}, \phi_{N_s+1}; t\right) \tag{4.1}$$

where $N_S$ is the number of chemical species in the reaction mechanism. This vector has a corresponding joint scalar MDF that is expressed as:

$$F_{\boldsymbol{\phi}} = F_{\boldsymbol{\phi}}\left(\psi_1, \ldots \ , \psi_{N_s}, \psi_{N_{S+1}}; t\right) \tag{4.2}$$

with $\psi$ being a realization of the random variables $\phi$. In addition, as proposed in the partially stirred plug flow reactor (PaSPFR) [104], it is assumed that probabilities of all scalar variables are independent of position, i.e., statistical homogeneity applies. This implies that the MDF does not vary spatially within the cylinder. Given the mentioned assumptions, the transport equation of the MDF can be written as:

$$\frac{\partial}{\partial t} F_{\boldsymbol{\phi}} + \frac{\partial}{\partial \psi_i}\left(Q_i(\psi) F_{\boldsymbol{\phi}}(\psi, t)\right) + \frac{\partial}{\partial \psi_{k+1}}\left(Q_{ht}\left(\psi_{k+1}\right) F_{\boldsymbol{\phi}}\right) \ = mixing\ term \tag{4.3}$$

Equation (4.3) describes the PaSPFR and serves as a base for the description of the stochastic reactor models for engine applications. The mixing term on the right-hand side is discussed in the next section. The term $Q_i$ on the left-hand side of equation (4.3) is, in general, a source/sink operator that depends on the phenomena under consideration such as the change of the MDF due to chemical reactions, volume changes due to piston motion, and fuel injection. The term $Q_{ht}$ refers to the convective heat loss to the cylinder walls. These terms are calculated based on the species and energy conservation equations that for DI engines can be expressed as (for details see, [105]):

$$Q_i = \frac{W_i}{\rho} \sum_{i=1}^{N_S} \omega_{i,j} + \frac{\dot{m}_f}{V}\left(Y_{i,f} - Y_i\right) \tag{4.4}$$

$$Q_{N_s+1} = \frac{1}{\rho c_p}\frac{dp}{dt} - \frac{1}{c_p}\sum_{i=1}^{N_S} h_i \frac{W_i}{\rho} - \sum_{j=1}^{N_R} \omega_{i,j} + \frac{1}{\rho c_p}\frac{\dot{m}_f}{V}\sum_{i=1}^{N_S} Y_{i,f}\left(h_{i,f} - h_i\right) \tag{4.5}$$

$$Q_{ht} = \frac{h_g A}{m c_p}(T - T_W) \tag{4.6}$$

In the equations above, $\omega_{i,j}$ and $Y_i$ denote the molar net rate of formation of species $i$ due to reaction $j$ and the mass fraction of species $i$ respectively. The subscript $f$ refers to the injected fuel. $W_i$ denotes molar mass of species $i$, $\rho$ is the density, $T$ is the mean temperature of the gas, $T_W$ is the cylinder wall temperature, $c_p$ is the specific heat capacity at constant pressure, $h_g$ is the heat transfer coefficient, $A$ is the heat transfer area, $h_i$ is the specific enthalpy of species $i$, $p$ is the pressure and $N_R$ and $N_S$ stand for the number of reactions and species, respectively. In equation (4.4) the terms on the right-hand side represent changes in composition space due to chemical reactions and fuel injection, respectively. Equation (4.5) contains terms describing temperature changes caused by work due to piston movement, chemical reactions, and fuel injection, respectively. Equation (4.6) shows the convective heat transfer term. The total wall heat transfer is calculated through Woschni's model (for details see, e.g., [106]). The distribution of the heat transfer over the particles follows a stochastic approach, explained by Bhave and Kraft [107]. Details of the fuel injection sub-model are explained in the work by Samuelsson et al. [108]. The right-hand side of equation (4.3) represents the time evolution of the MDF in composition and temperature space due to molecular mixing. For the SRM the right-hand side is modeled using a particle interaction model and a time dependent turbulent mixing time.

In addition to the local variables, global quantities are distinguished. These are the total mass $m$, volume $V$, and mean in-cylinder pressure $p$, which are assumed to not vary spatially in the combustion chamber. The volume change, in terms of crank angle degree, is calculated based on the known engine geometry. The pressure is calculated from the equation of state as

$$p(t) = \frac{\overline{\rho}(t)R\overline{T}(t)}{\overline{w}} \tag{4.7}$$

where the mean density $\overline{\rho}$ is calculated as $\overline{\rho}(t) = \frac{m}{V(t)}$ and $\overline{T}$ and $\overline{\mathrm{w}}$ are the mean temperature and mean molecular weight, respectively. Equation (4.3) is solved numerically using a Monte Carlo particle method (e.g., Pope [109]) with the operator splitting technique as previously presented by Maigaard et al. [110]:

$$\frac{\partial F_{\phi}}{\partial t} = \left(\frac{\partial F_{\phi}}{\partial t}\right)_{\Delta V} + \left(\frac{\partial F_{\phi}}{\partial t}\right)_{inj} + \left(\frac{\partial F_{\phi}}{\partial t}\right)_{FP} + \left(\frac{\partial F_{\phi}}{\partial t}\right)_{mix} + \left(\frac{\partial F_{\phi}}{\partial t}\right)_{chem} + \left(\frac{\partial F_{\phi}}{\partial t}\right)_{ht} \quad (4.8)$$

where the subscripts stand for: $\Delta V$ piston movement, $inj$ fuel injection, $FP$ flame propagation (considered for SI engine only), $mix$ the particle interaction process, $chem$ the chemical reactions and $ht$ heat transfer to the walls. The term $\frac{\partial F_{\phi}}{\partial t}$ is solved under the assumption of constant pressure, therefore a pressure correction at the end of time step is necessary and is calculated as in (4.9) with $x$ representing each of the operator split terms in equation (4.8)

$$p_{c,x} = \frac{\partial}{\partial \psi_{N_S+1}} \left( V \frac{1}{c_p} \left[\frac{dp}{dt}\right]_x F_{\phi} \right) \quad (4.9)$$

In the following sub-paragraphs, a more detailed description of the sub-models used in this work for fuel injection, flame propagation, turbulent mixing, particle interaction, chemical reactions and heat transfer are given.

### 4.1.1. Fuel Injection

Although more advanced approaches are implemented in the SRM code [111], in the present work, the liquid fuel is assumed to undergo vaporization at start of injection. Hence the injection profile given in the model is usually shifted by a few crack angles to account for the time needed by the fuel to vaporize. In other words, the inputted fuel mass injection curve is rather a vaporized mass injection curve. The energy needed for the vaporization is taken from the cylinder gas, as a consequence of mixing. The fuel is mixed with the corresponding amount of gas needed for supplying the vaporization energy. The amount of gas required for this purpose is referred in the text as mixing mass ($m_{mix}$). To account for the injection of mass in the system, new particles are added to the MDF and the total mass in the system is changed accordingly. In Figure 4.2 a schematic summary of the particle handling process is presented.

When fuel is added to the cylinder, the mass fractions and the temperatures of the current set of particles is changed depending on the composition of the fuel and its liquid injection temperature. Thus, for each particle the source terms need to be supplemented by the extra terms introduced in equations (4.4) and (4.5).

The mixing mass needed to vaporize the fuel is calculated assuming that injected fuel and bulk gas have the same pressure (see equation (4.10)).

$$m_{mix} = \frac{h_{f,liq}(T_f) - h_{f,gas}(T_v)}{h_m(T_v) - h_m(T_m)} m_f \quad (4.10)$$

The subscripts $f$ and $v$ denote fuel and vaporization, respectively. If the fuel is a mixture of several species, each species is dealt with separately, with respect to equation (4.10), as each molecule has a specific vaporization temperature. The final temperature of both the injected fuel and the mixing mass after completion of the process will be equal to the vaporization temperature ($T_v$) at the given pressure, which is known from the liquid properties of the injected fuel (also given as input to the SRM).

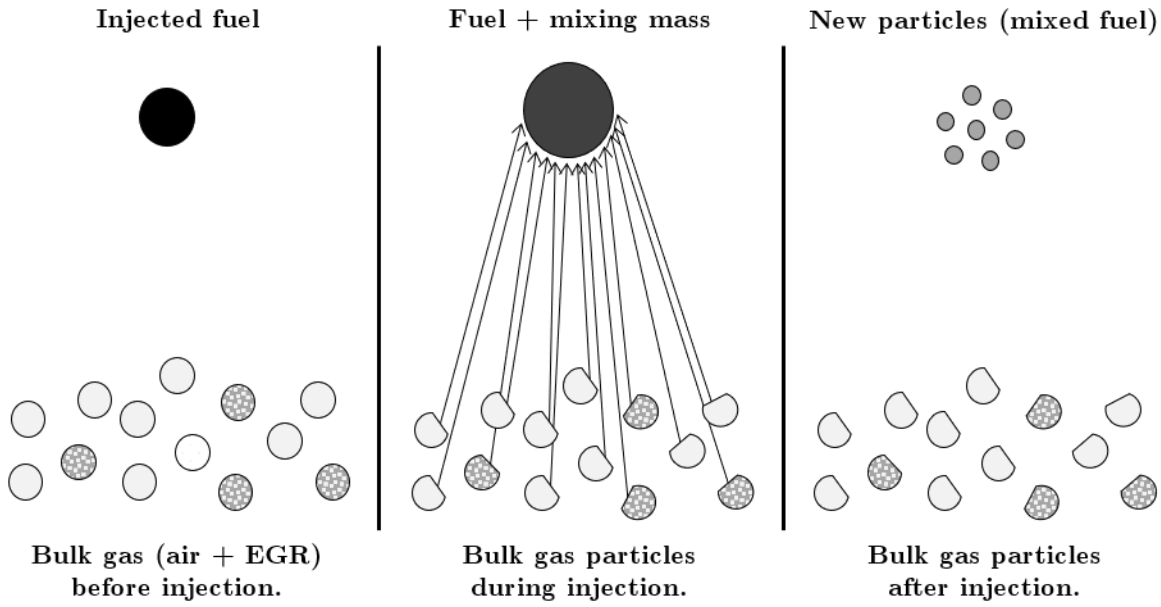


**Figure 4.2** Schematic representation of the particle handling strategy during injection.

### 4.1.2. Flame Propagation

For spark ignition engine simulations, a two-zone approach is used in the SRM framework. Particles in the unburnt and the burnt zone can mix with particles in their own zone, but not with particles in the other zone. There is no interaction between unburnt and burnt zone, except for mass transfer from the unburnt to burnt zone. This mass transfer is governed by the turbulent flame propagation, which can be modelled using either the model proposed by Peters [112] (equation (4.11)), or the more advanced correlation proposed by Kolla [113] (equation (4.12)) and implemented by Bjerkborn et al. [114] in the SRM code.

$$\frac{s_t}{s_l} = 1 + C\left(\frac{u'}{s_l}\right)^n \tag{4.11}$$

$$\frac{s_t}{s_l} = \left\{ \left[ b - a \left( 1 + \left( \frac{u'}{s_l} \right)^{1.5} \left( \frac{\delta}{l} \right)^{0.5} \right)^{-0.4} \right] \frac{(T_{ad} - T_u)}{T_{ad}} \frac{\delta}{l} \frac{u'}{s_l} + d \left[ \left( \frac{u'}{s_l} \right)^2 + \left( \frac{\delta}{l} \right)^{-0.25} \left( \frac{u'}{s_l} \right)^{-2.25} \right]^{-1} \right\}^{0.5} \tag{4.12}$$

Both approaches propose a correlation between the turbulent ($s_t$) and the laminar flame speed ($s_l$). The fluctuation of the turbulent velocity is noted as $u'$ in both correlations. The constant $C$ in (4.11) is a function of the turbulent length scale ($l$) and the laminar flame thickness ($\delta$); while the model constant ($n$) in (4.11) can be tuned in the range $[0.5 - 1.0]$. In (4.12) $T_u$ represents the unburned zone temperature and $T_{ad}$ is the adiabatic flame temperature; all the other values in (4.12) are assigned by the user and their reference values are reported in Table 4.1 (see also [114, 113]).

**Table 4.1.** Typical turbulent flame propagation model constants in equation (4.12)

| $\delta$ | $l$ | $a$ | $b$ | $d$ | $C_m$ | $\beta'$ | $C_\mu$ |
|---|---|---|---|---|---|---|---|
| 0.6 | 4.0 | 0.665 | 0.967 | 1.654 | 0.7 | 6.7 | 0.09 |

The laminar flame speed $s_l$ is pre-calculated and stored in a look-up table as a function of equivalence ratio ($\phi$), temperature, pressure and EGR and retrieved during run-time assuming averaged properties of the unburned zone. Starting at the spark instance, the flame front is tracked via a quasi-dimensional approach introduced in [114] and validated in several work for single and multiple spark plugs engine configurations [115, 116]. In Figure 4.3 an exemplary evolution of the spherical flame front calculated using the quasi-dimensional approach is presented based on the results obtained by Pasternak et al. in [115].

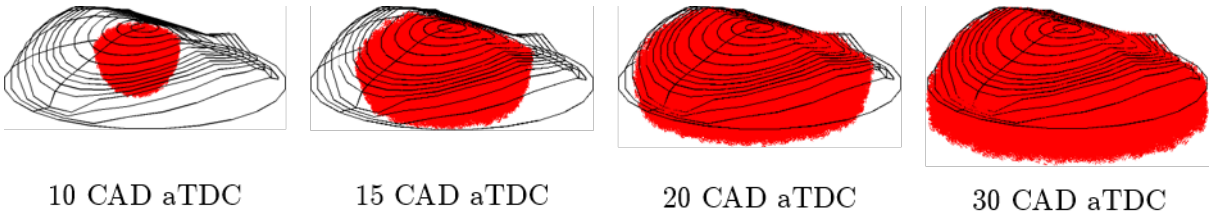


**Figure 4.3.** Exemplary visualization of flame front evolution in the SI-SRM. Figure reprinted based on the results presented in [115].

### 4.1.3. Turbulence Modeling

Turbulence is arguably one of the most important aspects to be addressed during model formulations for turbulent combustion simulations. Within the SRM framework

it is a crucial part from the model predictive capability stand-point. Based on the well-known energy cascade and dimensional analysis, the velocity fluctuation $u'$ is given by the ratio of the integral length scale l and the turbulent mixing time $\tau_{t,mix}$. Integral length scale and velocity fluctuations can be related to the turbulent kinetic energy $k$ and its dissipation $\epsilon$, thus resulting in [56]:

$$\tau_{t,mix} = \frac{l}{u'} \approx \frac{k}{\epsilon} \tag{4.13}$$

In the SRM the scalar mixing time $\tau_{mix}$ is the main model parameter and must be either imposed or calculated on the fly. Turbulent and scalar mixing time can be related using the mixing time constant $C_\tau$, that represents velocity scalar decay time [112]:

$$\tau_{mix} = \frac{\tau_{t,mix}}{C_\tau} \tag{4.14}$$

The mixing time governs the intensity of mixing between particles which in turn influences mixture inhomogeneities in the gas phase for scalars such as species mass fractions and temperature, which have a strong influence on the auto-ignition process, the local rates of heat release and pollutant formation. The shorter the mixing time, the higher the intensity of the mixing operations on particles and vice versa.

A simple approach to construct the mixing time history is by using a set of empirical constants as done by Pasternak et al. [117] for Diesel combustion studies. A more comprehensive approach is to calculate $\tau_{mix}$ during run-time by employing a phenomenological turbulence model. Depending on whether a Diesel or a gasoline engine simulation is concerned, different phenomenological models have been implemented in the SRM code. In Figure 4.4 exemplary profiles of the scalar mixing times (calculated with the two mentioned phenomenological models) are presented to underline how different $\tau_{mix}$ may evolve during the firing phase of CI and SI combustion regimes.

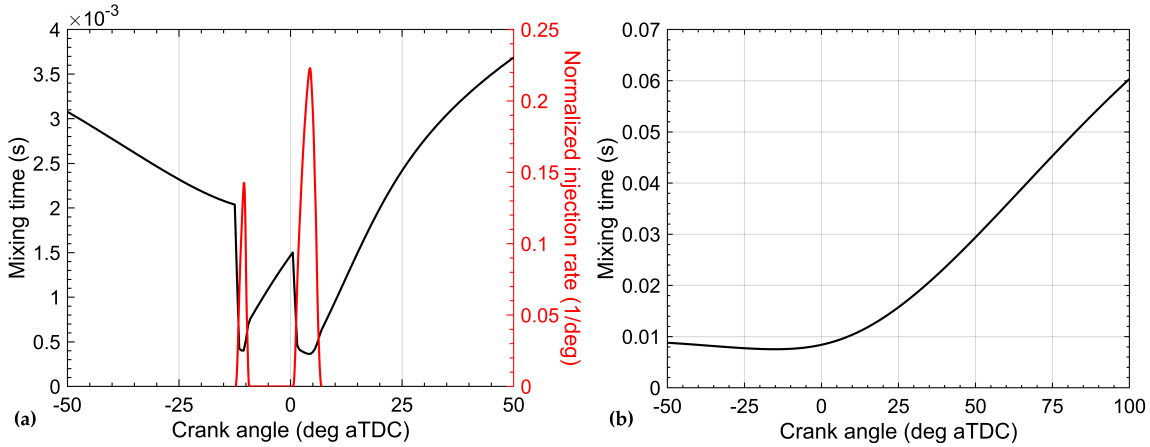


**Figure 4.4.** Exemplary mixing time histories computed using turbulence models for: **a)** Diesel engine condition [118]; **b)** port fuel injected SI engine condition [119].

In the following sub-paragraphs, an overview on the models' formulation is given for the parametrized mixing time model [120] as well as for the $k$-$\epsilon$ and the $K$-$k$ models that have been used in the present work. Equations and terms explanations have been mainly extracted from [120], [118] and [119].

#### 4.1.3.1. Empirical Turbulence Model

In this approach, the evolution scalar mixing time profile is governed by four empirical parameters (per single fuel injection shot) noted as $\tau_0$, $\tau_1$, $\tau_2$ and $\tau_3$. In Figure 4.5 an exemplary mixing time profile obtained with this method is shown. Each parameter is representative of a different engine in-cylinder process occurring during the firing phase of the engine cycle. The parameter $\tau_0$ controls mixing from the intake valve closure to start of injection, the parameter $\tau_1$ corresponds approximately to the fuel injection duration, $\tau_2$ is associated with the diffusive part of the combustion, and $\tau_3$ describes the late combustion phase until the exhaust valve opening. Each of these quantities is considered as a calibration parameter.

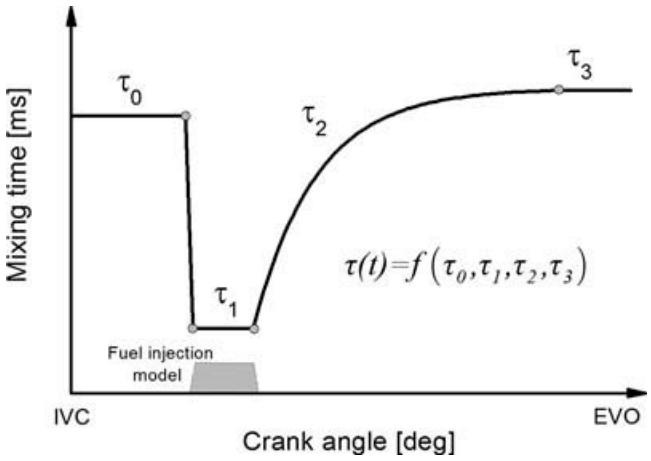


**Figure 4.5.** Schematic representation of a parametrized scalar mixing time for a single injection Diesel engine operating point. Figure reprinted from [117].

This approach has been validated in several studies and delivered good agreement with experimental data for large sets of Diesel engine cases and fuels [121, 12, 117, 48]. However, especially for multiple injection cases, the calibration process may require considerable efforts due to the implicit lack of physicality of the model parameters.

#### 4.1.3.2. Phenomenological Turbulence Model for Diesel Combustion

The evolution of the turbulent kinetic energy $k$ is calculated using the method proposed by Kozuch [118]. The model is based on a one-equation approach where $k$ is affected by the changes in density, kinetic energy dissipation, squish flow, fuel injection and swirl motion. The kinetic energy in the cylinder is assumed to be homogeneous and isotropic in space. The change of the turbulent kinetic energy over time $t$ is formulated

as in (4.15), where also the main model calibration parameters ($C_{den}$, $C_{diss}$, $C_{sq}$, $C_{inj}$ and $C_{sw}$) are included.

$$\frac{dk}{dt} = \left( \underbrace{-C_{den}\frac{2}{3}\frac{k}{V_{cyl}}\frac{dV_{cyl}}{dt}}_{Volume\ change} + \underbrace{\left[C_{sq}\, k_{sq}^{\frac{3}{2}}\right]_{\phi>TDC}}_{Squish\ flow} + \underbrace{C_{inj}\frac{dk_{inj}}{dt}}_{Injection} + \underbrace{C_{sw}\frac{c_m^3}{l}}_{Swirl\ motion} + \epsilon \right)\frac{1}{6n} \tag{4.15}$$

The influence of density on turbulent kinetic energy is described by the change in the cylinder volume $V_{cyl}$. If the cylinder volume decreases the length scales are reduced and the turbulent kinetic energy increases and vice versa. The kinetic energy dissipation $\epsilon$ and length scale (l) are presented in equations (4.16) and (4.17) respectively, followed by the definition of the scalar mixing time (including its scaling factor $C_\tau$) in (4.18).

$$\epsilon = \underbrace{C_{diss}\frac{k^{\frac{3}{2}}}{l}}_{Dissipation} \tag{4.16}$$

$$l = \left(\frac{6\, V_{cyl}}{\pi}\right)^{\frac{1}{3}} \tag{4.17}$$

$$\tau_{mix} = C_\tau \frac{k}{\epsilon} \tag{4.18}$$

For ω-shaped piston bowls a significant mass flow between the bowl and squish zone is observed close to top dead center. During the compression stroke the mass in the squish zone is pushed into the bowl zone. During the expansion stroke, the mass is flowing back into the squish zone because of the pressure difference. When the mass is flowing out of the bowl zone it detaches from the bowl rim and generates turbulent eddies. Measurements showed that the squish flow effect on turbulent kinetic energy is only dominant after TDC [118]. The squish term $k_{sq}$ depends on $w_{sq}$, which consists of an axial and radial velocity component calculated as in the equations below.

$$w_{sq} = \frac{1}{3}\left( w_r \left[1 + \frac{d_{bowl}}{d_{cyl}}\right] + w_a \left[\frac{d_{bowl}}{d_{cyl}}\right]^2 \right) \tag{4.19}$$

$$w_r = \frac{dV_{cyl}}{dt} \frac{V_{bowl}}{V_{cyl}\left(V_{cyl} - V_{bowl}\right)} d_{cyl}^2 - \frac{d_{cyl}^2}{4\, d_{bowl}} \tag{4.20}$$

$$w_a = \frac{dV_{cyl}}{dt} \frac{s_{bowl}}{V_{cyl}} \tag{4.21}$$

The axial $w_a$ and radial $w_r$ velocity components depend on the geometric measures of the combustion chamber, which are schematically reported in Figure 4.6. The quantity noted as $d_{cyl}$ is the cylinder bore, $V_{cyl}$ is the instantaneous cylinder volume, $d_{bowl}$ is the mean bowl diameter, $V_{bowl}$ is the bowl volume and $s_{bowl}$ is the maximum bowl depth. The contribution of swirl motion to turbulent kinetic energy is assumed to be proportional to the mean piston velocity $c_m$ and the length scale l. Modern Diesel engine injection systems utilize rail pressures between 300bar and 2000bar. Hence, the fuel jet entering the cylinder through the injector nozzles has a high kinetic energy, which affects the in-cylinder turbulent kinetic energy.

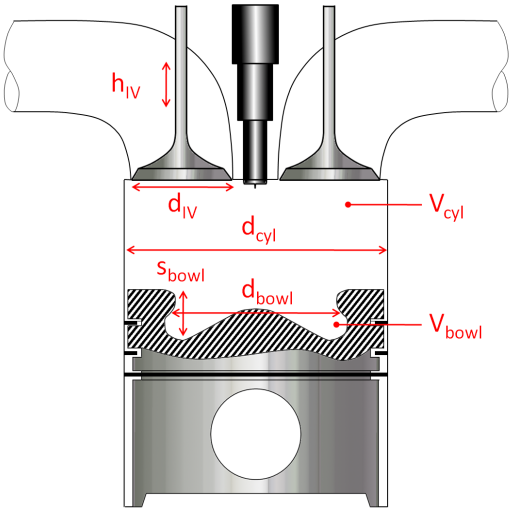


**Figure 4.6.** Engine geometrical quantities used as input for the $k$-$\epsilon$ turbulence model. Figure reprinted from [122].

The rate of change of turbulent kinetic energy due to direct injection $k_{inj}$ is reported below:

$$\frac{dk_{inj}}{dt} = \frac{1}{2} \dot{m}_{inj}\, u_{D_{r,0}}^2 \frac{1}{m_{cyl}} \tag{4.22}$$

$$u_{D_{r,0}}^2 = \frac{2\Delta p}{\rho_{fuel}} \tag{4.23}$$

In equation (4.22) $\dot{m}_{inj}$ corresponds to the fuel injection rate and $m_{cyl}$ is the total mass in the cylinder. The droplet velocity $u_{Dr,0}$ is calculated based on the Bernoulli equation in (4.23). The equation considers the pressure difference between rail pressure and cylinder gas pressure ($\Delta p$) and the liquid fuel density $\rho_{fuel}$. As initial condition, the turbulent kinetic energy at intake valve closure is approximated assuming the following formulation:

$$k_{IVC} = \frac{1}{8}\left(\frac{c_m\, d_{cyl}^2\, \eta_V}{d_{IV}\, h_{IV}}\right) \tag{4.24}$$

where $\eta_V$ is the volumetric efficiency, $d_{IV}$ is the intake valve diameter and $h_{IV}$ is the maximum intake valve lift.

#### 4.1.3.3. Phenomenological Turbulence Model for SI Combustion

For SI engine simulations in the SRM, the quasi-dimensional model proposed by Dulbecco et al. [119] has been implemented. The rate of change of kinetic energy $K$ and turbulent kinetic energy $k$ are reported in equations(4.25) and (4.26) respectively:

$$\frac{dK}{dt} = \underbrace{\frac{1}{2} C_{tke} \frac{\dot{m}_{in}}{m_{cyl}} v_{in}^2}_{Intake} + \underbrace{C_{inj} \frac{dK_{inj}}{dt}}_{Injection} + K\left[\underbrace{\frac{\dot{m}_{out}}{m_{cyl}}}_{Exhuast} + \underbrace{C_{comp}\frac{\dot{\rho}}{\rho}}_{Compressibility} \underbrace{-\left(\frac{\dot{\rho}}{\rho}+\frac{\dot{V}}{V}\right)}_{Explicit\ closure}\right] - P_K \tag{4.25}$$

$$\frac{dk}{dt} = \frac{1}{2}(1 - C_{tke})\,\frac{\dot{m}_{in}}{m_{cyl}} v_{in}^2 + C_{inj}\frac{dk_{inj}}{dt} + k\left[\frac{\dot{m}_{out}}{m_{cyl}} + C_{comp}\,\frac{\dot{\rho}}{\rho} - \left(\frac{\dot{\rho}}{\rho}+\frac{\dot{V}}{V}\right)\right] \tag{4.26}$$
$$-P_k - C_{diss}\,\epsilon$$

The quantity noted as $\dot{m}_{in}$ is the intake valve mass flow, $m_{cyl}$ is the trapped mass in the cylinder, $v_{in}$ is the intake valve flow velocity, $K_{inj}$ is the kinetic energy from the direct injection, $\dot{m}_{out}$ is the exhaust valve mass flow, $\dot{\rho}$ and $\dot{V}$ are the density and cylinder volume change respectively with $\rho$ and $V$ being density and instantaneous cylinder volume. The dissipation $\epsilon$ is derived via the integral length scale $l$, which is based on the instantaneous cylinder volume, as noted in equations (4.27) and (4.28).

The term $P_k$ is the production term for turbulent kinetic energy from tumble motion decay and its formulation is reported in equation (4.29).

$$\epsilon = \underbrace{\frac{\left(\frac{2}{3}k\right)^{\frac{3}{2}}}{l}}_{Dissipation} \tag{4.27}$$

$$l = C_{len}\, V^{\frac{1}{3}} \tag{4.28}$$

$$P_k = 0.3307\, C_\beta\, l\, k^{\frac{1}{2}}\, \frac{K}{\Delta} \tag{4.29}$$

$$\Delta = min\left(C_{\Delta,1} V^{1/3}, C_{\Delta,2}\, min\left(h_{cyl}, d_{bore}\right)\right) \tag{4.30}$$

$$\tau_{mix} = C_\tau \frac{k}{\epsilon} \tag{4.31}$$

The parameters $C_{inj}$, $C_{comp}$, $C_{tke}$, $C_{diss}$, $C_{len}$, $C_\beta$, $C_{\Delta,1}$, $C_{\Delta,2}$ and $C_\tau$ are the main model constants that need to be trained during model calibration for the given engine. As done in the compression ignition turbulence, the scalar mixing time $\tau_{mix}$ is eventually calculated as the quotient of $k$ and $\epsilon$ for each computed crank angle degree.

### 4.1.4. Particle Interaction Modeling

The modeling of the particle interaction in the SRM governs how the gas-phase particle composition vectors evolve and is needed to mimic the composition change of real fluid parcels due to mixing caused by the turbulence. In the SRM the particle interaction sub-model strongly affects the complex chemistry of emission formation and describes the local character of turbulent flow and chemistry interaction. The particle mixing term in the SRM model formulation is given below (see also equation (4.3)):

$$mixing\ term = \frac{C_\phi \beta}{\tau_{mix}} \left( \int_{\Delta\phi} F_{\boldsymbol{\phi}}(\psi - \Delta\psi, t) F_{\boldsymbol{\phi}}(\psi + \Delta\psi) d(\Delta\phi) - F_{\boldsymbol{\phi}} \right) \tag{4.32}$$

In this work two different approaches have been used: the Coalescence/Dispersal model (also known as the Curl model [123]) and a modified version of the Euclidean Minimum Spanning Tree (EMST - proposed by Subramaniam et al. [124]).

The basic idea of the Curl model is that two randomly chosen particles from a set of p particles, where $p < N_p$ and $N_p$ is the total number of particles, are mixed to their mean. Figure 4.7 schematically illustrates the Curl model where the randomly chosen particle $m$ with its properties $\phi(m)$ at time $t$ is mixed with the randomly chosen particle $n$. At the time setup $t + \Delta t$, their properties are equal and the mean of their sum at t; in the next mixing step, the particles are mixed with another particle if again chosen to be in the set $n$.

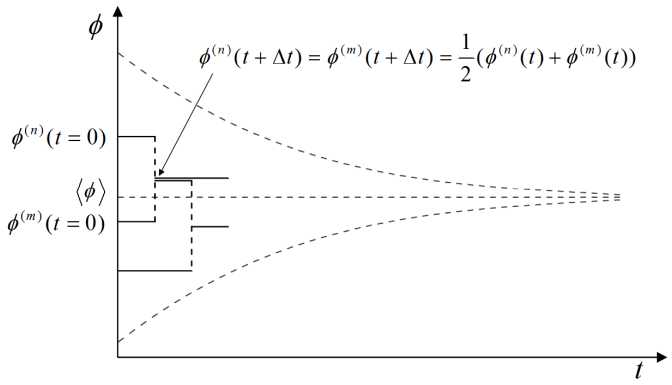


**Figure 4.7.** Mixing step in the Curl model. Figure rearranged from [111].

The mean values of a property of the computational domain and the number of particles are not changed during the mixing. Unlike pairwise exchange models such as Curl, in the EMST model particles' interaction is governed by their position in composition space. At each time step a Euclidean spanning tree is constructed through connecting unordered pairs of SRM particles (called edges) based on actual composition and enthalpy space. Thereafter, particle interaction is only allowed between neighbor particles in composition space. Furthermore, the interaction rate between two particles at either end of the edge depends on the morphology of the constructed spanning tree in the given scalar dimension. In other words, this method allows for a more realistic particle interaction representation since locality in composition and enthalpy space is considered. For an MDF particle, the evolution equation for the particle composition vector $\boldsymbol{\phi}_i = \phi_{\beta_i}$, where $\beta = 1, \ldots, N_{Scalars}$ and $i = 1, \ldots, N_P$, can be written as:

$$\frac{w_i d\boldsymbol{\phi}_i}{dt} = -\alpha \sum_{v=1}^{N_P - 1} B_v \left\{ \left(\boldsymbol{\phi}_i - \boldsymbol{\phi}_{n_v}\right) \delta_{im_v} + \left(\boldsymbol{\phi}_i - \boldsymbol{\phi}_{m_v}\right) \delta_{in_v} \right\} \tag{4.33}$$

where $w_i$ is the particle weight, the $v^{th}$ edge connects the particle pair $(m_v, n_v)$, $\delta$ represents the Kronecker delta and $B_v$ is an edge coefficient that depends linearly on the edge weight. The parameter $\alpha$ is determined at each time step under the constraint that scalar variances decay at a prescribed rate. More details on the derivation of $\alpha$

can be found in [124]. In the present thesis, a special constraint for the construction of the EMST has been assumed: scaling factors have been specified for each scalar included in the particle composition vector in order to differentiate which dimension is dominant during EMST construction. Independently on the chemistry solver, scaling factors have been assumed such that among all scalars involved in the particle composition vector $(Y_1, \ldots, Y_{N_{species}}, Z, h, etc.)$ mixture fraction $(Z)$ has the biggest impact on the construction of the spanning tree. From the modeling perspective this assumption implies that during fuel injection and onwards the mixing between rich and lean particles always occurs at a higher rate. Furthermore, mixture fraction was used to avoid artifacts occurring during tree construction if all dimensions (mostly composed of species) had the same weight. From the physical point of view, this approach mimics better the typical air entrainment phenomenon occurring in Diesel sprays much better than other models (i.e., [123]).

To better illustrate the importance and impact of the choice of the particle interaction model, in Figure 4.8 a comparison of two SRM Diesel engine simulations using Curl and EMST are shown in terms of in-cylinder pressure and rate of heat release. The experimental data, and model setup, are taken from a low-load, low-speed operating point with double injection ($SOI_{pilot} = -14.0$ CAD aTDC and $SOI_{main} =$ 4.0 CAD aTDC). Correct prediction of the pilot injection heat release is particularly challenging in this part of the engine map. Due to the very low amounts of injected fuel, depending on the particle interaction model, the mixture may easily become too lean, or stay too rich, in the computational domain and result in poor agreement with experimental values.

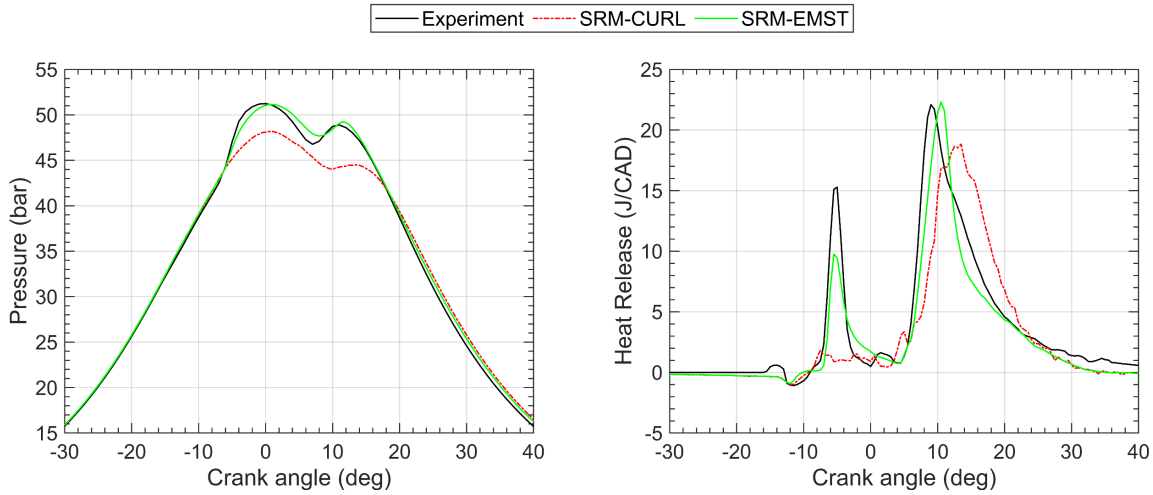


**Figure 4.8.** In-cylinder pressure (left) and apparent rate of heat release (right) for a low-load low-speed double injection Diesel engine operating point.

In Figure 4.9, scatter plots in temperature and equivalence ratio space are shown together with contours of the fuel mass fraction in each SRM particle. Three instances have been depicted based on the combustion predictions shown in Figure 4.8. The first instance (Figure 4.9 a)) displays the difference in the mixture formation process

occurring 4 crank angles after the pilot start of injection. Thanks to the composition driven particle mixing, the EMST computes a more realistic distribution of equivalence ratios in the combustion chamber.

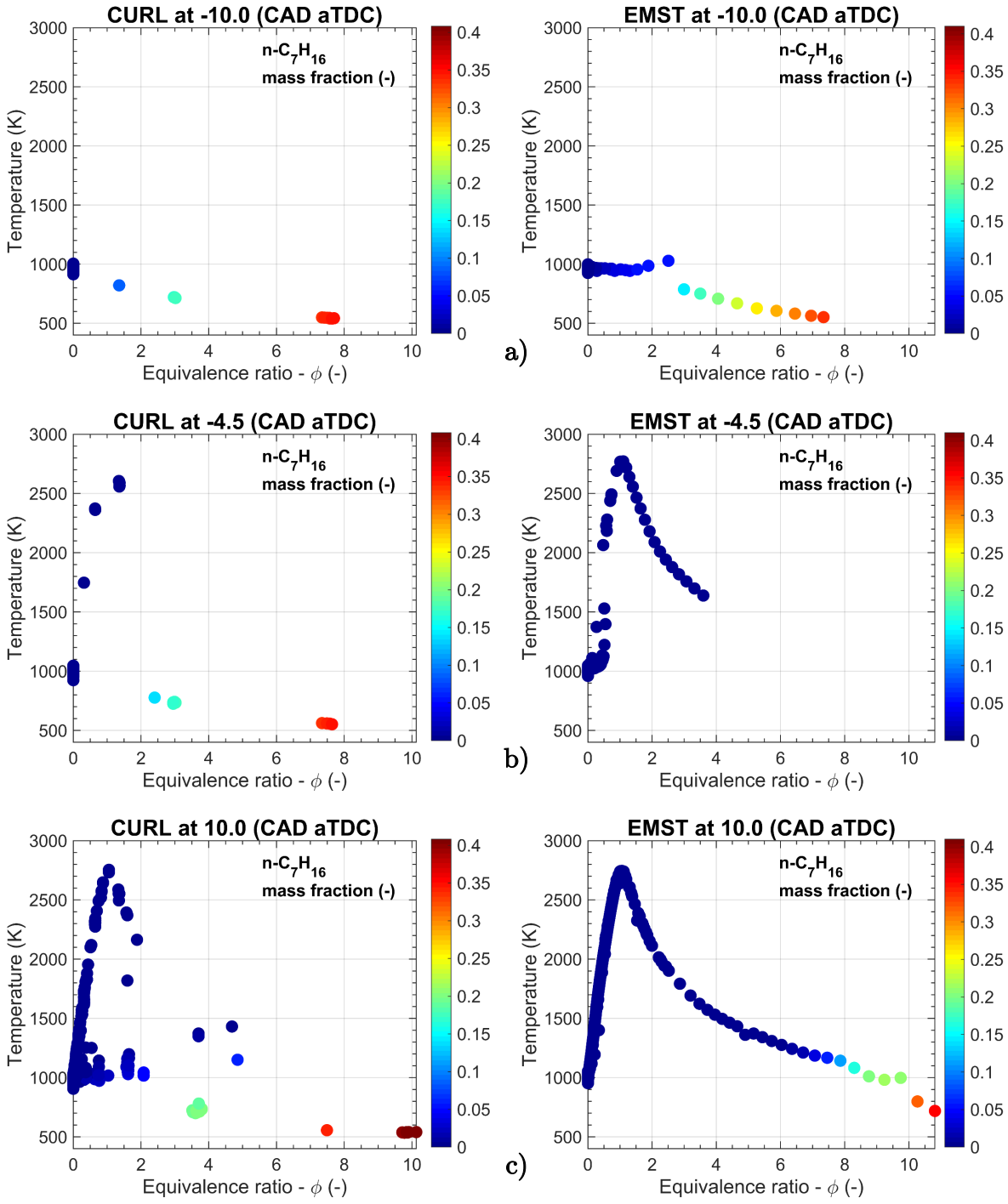


**Figure 4.9.** Scatter plots in mixture fraction vs. temperature space with fuel mass fraction contours at **a)** pilot injection mixture formation instance; **b)** pilot injection heat release peak instance; **c)** main injection mixture formation instance.

This aspect is also facilitating a faster auto-ignition than in the Curl simulation, thanks to the higher number of particles in the nearness of stoichiometry. In Figure 4.9 b) it can be seen that the in the EMST-based simulation most of the fuel has fully mixed and undergone combustion, while in the Curl-based simulation a noticeable number of rich particles have not yet mixed with the bulk gas. Similarly to the pilot injection, better mixture preparation can be seen also during the main injection event in the EMST-based simulation compared to the Curl results.

In conclusion, during the various simulation campaigns performed in this work, the Curl mixing model delivered a generally acceptable agreement, and it can be confidently used for single injection cases. The EMST proved to give remarkably better combustion predictions than Curl for multiple-injection cases featuring very small amounts of pilots. However, the EMST was also found to deliver worse engine-out emission predictions than Curl due to the generally faster combustion rate (independently of the mixing time tuning). For this reason, in the SRM code it was implemented a hybrid mixing mode where the EMST mixing model is used during pilot injection instances, while for the main injection and onwards the Curl model is used instead. This proved to be the optimal solution especially for engine cases having complex multi-injection strategies.

### 4.1.5. Chemical Reactions

Depending on whether the online or the chemistry solver is used in the simulation, different operations are performed in this step of the operator split. In Figure 4.10 a summary of the transported quantities in each SRM particle is shown.

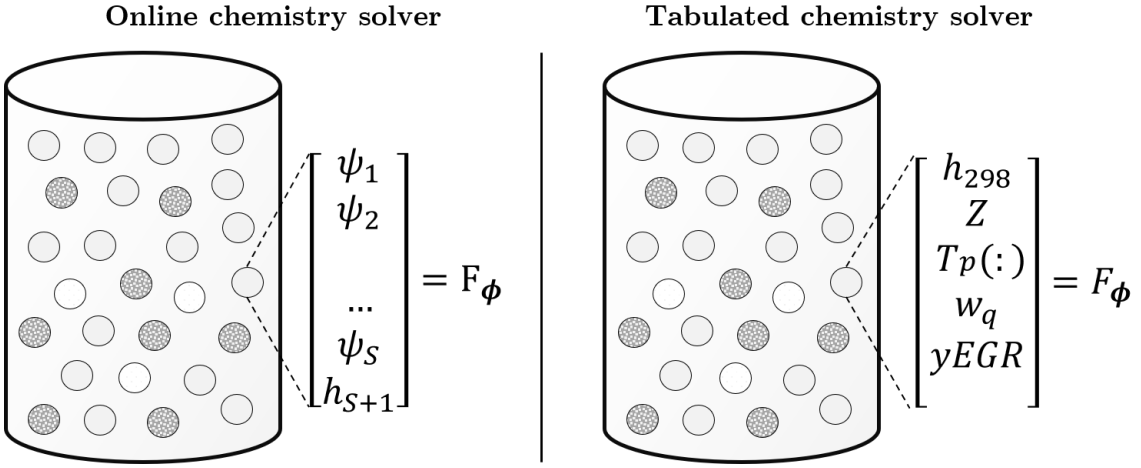


**Figure 4.10.** Schematic representation of the transported quantities in each SRM particle when using (left) the online chemistry solver and (right) the tabulated chemistry solver.

When using the online chemistry solver, a set of PDEs must be solved to calculate the species source terms $\omega(\phi)$ in each particle as per equation (4.34).

$$\left(\frac{\partial F_\phi}{\partial t}\right)_{chem} = \frac{\partial}{\partial \psi_{S+1}}\left(\frac{1}{c_p}\sum_{s=1}^{N_S} h_s \frac{w_s}{\rho}\omega(\phi)F_\phi\right) - \sum_{s=1}^{N_S}\frac{\partial}{\partial \psi_s}\left(\frac{w_s}{\rho}\omega(\phi)F_\phi\right) \tag{4.34}$$

This step needs sub-cycling since the governing equations are highly nonlinear and may present stiffness depending on the reaction mechanism adopted. A standard backward differential function (BDF) method combined with a Newton algorithm is used to solve this system of equations. The result is the new chemical composition for the particle at the new timestep.

When using the tabulated chemistry solver, the chemistry solution is already available. Hence, in CPV-SRM coupled runs a table look-up is performed at each time-step and for each particle, based on the local values of mixture fraction ($Z$), mass fraction EGR ($yEGR$), unburned temperature, pressure and reaction progress variable $C$ (calculated based on the transported $h_{298}$, see equation (3.11)). Based on the retrieved mixture averaged thermodynamic polynomials ($T_p$) and mean molecular weight of the mixture ($w_q$) as well as the source terms for progress variable and emissions (NO and Soot) the new properties of the particles are updated (i.e., Temperature) as well as any of the user-defined transported species profile.

### 4.1.6. Heat Transfer

In the SRM framework each particle may have a different temperature and hence, transfer different amounts of heat to the walls. This, on top of the stochastic nature of the mixing process, makes the SRM capable of accounting for in-homogeneity effects leading to cycle-to-cycle variations. A stochastic approach, introduced in [125] and validated in [126] against DNS data, is employed to decide the heat transfer distribution over the particles. A stochastic heat transfer constant $C_{ht}$ is also defined to tune the heat transfer distribution. A lower value leads to a larger amount of heat transfer for each particle and fewer particles participating in the exchange with the walls. Consequently, a larger value of $C_{ht}$ leads to less heat transfer for each particle and consequently to a larger number of particles participating to fulfil the total amount of heat transfer at each time step. With the stochastic heat transfer constant going towards infinity, a deterministic heat transfer calculation would be reproduced.

In the present work, the Woschni correlation has been used to calculate the total heat transfer for all the SRM simulation campaigns. The recommended parameters, as presented in [127], have been used together with $C_{ht} = 15$. The heat transfer coefficient $h_g$, as already noted in equation (4.6), is calculated as follows [127]:

$$h_g = 3.26\, d^{-0.2}\, p^{0.8}\, T^{-0.53}\left[C_1\, c_m + C_2 \frac{V T_0}{p_0 V_0}(p - p_{mot})\right] \tag{4.35}$$

$C_1$ and $C_2$ are model constants, $d$ is the cylinder bore, $p$, $V$ and $T$ are the in-cylinder pressure, volume and temperature respectively, $c_m$ is the mean piston speed

and $p_{mot}$ is the motored cylinder pressure. The subscript 0 refers to properties being taken at the reference condition.

Once the total heat transfer $Q_{ht}$ (equation (4.6)) is calculated in the timestep $\Delta t$, a time jump parameter $t_{jp}$ (4.36) is computed proportionally to the stochastic heat transfer constant and the number of particles $N_P$, followed by the calculation of a sub-time step $t_{sub}$ (4.37).

$$t_{jp} \propto \frac{C_{ht} N_P}{Q_{ht}} \tag{4.36}$$

$$t_{sub} = t_{start} - \frac{1}{t_{jp}} \, log\left(RN_{P,0}\right) \tag{4.37}$$

$$h_n = T_n - \frac{T_{wall}}{C_{ht}} \quad ; \quad T_n = T_{wall} - h_n \tag{4.38}$$

At this point a random particle n is selected, and the heat transfer through the fluctuation in heat between the particle and the wall $h_n$ is calculated. The particle properties are then updated based on the updated temperature $T_n$ as per equation (4.38). This sub-stepping process is then re-iterated until the full timestep $\Delta t$ is computed.

## 4.2. Combustion Modeling in 3-D CFD RANS

The in-cylinder combustion process is certainly among the most challenging problems for 3-D CFD modelers. A reactive ICE simulation involves in fact a remarkable amount of interdependent sub-models, which are needed to account for the diverse fluid-dynamic, multi-phase flow and chemical phenomena involved, such as liquid fuel injection, spray evaporation, turbulence chemistry interaction, gas and solid phase pollutant formation mechanisms. In the present work, specifically in Chapter 6, several sub-models have been used in line with the engineering best practices for ICE simulations in RANS-CFD. To keep relevance with the main topic of the present thesis, this paragraph will only address the modelling aspects related to the combustion chemistry solvers used and implemented in the present work. Comprehensive descriptions of the governing equations as well as of the other sub-models for spray break-up, evaporation, turbulence and heat transfer used in Chapter 6 can be found in [21, 56, 128]. Details on the numerical aspects, such as meshing/time-stepping algorithms and their implementation in the CFD code, can be found in [20].

The combustion modelling community has proposed a wide number of approaches to model turbulent combustion in flames and engines. One of the main challenges to be addressed when modelling turbulent reactive flows lies in the closure of the chemistry source term. This is due to the fact that turbulence causes fluctuations of reactive

scalars and state variables. The simplest approach to tackle this problem consists in using a laminar source term closure for the chemical source term or, in other words, neglect fluctuations due to turbulence and rely on the cell mean quantities. This approach is often addressed in literature as well-stirred reactor (WSR) model and is among the most widely used methods by OEMs for ICE combustion analyses.

More complex approaches, where turbulence chemistry interaction (TCI) effects are considered, have been developed for RANS and LES frameworks and can be categorized in 1) models based on presumed probability density functions (i.e., flamelet-based methods), and 2) models based on transported PDFs. In depth discussions on the mentioned categories of models as well as on the challenges of turbulent combustion modeling with TCI can be found in [129, 53, 130].

As discussed in Chapter 3 the developed progress variable model relies on the tabulation of adiabatic constant pressure reactors where no TCI effects are taken into account. This implies that, to consistently assess CPV model accuracy in CFD, a WSR-based approach featuring on-the-fly chemistry calculation is the appropriate choice.

### 4.2.1. The Well Stirred Reactor Model

The main assumption behind the WSR model is that the mixture inside the computational reactor (i.e., a full CFD cell) is "well stirred" which is to say homogeneously mixed. This means that, on a cell level, the three-dimensional system is reduced to a zero-dimensional problem where no transport of momentum is needed within the cell. However, the transport of species between cells must be considered. Assuming Favre averaging, and the usual RANS assumption for the diffusion term, the transport equation for species s can be written as [21]:

$$\frac{\partial\left(\overline{\rho}\widetilde{Y}_s\right)}{\partial t}+\frac{\partial}{\partial x_i}\left(\overline{\rho}\widetilde{u}_i\widetilde{Y}_s\right)-\frac{\partial}{\partial x_i}\left(\overline{\rho}\frac{\mu_t}{Sc_{s,t}}\frac{\partial\widetilde{Y}_s}{\partial x_i}\right)=\overline{\dot{\omega}_s}+\overline{\dot{\omega}_{spray}}\,\delta_{s,f} \tag{4.39}$$

In equation (4.39) $Sc_{s,t}$ is the turbulent Schmidt number for species $s$; $\mu_t$ is the turbulent viscosity, $\widetilde{u}_i$ and $\widetilde{Y}_s$ are the mean components of the velocity over direction $i$ and the mass fraction of species $s$, respectively. On the right had side, the formation or consumption rate due to chemical reactions for the given species $s$ is notes as $\dot{\omega}_s$, while $\overline{\dot{\omega}_{spray}}$ is the spray source term in case the fuel species $f$ is injected in the system and $\delta_{s,f}$ is the Kronecker delta.

The chemical source term for the species can be calculated through a given reaction scheme which contains a certain number of species ($N_S$) and reactions ($N_R$). As described in [21], a multi-step chemical reaction mechanism can be formulated in the following fashion:

$$\sum_{s=1}^{N_S} \upsilon'_{s,r}\, X_s \leftrightharpoons \sum_{s=1}^{N_S} \upsilon''_{s,r}\, X_s \qquad for \qquad r = 1, 2, \ldots, N_R \tag{4.40}$$

where $\upsilon'_{s,r}$ and $\upsilon''_{s,r}$ are the stoichiometric coefficients for the reactants and products respectively, for species $s$ due to reaction $r$. For better readability, the following will be assumed:

$$\upsilon_{s,r} = \upsilon''_{s,r} - \upsilon'_{s,r} \tag{4.41}$$

From the reaction mechanism, the formation rate $\dot{\omega}_s$ of species $s$ is obtained by [21]:

$$\dot{\omega}_s = \sum_{s=1}^{N_S} \upsilon_{s,r} \left[ k_{f,r} \prod_{s=1}^{N_S} \left[X_s\right]^{\upsilon'_{s,r}} - k_{b,r} \prod_{s=1}^{N_S} \left[X_s\right]^{\upsilon''_{s,r}} \right] \tag{4.42}$$

$\left[X_s\right]$ is the molar concentration of species $s$, $k_{f,r}$ and $k_{b,r}$ are the forward and backward rate coefficients for reaction r, respectively. The forward rate coefficient can be determined by the Arrhenius law as:

$$k_{f,r}(T) = A_r T^{n_r} exp\left(-\frac{E_{a,r}}{RT}\right) \tag{4.43}$$

The activation energy $E_{a,r}$, the pre-exponential factor $A_r$ and temperature exponent $n_r$ are included in the reaction scheme for each reaction $r$. $R$ and $T$ are the universal gas constant and temperature, respectively. The backward rate coefficient is calculated via the equilibrium coefficient $K_{eq}$, which is determined from the thermodynamic properties [21]:

$$k_{b,r} = \frac{k_{f,r}}{K_b} \tag{4.44}$$

$$K_b = K_{eq} \left(\frac{p_{atm}}{RT}\right)^{\sum_{s=1}^{N_S} \upsilon_{s,r}} \tag{4.45}$$

$$K_{eq} = exp\left(\frac{\Delta S_r^0}{R} - \frac{\Delta H_r^0}{RT}\right) \tag{4.46}$$

In equation (4.45) $p_{atm}$ is the atmospheric pressure; in equation (4.46) $\Delta$ refers to the change that occurs when passing completely from reactants to products in the $r^{th}$ reaction; $S$ and $H$ denote entropy and enthalpy, respectively.

$$\frac{\Delta S_r^0}{R} = \sum_{s=1}^{N_S} \upsilon_{s,r} \frac{S_s^0}{R} \tag{4.47}$$

$$\frac{\Delta H_r^0}{RT} = \sum_{s=1}^{N_S} \upsilon_{s,r} \frac{H_s^0}{R} \tag{4.48}$$

The calculated species reaction rate $\dot{\omega}_s$ is then used to calculate the formation or consumption of species $s$ in a cell as follows:

$$\frac{dY_s}{dt} = \dot{\omega}_s \frac{w_s}{\rho} \tag{4.49}$$

The change in temperature according to the reactions is then calculated via the energy equation assuming constant-pressure as:

$$\frac{dT}{dt} = \frac{\left(\frac{\dot{Q}}{V}\right) - \sum_s \left(\overline{h_s}\, \dot{\omega}_s\right)}{\sum_m \left(Y_s \overline{c_{p,s}}\right)} \tag{4.50}$$

$\dot{Q}$ is the heat release rate, $V$ is the volume while $\overline{h_s}$ and $\overline{c_{p,s}}$ are the specific enthalpy and heat capacity at constant pressure for species s, respectively. The equations above must be solved at each computational time-step so that the species concentration can be updated appropriately. Because the species reaction rates $\dot{\omega}_s$ can be vastly different, the timescales of change of different species concentrations can vary significantly. Therefore, the system of equations can be stiff and usually require specialized numerical integration routines for their solution.

In CONVERGE, the SAGE kinetic solver [131] is employed to solve the system of ordinary differential equations (ODEs) using either a CVODE-based solver [132] or a sparse linear equation solver based on [133]. The temperature obtained via equation (4.50) is used to update only the rate coefficients solved by the SAGE solver and is not used to update the cell temperature [20]. The cell temperature is updated after the detailed chemistry calculation has converged using the computed species concentrations. Especially for large chemical mechanisms, long computational times due to the solution of the chemistry in each cell can be reduced by grouping together similar computational cells and then invoking the chemistry solver once per group rather than once per cell. One of these methods is the adaptive zoning algorithm [134] and is fully integrated into CONVERGE. Additionally, a cut-off temperature $T_{cut}$ (600

K in this thesis) and a cut-off mole fraction $HC_{min}$ (defined as sum of CO, $H_2$ and hydrocarbons species) are defined. If temperature and/or mole fraction of the given cell (or zone) fall below the defined cut-off values, the kinetic solver will not be called [20].

In the present work, the tabulated chemistry solver has been compared to CONVERGE runs using the SAGE solver with adaptive zoning. Default model parameters for the zoning algorithm and kinetics solver have been used. For more details, please refer to [20].

### 4.2.2. CPV Model Implementation in CFD

Compared to a CONVERGE run using the built-in WSR chemistry solver, in CPV coupled runs the combustion model is replaced entirely and the chemistry solution is fully handled via user coding. The transport of species and passive scalars needed for the chemistry look-up is handled by the 3-D CFD code instead.

The case specific fuel species as well as a set of standard species ($O_2$, $N_2$, $CO_2$, $H_2O$, CO, $H_2$, $C_2H_2$, $C_2H_4$, H, O, OH, N, NO) are defined as the only active scalars in the computational domain independently on the mechanism used during tabulation. These species are necessary to calculate the thermodynamic properties of the in-cylinder content and, in turn, engineering quantities such as the rate of heat release. The transport equation for these species is formulated as in (4.39) and the source terms are passed to CONVERGE based on the retrieved values from the CPV table.

To correctly evaluate the look-up parameters for the auto-ignition and emissions source terms table, the following passive scalars are also defined and transported in the computational domain: mixture fraction ($Z$), latent enthalpy ($h_{298}$), mass fraction EGR ($yEGR$), soot moments ($M_0$ and $M_1$) and the table-based NO species ($NO_{lib}$). In equations (4.51) and (4.52) the transport equations for mixture fraction and latent enthalpy are reported:

$$\frac{\partial \overline{\rho}\tilde{Z}}{\partial t} + \frac{\partial}{\partial x_i}\left(\overline{\rho}\widetilde{u_i}\tilde{Z}\right) - \frac{\partial}{\partial x_i}\left(\overline{\rho}\frac{\mu_t}{Sc_t}\frac{\partial \tilde{Z}}{\partial x_i}\right) = \overline{\dot{\omega}_{Z,spray}} \tag{4.51}$$

$$\frac{\partial\left(\overline{\rho}\widetilde{h_{298}}\right)}{\partial t} + \frac{\partial}{\partial x_i}\left(\overline{\rho}\widetilde{u_i}\widetilde{h_{298}}\right) - \frac{\partial}{\partial x_i}\left(\overline{\rho}\frac{\mu_t}{Sc_{s,t}}\frac{\partial \widetilde{h_{298}}}{\partial x_i}\right) = \overline{\dot{\omega}_{h_{298}}} + \overline{\dot{\omega}_{h_{298},spray}} \tag{4.52}$$

In equations (4.51) and (4.52) the terms on the left-hand side are handled by the CFD code. Depending on the spray evaporation model used, the CFD code also provides the fuel species source term due to fuel injection. This quantity is then used to derive the spray terms ($\overline{\dot{\omega}_{Z,spray}}$ and $\overline{\dot{\omega}_{h_{298},spray}}$) on the right hand side of equations (4.51) and (4.52). The enthalpy source term $\overline{\dot{\omega}_{h_{298}}}$ due to chemical reactions is entirely handled via user-coding. It must be noted that the normalized progress variable as defined in equation (3.11)) is not transported itself. The combustion progress is calculated form the transported mixture fraction ($Z$) and $h_{298}$ in each cell. The

pressure $p$ is provided by the CFD code data structure while the unburned temperature ($T_u$) is evaluated based on the cell local: equivalence ratio ($\phi$), mass fraction EGR and total enthalpy. Hence, after all necessary look-up variables are evaluated ($p$, $T_u$, $\phi$, $yEGR$, $C$), the updated species mass fractions are retrieved, together with the source terms for mixture fraction, and latent enthalpy.

# Chapter 5

# CPV Validation using 0-D Stochastic Reactor Models

This chapter covers the results of three SRM simulation campaigns. The first two are based on a set of experimental data from a passenger car and a heavy-duty Diesel engine, respectively. The third campaign was conducted based on single cylinder spark ignition engine data. In each paragraph, a brief description of the experimental data and computational setups is presented, followed by a result comparison between measurements, the online and the tabulated chemistry solvers (see paragraph 4.1.5) with respect to engine performance parameters and engine-out emissions. All the simulation results in this chapter have been obtained using the software LOGEengine [18].

## 5.1. Light-Duty Diesel Engine Simulations

The simulation setups refer to experimental data from a direct injected EURO 6 1.5 liters passenger car engine. Some details on the experimental campaign and engine geometry can be found in [121]. However, experimental pressure traces are omitted in this paragraph so to comply with confidentiality agreements.

A total of 10 operating conditions with multiple injection strategies have been selected in order to assess performance of the tabulated chemistry methodology against the online chemistry solver. The operating conditions have been chosen so that EGR, speed, load and injection strategy variations are considered. In Table 5.1 the details of the investigated operating conditions are reported.

Commercial Diesel fuel was used during experiments, whereas in the simulations n-heptane was used as surrogate fuel model employing the mechanism presented in [89]. A liquid fuel properties comparison is summarized in Table 5.3. The liquid properties of n-heptane differ from the diesel properties in terms of lower heating value (LHV), density and viscosity. Cetane number on the other hand compares well to Diesel fuel and makes it a good candidate to match the ignition delay of the EU commercial Diesel. The C:H ratio of Diesel is 1:1.87 and differs from n-heptane with 1:2.29, which impacts the emission formation characteristics of the two fuels. Because of the larger LHV of

n-heptane compared to Diesel, the total injected fuel mass in the SRM simulations has been decreased, with respect to the measured values, to ensure consistency with the energy content in both experimental and computational systems.

**Table 5.1.** Light-duty Diesel engine operating conditions.

| Case Name | Speed (rpm) | IMEP (bar) | EGR (mass%) | Injection pulses (#) |
|---|---|---|---|---|
| LD01 | 1500 | 2.1 | 4.2 | 2 |
| LD02 | 1500 | 2.1 | 25.0 | 2 |
| LD03 | 1500 | 2.1 | 40.0 | 2 |
| LD04 | 1500 | 10.5 | 4.2 | 2 |
| LD05 | 2000 | 2.1 | 4.2 | 2 |
| LD06 | 2000 | 7.0 | 4.2 | 2 |
| LD07 | 2000 | 23.5 | 4.2 | 2 |
| LD08 | 3000 | 10.5 | 4.2 | 2 |
| LD09 | 4000 | 10.5 | 4.2 | 1 |
| LD10 | 4000 | 16.0 | 4.2 | 1 |

Boundary conditions for the SRM simulations, computed for the part of the engine cycle between IVC and EVO, were obtained via the thermodynamic analysis module of LOGEengine [18], using the measured pressure traces as inputs.

**Table 5.2.** SRM main model settings for the light-duty Diesel engine simulations.

| Parameter | Value |
|---|---|
| Particle interaction model | EMST |
| Number of particles (-) | 500 |
| Simulation time-step (CAD) | 0.5 |
| Number of consecutive cycles (-) | 10 |
| Heat transfer model | Woschni |
| Stochastic heat transfer constant (-) | 15 |

**Table 5.3.** Liquid properties of the experimental and surrogate fuel mixture used in the light-duty Diesel engine simulation campaign [135].

| Fuel | Lower heating value (MJ/kg) | Density at 15 °C (kg/m³) | Cetane Number (-) | C (w%) | H (w%) | O (w%) |
|---|---|---|---|---|---|---|
| Diesel | 40.6 | 836 | 53 | 86.0 | 13.4 | 0.6 |
| n-Heptane | 44.6 | 686 | 56 | 84.0 | 16.0 | 0.0 |

In Figure 5.1 the injection profiles for the simulated operating conditions are shown. The model calibration procedure for the presented operating conditions was carried out in using a genetic algorithm and under the assumption of empirically defined mixing time (see 4.1.3.1). Please refer to [122] for more details on how the mixing time parameters were calibrated using the online chemistry solver. In the present simulation

campaign, the SRM model parameters optimized in [122] were applied to the tabulated chemistry solver setups without any further change.

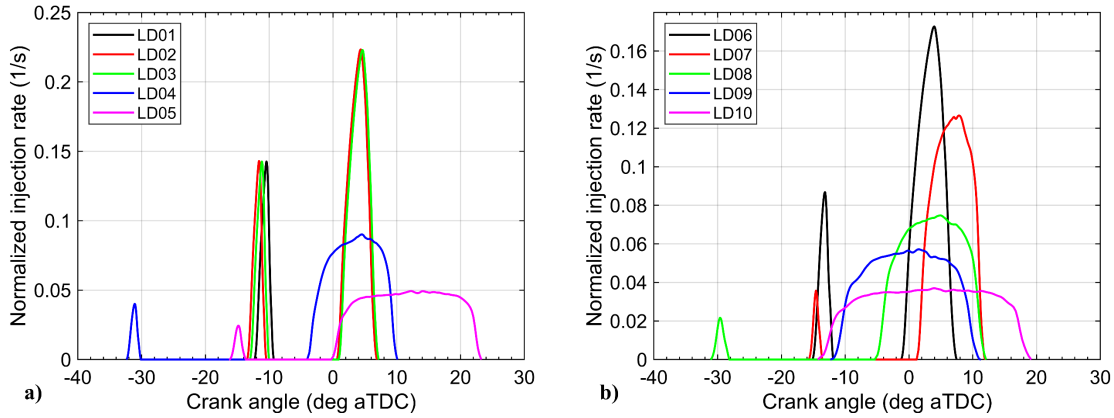


**Figure 5.1.** Fuel injection rates for operating conditions from 1-5 **a)** and 6-10 **b)** as listed in Table 5.1.

In Figure 5.2, Figure 5.3 and Figure 5.4 comparisons of predicted in-cylinder pressure history and chemical rate of heat release are shown for all investigated operating points (see Table 5.1). For the whole range of conditions, the online and the tabulated chemistry solver show a very close match with respect to the heat release rate due to the main injection events. The most noticeable differences are seen in the pilot injection heat release histories, especially in the low-speed low-load region (see Figure 5.2 a), b) and c)). While the start of combustion is closely matched between the two solvers, the evolution of the pilot injection heat release starts to differ. More in detail, the tabulated chemistry solver computes a generally faster burn rate than the online solver in the early phase. Nevertheless, during the main injection event the predicted chemical heat release rates match very well.

In Figure 5.5 comparisons of the main engine combustion phasing parameters (CA05, CA10, CA50 and CA90), the peak cylinder pressure (value and location in CAD) as well as computed IMEP are compared in a normalized form with reference to the online solution. The most relevant differences in combustion predictions can be seen in the CA05 and the CA10 histograms especially for LD03 (low-load high EGR case). Under such conditions the fuel undergoes the NTC behavior. It is likely to happen that the interpolation error starts to play a significant role. It has also to be considered that, given the fact that the CPV solver is called in each stochastic particle (500 in total have been used in this campaign), an error propagation/compensation effect may be observed in these simulations. Nevertheless, from a purely engineering standpoint, the reported discrepancies between the two solvers, lie within a comparable order of magnitude of what experimentally is observed as cycle-to-cycle variability.

As for engine out emissions, no comparisons are presented since the scope of the present campaign was to first establish a computationally efficient methodology for combustion prediction using tabulated chemistry within the SRM framework. In the following paragraphs, combustion and emissions are broadly discussed instead.

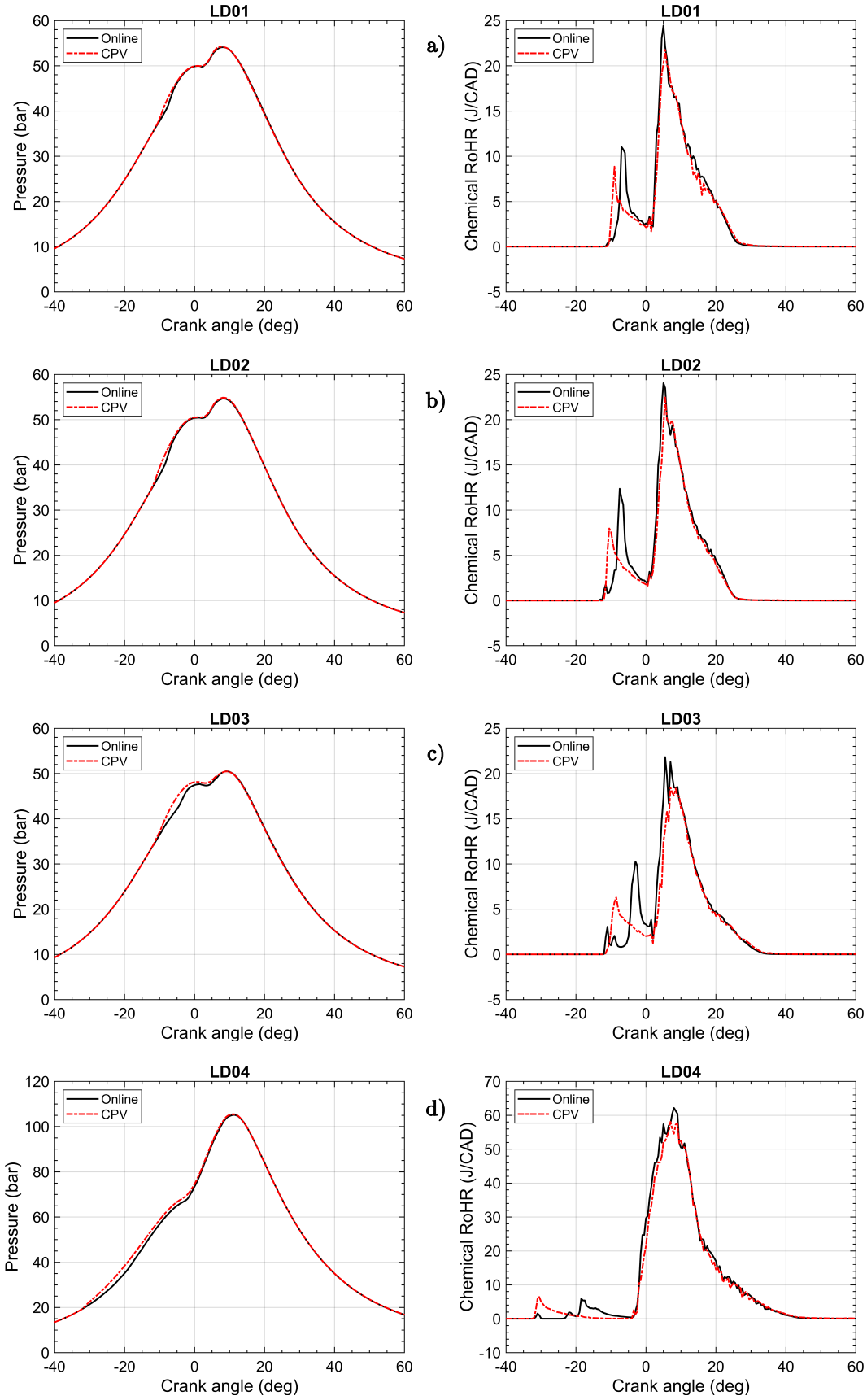


**Figure 5.2.** In-cylinder pressure history (left) and chemical heat release rate (right) comparison between SRM with online and CPV solvers for **a)** operating conditions LD01, **b)** LD02, **c)** LD03 and **d)** LD04 as noted in Table 5.1.

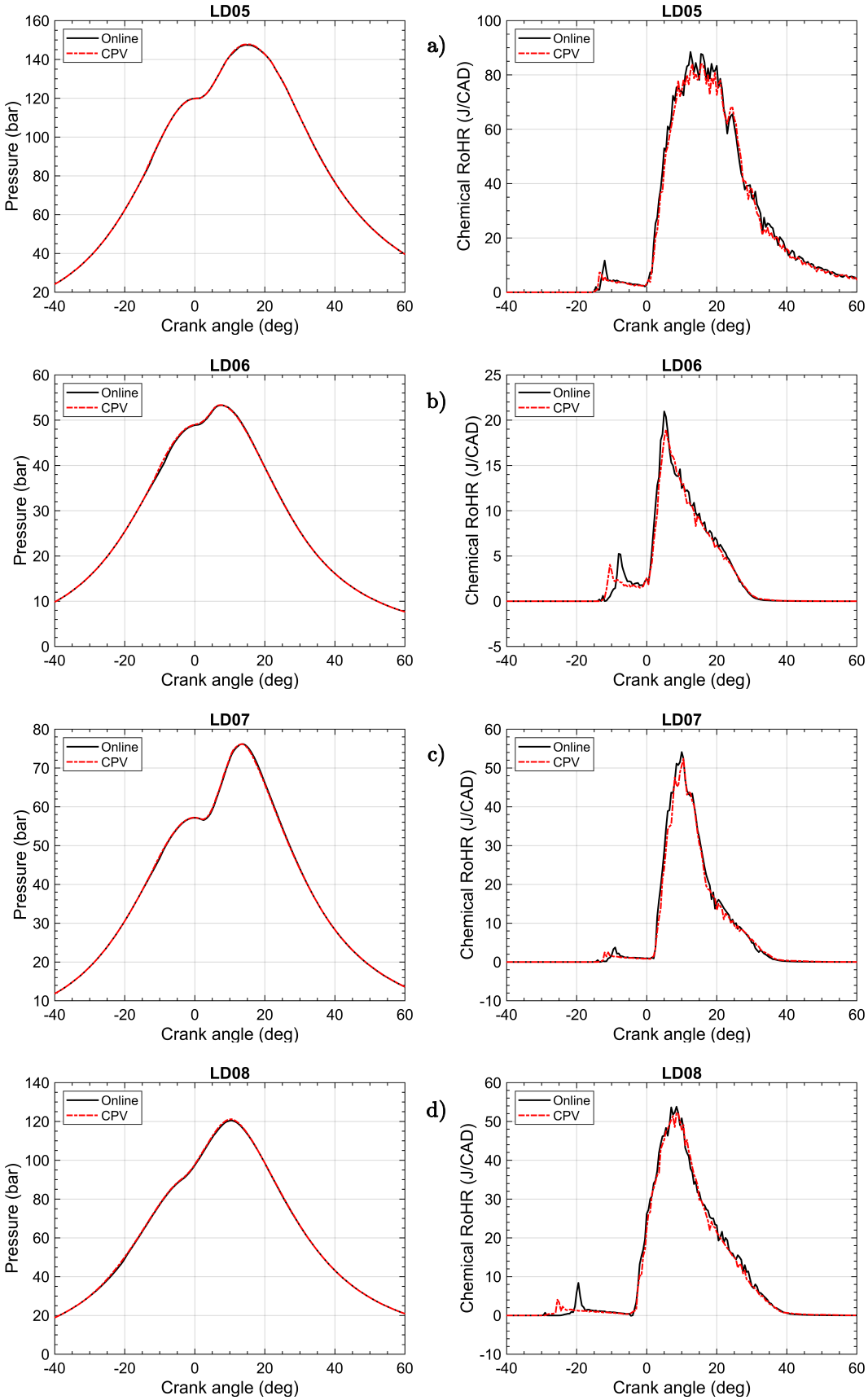


**Figure 5.3.** In-cylinder pressure history (left) and chemical heat release rate (right) comparison between SRM with online and CPV solvers for **a)** operating conditions LD05, **b)** LD06, **c)** LD07 and **d)** LD08 as noted in Table 5.1.

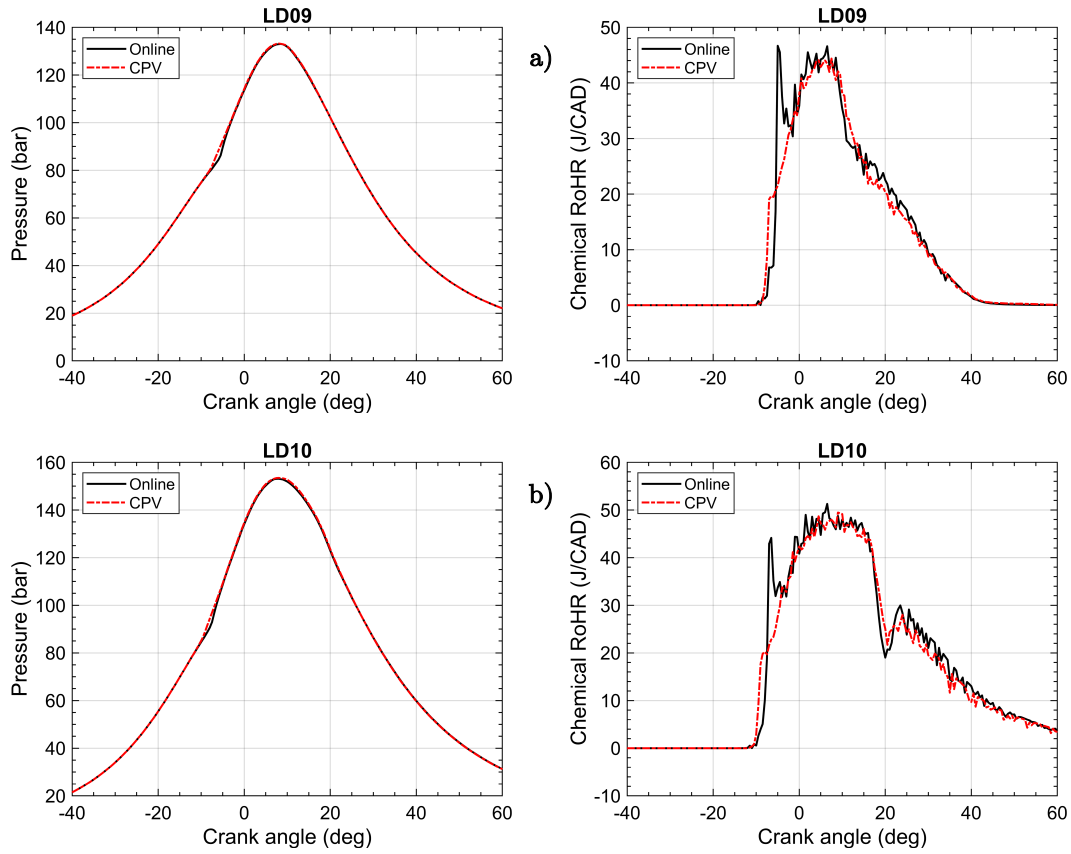


**Figure 5.4.** In-cylinder pressure history (left) and chemical heat release rate (right) comparison between SRM with online and CPV solvers for **a)** operating conditions LD09, and **b)** LD10 as noted in Table 5.1.

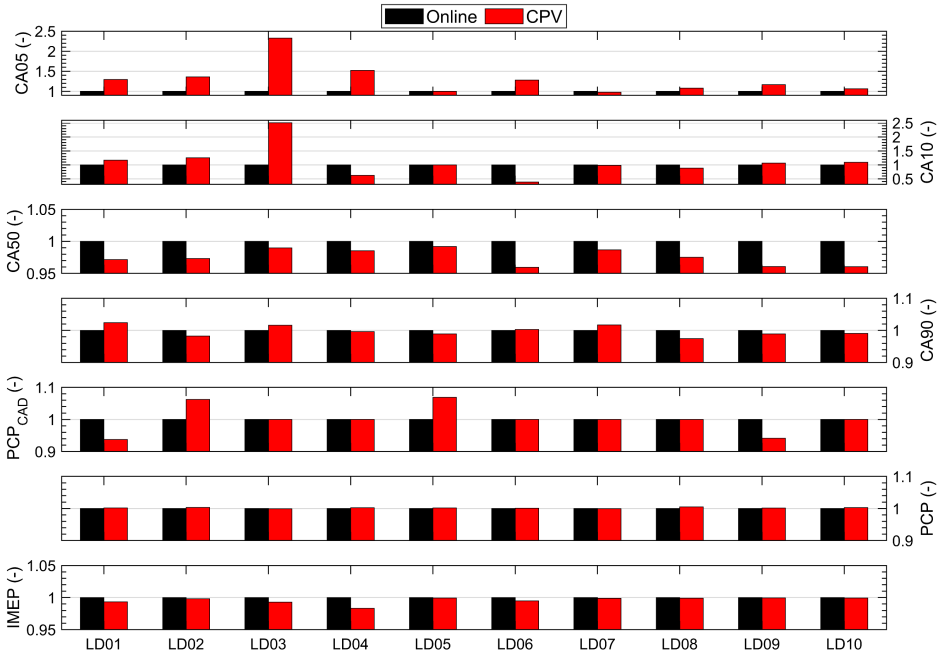


**Figure 5.5.** Simulated engine performance parameters and major emissions at EVO for SRM with online CPV solvers over all 10 operating conditions listed in Table 5.1.

## 5.2. Heavy-Duty Diesel Engine Simulations

The simulation setups were constructed based on experimental data from a heavy-duty (HD) 13.0 liters Diesel engine. A direct injection system is mounted to the engine that allows injection pressures up to 2000 bar. The measurements are without external EGR, while the engine itself has an external EGR system in-built. The measurement data consist of 10 operating points from 1000 rpm to 1700 rpm engine speed and 6 bar to 22 bar indicated mean effective pressure. The operating points are outlined in Table 5.4. The operating points 1 to 9 have a single injection rate profile, while the operating point 10 has a double injection rate profile (pilot + main) as presented in Figure 5.6. The crank-angle resolved pressure profile is measured for one cylinder and used to calibrate the combustion of the 0-D SRM.

**Table 5.4.** Heavy-Duty engine operating conditions.

| Case Name | Speed (rpm) | IMEP (bar) | EGR (mass%) | Injection pulses (#) |
|---|---|---|---|---|
| HD01 | 1700 | 19.0 | 4.0 | 1 |
| HD02 | 1300 | 22.0 | 4.0 | 1 |
| HD03 | 1300 | 14.5 | 4.0 | 1 |
| HD04 | 1300 | 6.0 | 4.0 | 1 |
| HD05 | 1200 | 6.0 | 4.0 | 1 |
| HD06 | 1200 | 14.5 | 4.0 | 1 |
| HD07 | 1200 | 22.0 | 4.0 | 1 |
| HD08 | 1000 | 6.0 | 4.0 | 1 |
| HD09 | 1000 | 11.0 | 4.0 | 1 |
| HD10 | 1000 | 22.0 | 4.0 | 2 |

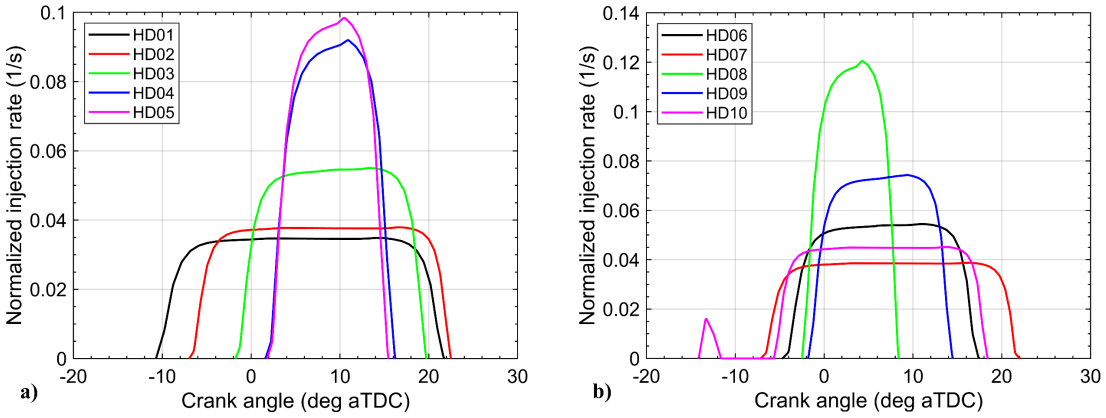


**Figure 5.6.** Fuel injection rates as a function of crank angle degree (assuming 0 as firing TDC) for operating conditions **a)** from 1-5 and **b)** 6-10 as listed in Table 5.4.

Commercial Diesel fuel was used during experiments, whereas in the simulations a mixture of *n*-decane and $\alpha$-methylnaphthalene (75% - 25% mass fractions respectively, also noted as IDEA mixture) was employed as surrogate fuel model. A liquid fuel properties comparison is summarized in Table 5.5.

**Table 5.5.** Liquid properties of the experimental and surrogate fuel mixture used in the heavy-duty Diesel engine simulation campaign.

| Fuel name | Lower heating value (MJ/kg) | Density at 15 °C (kg/m³) | Cetane Number (-) | C (w%) | H (w%) | O (w%) |
|---|---|---|---|---|---|---|
| EU Diesel | 41.60 | 820.0 | 49.0 | 86.0 | 13.40 | 0.6 |
| IDEA surrogate fuel | 42.94 | 783.0 | 52.3 | 86.62 | 13.38 | 0.0 |

The chemical kinetic scheme has been taken from the LOGEfuel database [18]. The mechanism is an improved version of the detailed model from Wang X. [47]. It features oxidation models for *n*-decane, *α*-methylnaphthalene and methyl decanoate as main fuel species as well as a detailed PAH growth mechanism [90] and thermal $NO_x$ model. The detailed reaction scheme was reduced to a size of 189 species using the method described in [15].

The measured pressure profile was analyzed using the thermodynamic analysis of LOGEengine [18]. This procedure provided chemical kinetics-based estimations of wall temperature, in-cylinder temperature at IVC, internal EGR fraction and the apparent rate of heat release (RoHR). The SRM model calibration for the presented operating conditions was carried out using the procedure described in [13] and the Curl [123] particle interaction sub-model was used. In Table 5.6 and Table 5.7 the main SRM model parameters and the calibrated *k*-ϵ model constants are presented respectively [118]. To ensure consistency during chemistry solver comparisons, the same set of model parameters and constants were applied to both the online and tabulated chemistry solver runs without any re-calibration.

**Table 5.6.** SRM main model settings for the heavy-duty Diesel engine simulation campaign.

| Parameter | Value |
|---|---|
| Number of particles (-) | 500 |
| Simulation time-step (CAD) | 0.5 |
| Number of consecutive cycles (-) | 30 |
| Woschni constant C1 | 2.28 |
| Woschni constant C2 | 0.0035 |
| Stochastic heat transfer constant (-) | 15 |

**Table 5.7.** Calibrated constants for the *k*-ϵ turbulence model. See paragraph 4.1.3.2.

| $C_{sq}$ | $C_{inj}$ | $C_{sw}$ | $C_{diss}$ | $C_{\tau}$ |
|---|---|---|---|---|
| 1.0 | 11.0 | 136.0 | 9.1 | 0.35 |

In Figure 5.7, Figure 5.8 and Figure 5.9 comparisons of experimental and simulated in-cylinder pressure histories, rate of heat release, combustion phasing parameters and normalized engine-out emissions are presented for all the investigated operating points.

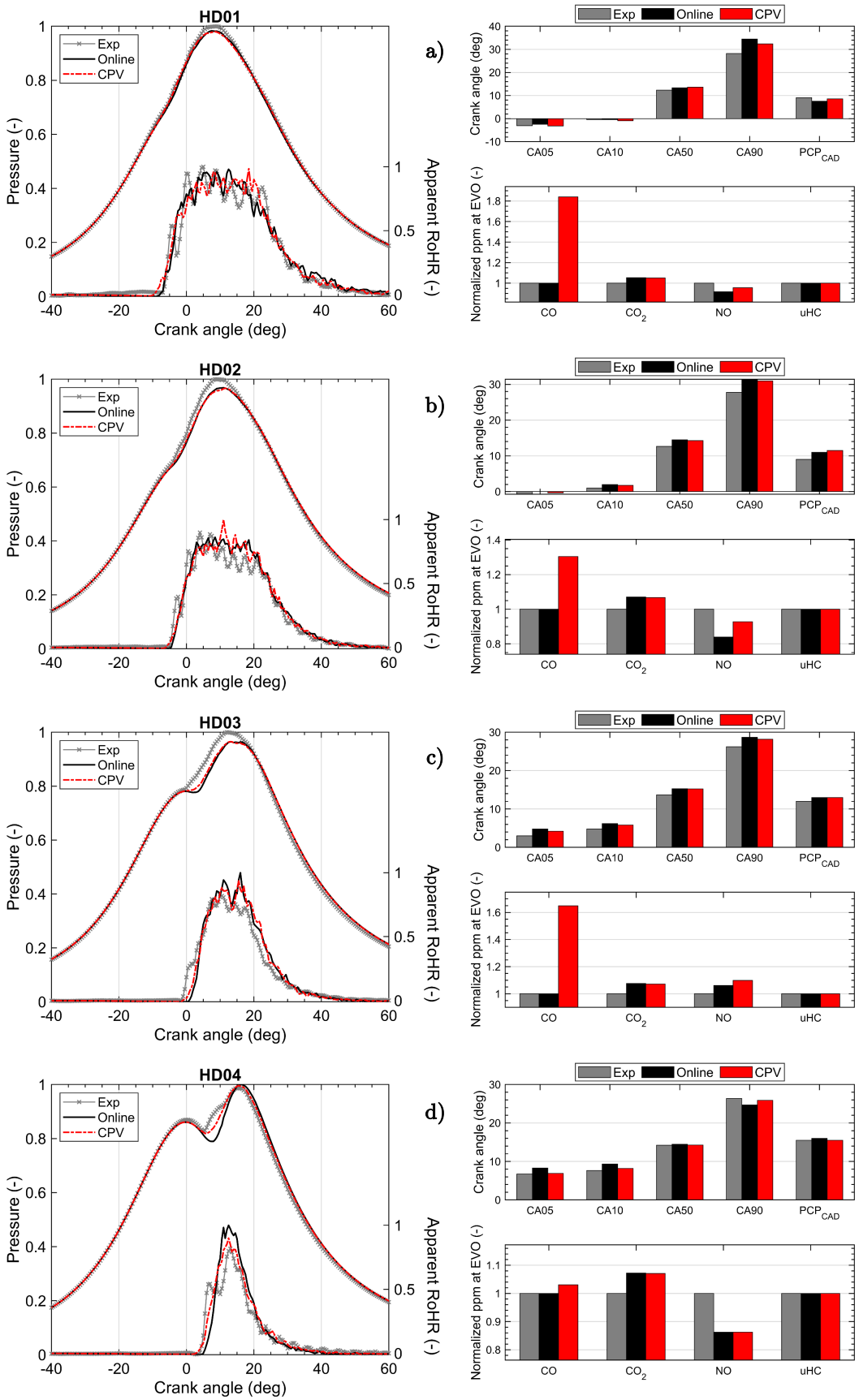


**Figure 5.7.** In-cylinder pressure and apparent heat release histories (left), combustion phasing parameters (top right) and normalized engine-out emissions (bottom right) for operating points **a)** HD01, **b)** HD02, **c)** HD03 and **d)** HD04 (see Table 5.4).

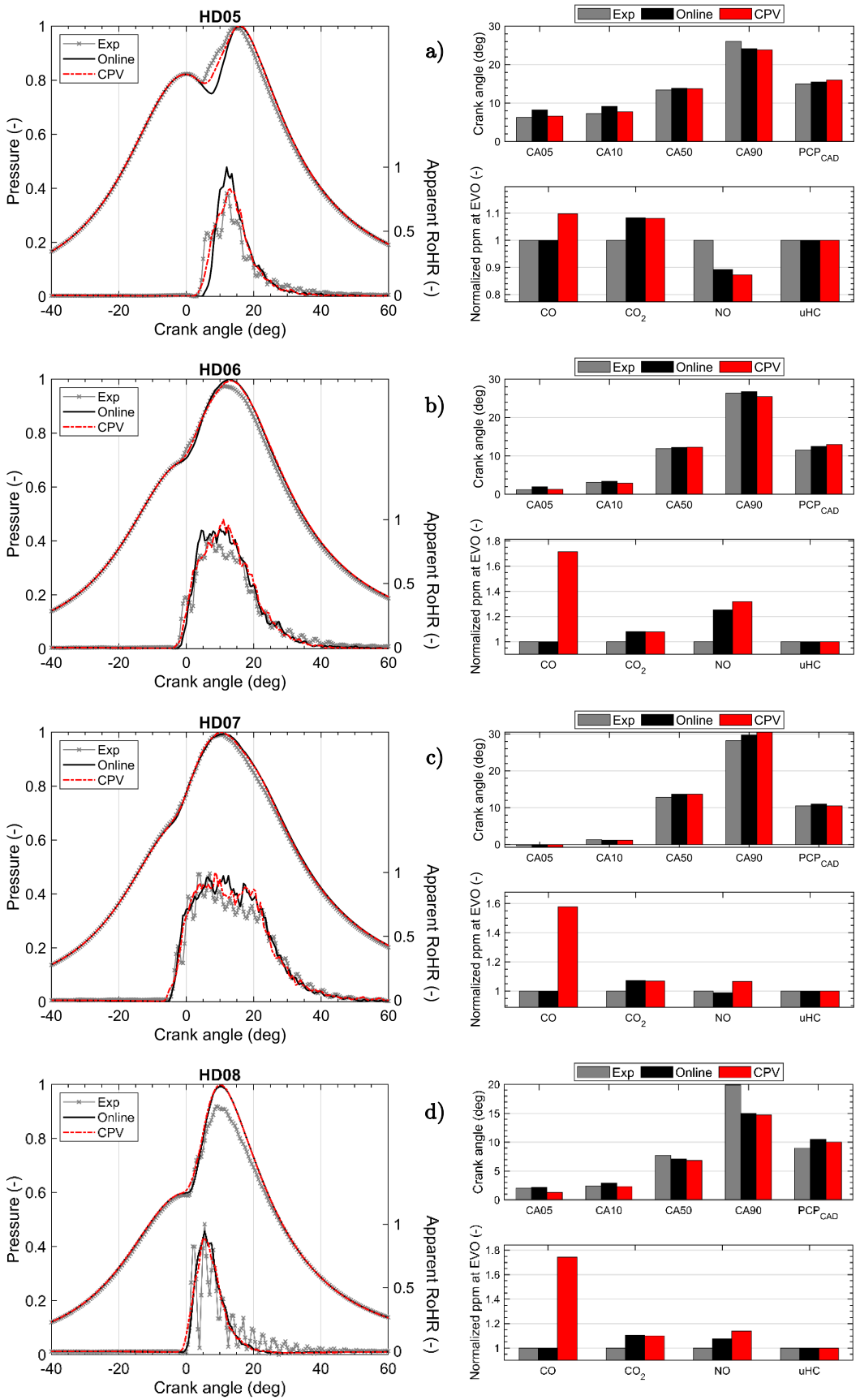


**Figure 5.8.** In-cylinder pressure and apparent heat release histories (left), combustion phasing parameters (top right) and normalized engine-out emissions (bottom right) for operating points **a)** HD05 , **b)** HD06, **c)** HD07 and **d)** HD08 (see Table 5.4).

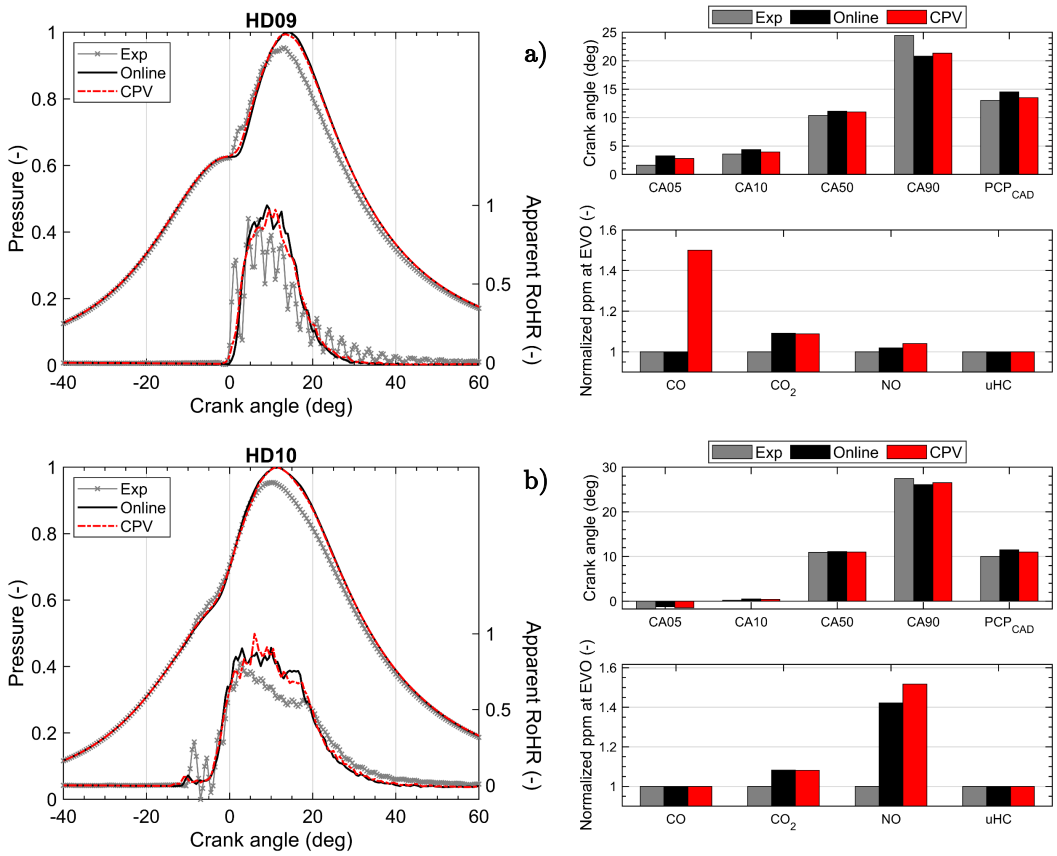


**Figure 5.9.** In-cylinder pressure and apparent heat release histories (left), combustion phasing parameters (top right) and normalized engine-out emissions (bottom right) for operating points **a)** HD09 and **b)** HD10 (see Table 5.4).

In Figure 5.10 comparisons of the CA50, Peak Cylinder Pressure location in CAD ($PCP_{CAD}$), as well as CO $CO_2$, unburned hydrocarbons (uHC) and NO at EVO are shown for all operating points.

To comply with data confidentiality restrictions, all the results shown in this simulation campaign are presented in a normalized fashion. With respect to engine out emissions different normalization strategies have been applied to ensure meaningfulness of the shown comparisons. More in details, for $CO_2$ and NO, the simulated ppm values have been normalized with respect to the experimental measurements. For CO and uHC instead, the normalization has been computed based on the difference in ppm between simulated and experimental data with a threshold value set to approximately 100 ppm. In other words, if simulated HC or CO present a normalized factor of 2.0, it means that the absolute difference between experimental and simulated values is approximately 200 ppm. On the other hand, if simulated and experimental HC or CO differ by less than 100 ppm, then the factor is set to 1.0, so to underline an acceptable agreement. Such formulation was considered necessary to cope with the fact that the measured CO and uHC are in absolute terms very low. Hence a standard normalization would have resulted in a set of misleadingly high factors for CO and uHC from the engineering standpoint. For uHC in particular, the difference between experimental and simulated engine-out ppm values never exceeded 30 ppm across all the operating

points, therefore the set of comparison factors for uHC in Figure 5.10 is homogeneously set to 1.0.

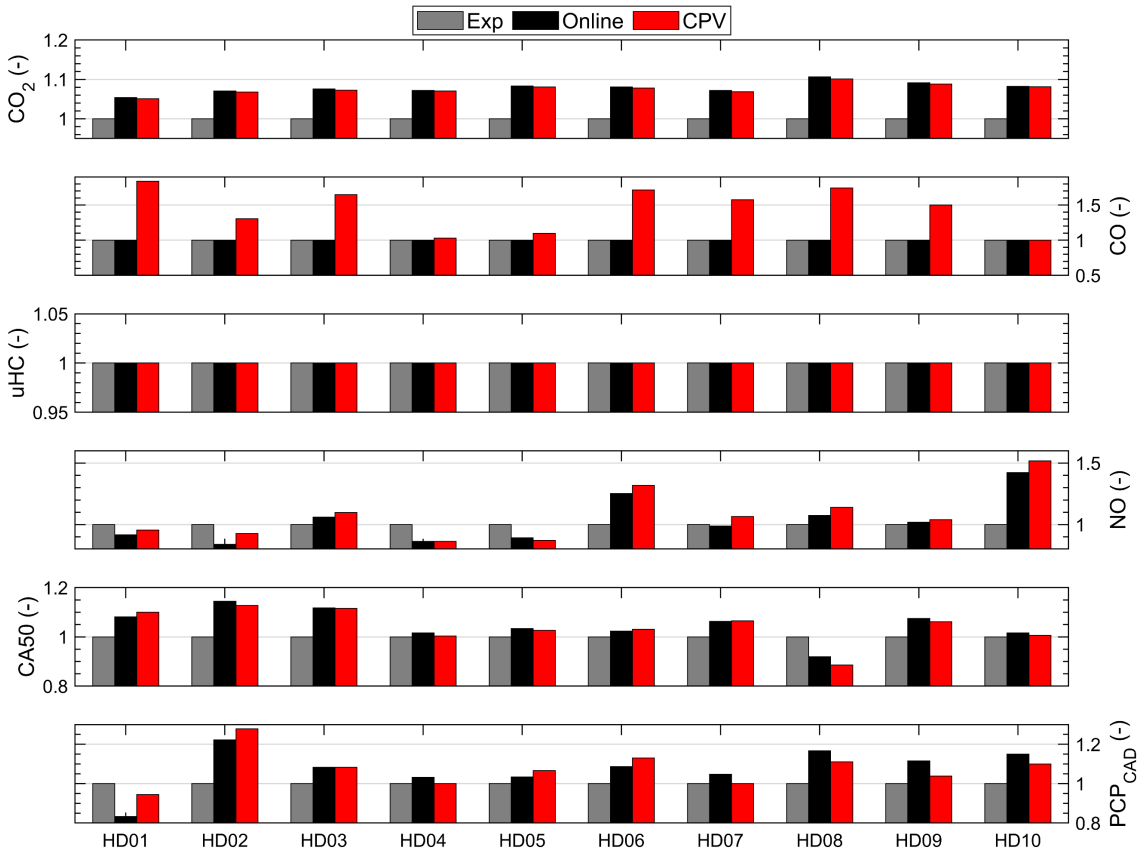


**Figure 5.10.** Experimental and simulated engine-out emissions as well as performance parameters (CA50 and PCP location) for all operating conditions of the heavy-duty engine simulation campaign. Data have been normalized with respect to experimental values.

With respect to combustion phasing, the SRM results are in good agreement with experimental data for most of the analyzed operating conditions. Visible discrepancies can be observed in terms of peak cylinder pressure predictions in HD08 and HD09. However, such result was considered acceptable considering that on the experimental side these operating point showed a strong cycle-to-cycle variability, as it can be noticed via the large fluctuations of the heat release rate between 0 and 40 crank angle degrees after TDC (see Figure 5.8 d) and Figure 5.9 a)).

As for the online versus CPV simulation results, both simulations resulted to be in close agreement with each other across the whole range of simulated data. The tabulated chemistry solver predicted a combustion phasing within less than 0.5 CAD difference with the detailed online chemistry solver at the mid and high loads. For the low load points (HD04 and HD05) a slightly more noticeable difference (approximately 2.0 CAD) between online and tabulated chemistry solutions can be seen when comparing the predicted start of combustion (See Figure 5.7 d) and Figure 5.8 a)). At

low loads, combustion initiates while the mixture is the NTC region, which, as discussed in paragraph 3.4 is the most challenging regime for progress variable-based models. It is therefore likely to happen that under these conditions the interpolation error starts to play a visible role. Nevertheless, a 2 CAD discrepancy in start of combustion is well within a range typically considered acceptable for engine performance studies and considering accuracy of the sensors used during the experimental campaigns.

With respects to engine-out emissions, both solvers showed good agreement with experimental data for $CO_2$, uHC and NO. For carbon monoxide emissions, the online chemistry solver, showed a noticeably closer match (less than 120 ppm difference) with experimental data. While the CO predictions from the CPV solver lie within a more than acceptable range from the engineering point of view, it is important to note that correct tabulation of CO during the expansion phase is another challenging area when progress variable models are concerned. Unlike methods proposed by IFP-EN (i.e., [76]), the present method does not account for a time-scale dependent retrieval of the CO emissions from the table. This means that the accuracy of the final CO yield depends on how the close to (or far from) equilibrium the value stored in the table at progress 1 is. In the present thesis, the presented level of accuracy between online and tabulated chemistry solver-based CO values (within a 150 ppm discrepancy) was considered acceptable. In future studies however, a time-scale dependent CO retrieval strategy may be considered.

## 5.3. Spark-Ignition Engine Simulations

The experiments are conducted on a single cylinder research engine at the TU-Berlin [19]. Cylinder bore and stroke are 82.0 and 71.9 mm respectively, while the compression ratio is 10.75:1. The single cylinder engine is built for fundamental investigations and supports both port and direct fuel injection capabilities. The present engine experiments were conducted using a central direct fuel injection. More details on the experimental setup and measuring equipment used can also be found in the work of Kauf et al. [136]. The engine is equipped with low-pressure and high-pressure sensors to measure the cylinder and manifold pressures of 250 consecutive cycles. The centrally mounted direct injector is used to inject a RON95 E10 fuel with 150 bar injection pressure. The start of fuel injection is at -270 CAD aTDC. Eight fired operating points are selected from the available experimental database and are summarized in Table 5.8.

The fuel used during the experimental campaign was a RON95 E10 commercial gasoline. A four component mixture comprising mole percentages of 31.9% *iso*-octane, 11.4% *n*-heptane 35.6% toluene and 20.8% ethanol was used in the simulation campaign instead. Comparisons of the major fuel properties are listed in Table 5.9. The adopted reaction mechanism is based on the detailed ETRF scheme developed by Seidel [51] consisting of 475 species and 5160 reactions. The detailed reaction scheme was validated for different experiments and engine relevant conditions for both auto-ignition and laminar flame speed in several previous works [30, 137]. The SRM model calibration

for the presented operating conditions was carried out using the procedure described in [138].

**Table 5.8.** Spark-ignition engine operating conditions.

| Case Name | Speed (rpm) | IMEP (bar) | EGR (mass%) | Spark timing (CAD aTDC) |
|---|---|---|---|---|
| SI01 | 1500 | 15.0 | 1.7 | -1.5 |
| SI02 | 2000 | 5.0 | 9.1 | -4.0 |
| SI03 | 2000 | 10.0 | 4.9 | -6.0 |
| SI04 | 2000 | 15.0 | 2.0 | -3.0 |
| SI05 | 2000 | 20.0 | 1.1 | 2.0 |
| SI06 | 2500 | 5.0 | 9.4 | -9.0 |
| SI07 | 2500 | 10.0 | 4.9 | -5.0 |
| SI08 | 2500 | 15.0 | 2.0 | -5.0 |

**Table 5.9.** Liquid properties of the experimental and surrogate fuel mixture used in the SI engine simulation campaign.

| Fuel name | Lower heating value (MJ/kg) | Density at 15 °C (kg/m³) | RON / MON (-) | C (n) | H (n) | O (n) |
|---|---|---|---|---|---|---|
| E10 Gasoline | 41.78 | 748.7 | 96.7 / 85.8 | 6.6 | 12.8 | 0.21 |
| ETRF mixture | 41.14 | 756.4.0 | 96.7 / 87.4 | 6.3 | 11.8 | 0.21 |

In Table 5.10 and Table 5.11 the main SRM model parameters and the calibrated $K$-$k$ model constants [119] are presented, respectively. As done for the compression ignition engine campaign, the same set of model parameters and constants were applied to both the online and tabulated chemistry solver runs without any re-calibration.

**Table 5.10.** SRM main model settings for the spark-ignition engine simulation campaign.

| Parameter | Value |
|---|---|
| Number of particles (-) | 500 |
| Simulation time-step (CAD) | 0.5 |
| Number of consecutive cycles (-) | 30 |
| Woschni constant C1 | 2.28 |
| Woschni constant C2 | 0.0035 |
| Stochastic heat transfer constant (-) | 15 |

**Table 5.11.** Calibrated constants for the $K$-$k$ turbulence model [119]. See paragraph 4.1.3.3.

| $C_{inj}$ | $C_{comp}$ | $C_{diss}$ | $C_{tke}$ | $C_{len}$ | $C_{\beta}$ | $C_{\Delta,1}$ | $C_{\Delta,2}$ | $C_{\tau}$ |
|---|---|---|---|---|---|---|---|---|
| 0.005 | 0.67 | 1.0 | 0.85 | 0.30 | 0.25 | 0.073 | 0.1313 | 4.3 |

In Figure 5.11 a compact summary of engine-out emissions and major combustion phasing parameters are summarized for all the investigated operating conditions. All values are normalized to experimental data. With regard to engine-out emissions, while simulations and experiments agree acceptably well, for most of the cases, noticeable differences can be seen for CO and NO between online and tabulated chemistry solver.

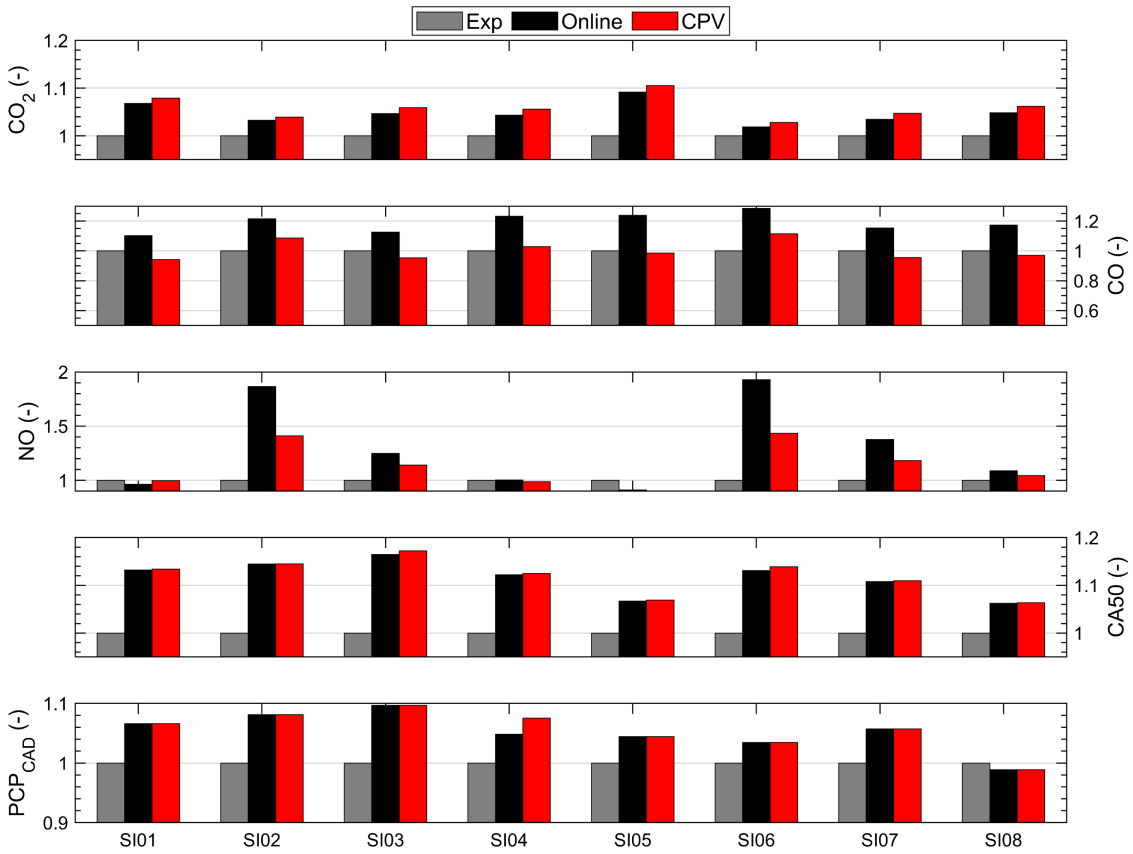


**Figure 5.11.** Experimental and simulated engine-out emissions as well as performance parameters (CA50 and PCP location) for all operating conditions of the SI engine simulation campaign. Data have been normalized with respect to experimental values.

Comparisons of experimental and simulated in-cylinder pressure histories, rate of heat release, combustion phasing parameters and normalized engine-out emissions are presented for all operating conditions in Figure 5.12 and Figure 5.13. Overall, the SRM simulation results show a very close match with experiment in terms of in-cylinder pressure for different operating conditions. Slight deviations can be seen for the operating points SI05 (2000 rpm and 20 bar IMEP) and SI06 (2500 rpm and 5 bar IMEP) in Figure 5.13 b) and c) in terms of start of combustion and peak cylinder pressure. However, the overall agreement is considered acceptable, especially considering cycle-to-cycle variability [136].

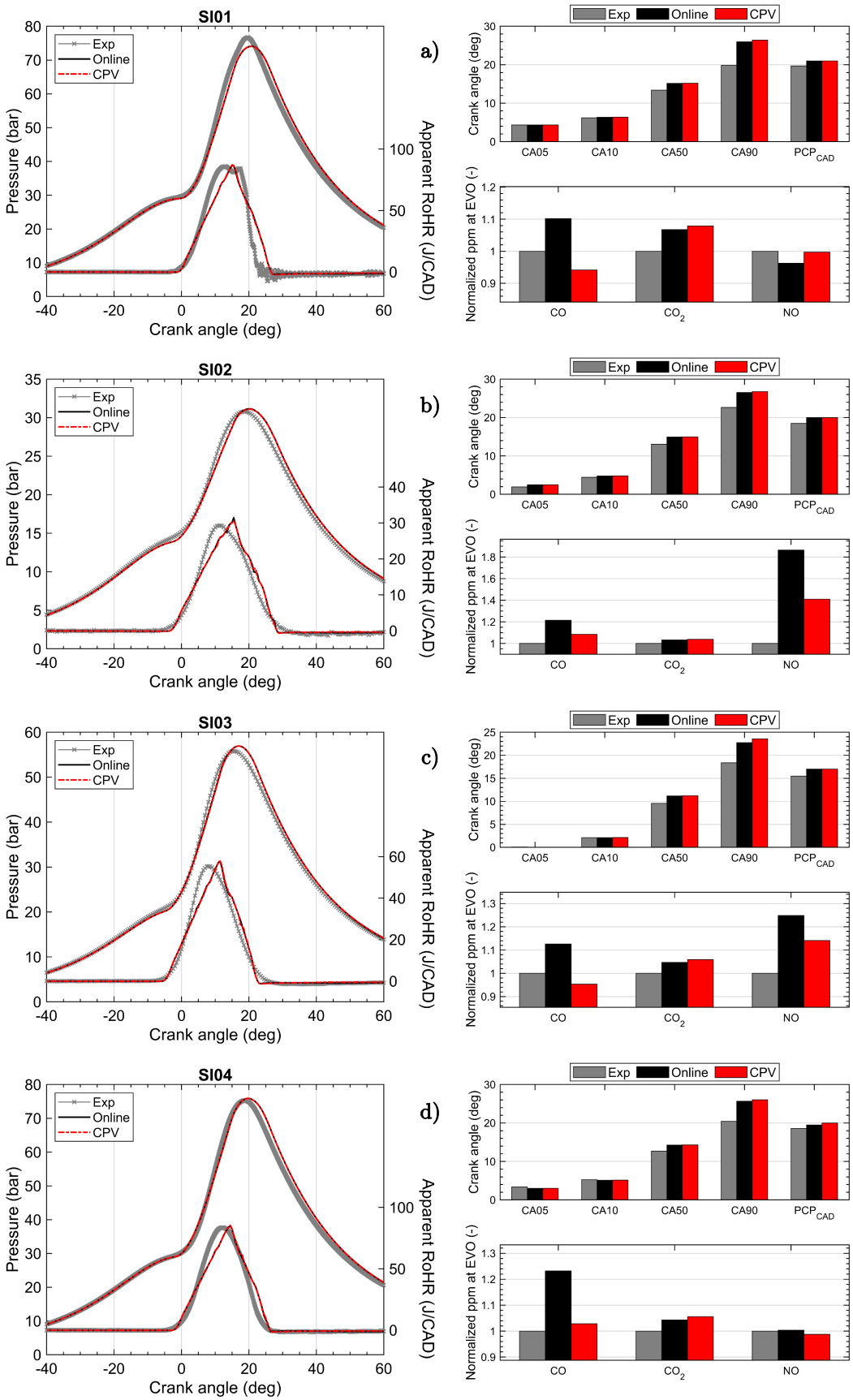


**Figure 5.12.** In-cylinder pressure and apparent heat release histories (left), combustion phasing parameters (top right) and normalized engine-out emissions (bottom right) for operating points **a)** SI01, **b)** SI02, **c)** SI03 and **d)** SI04 as noted in Table 5.8.

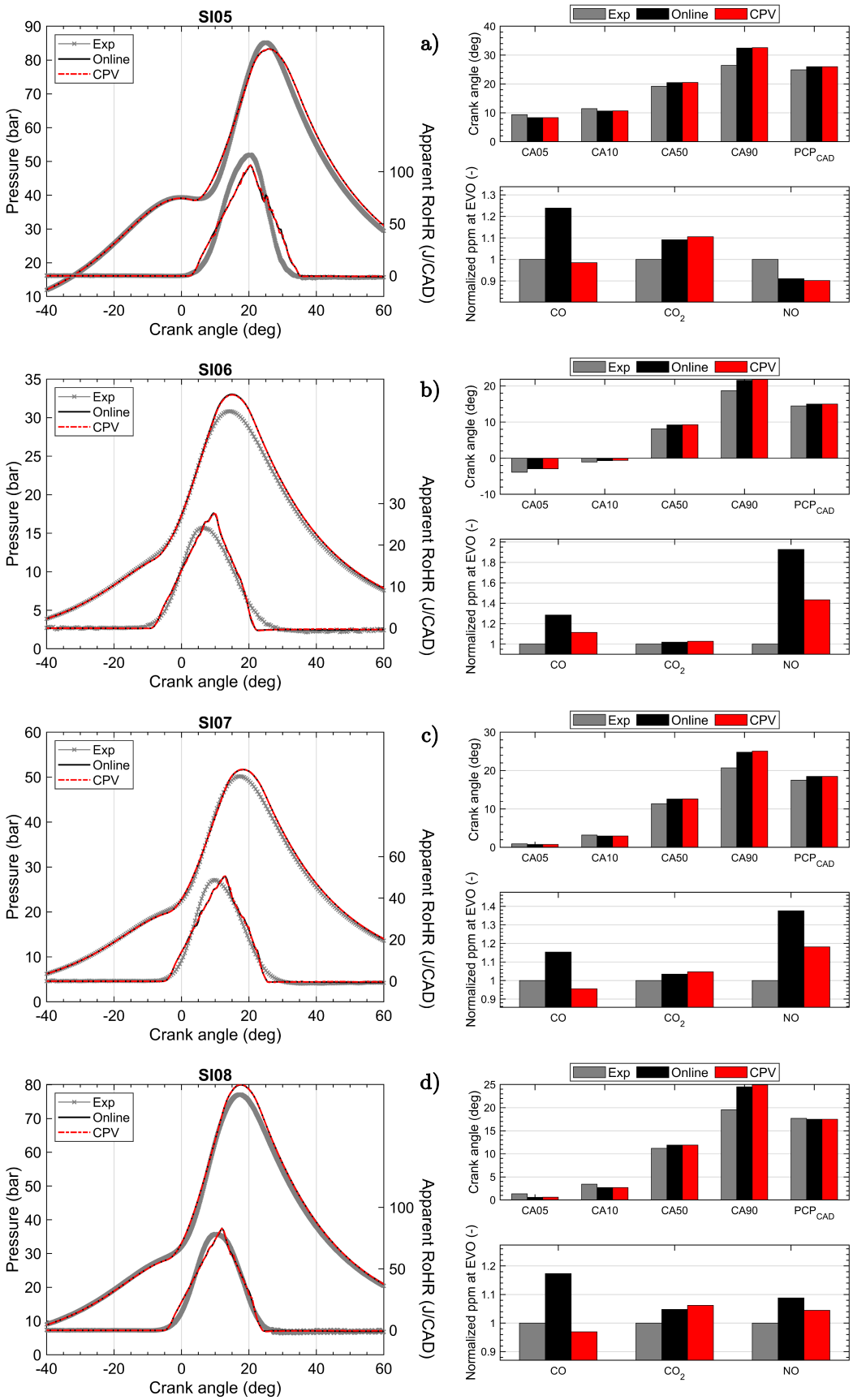


**Figure 5.13.** In-cylinder pressure and apparent heat release histories (left), combustion phasing parameters (top right) and normalized engine-out emissions (bottom right) for operating points **a)** SI05, **b)** SI06, **c)** SI07 and **d)** SI08 as noted in Table 5.8.

Compared to the Diesel engine campaign, a much closer match between online and CPV solver can be seen in the SI cases. This is explained by the fact that in SI mode, the dominant phenomenon is the flame propagation rather than mixing controlled combustion, where particles reach fully burned state ($C = 1$) much faster and are moved to the burned zone. In addition, given the early start of injection, the mixture is assumed to be homogeneous and close to stoichiometry. The homogeneity in lambda, together with the particles quickly reaching $C = 1$, make the interpolation particularly accurate. Stochastic effects are still present due to the SRM treatment of the heat transfer (see paragraph 4.1.6), however hardly any difference can be seen in terms of pressure and rate of heat release histories as well as in terms of combustion phasing parameters and peak cylinder pressure location.

Regarding NO, the differences are related to the fact that in the detailed scheme a more advanced formation mechanism for $NO_x$ is accounted for, while in the tabulated chemistry solver only thermal NO source terms are considered. As for CO, a similar discrepancy as in the Diesel simulation campaign can be seen. The operating point at 2500 rpm and 5 bar IMEP (SI06, Figure 5.13 b)) shows the largest difference for NO emission of 17 % because of larger differences in predicted combustion.

## 5.4. Computational Performance of CPV in SRM

Employing the 475 species reaction mechanism and carrying out calculations using the online chemistry solver in parallel on twenty four cores (Intel Xeon E5-2687W v4 @ 3.00GHz processors from the year 2016) the SRM takes 19 minutes/cycle (using 500 particles and 0.5 CAD as time-step). Thirty consecutive cycles would then result in a total CPU time per operating point of 9.4 hours. This CPU time, although shorter than that of a RANS 3-D CFD multicycle engine simulation, is several orders of magnitudes higher than the average simulation time needed for a typical 0-D/1-D run in a simulation tool used for engine performance mapping (i.e., multi-zone Viebe models). Furthermore, considering that the turbulence model calibration procedure [13, 138] needs to perform a few thousands of runs to find the optimal constants, application of the online chemistry solver with detailed chemical mechanisms becomes unfeasible for engineering applications.

It is well known that, given fixed simulation accuracy settings and fixed calculation time-step, the computational cost may increase exponentially as the number of species in the reaction mechanism. A CPU time performance analysis using the SRM with different reaction mechanisms of various sizes was carried out assuming 100 particles and a calculation time-step of 1.0 CAD in a Diesel engine. The computational performance of these simulations is reported in Figure 5.14. On the one hand, CPU time is much reduced thanks to the fast interpolation operation as opposed to the on-the-fly source/sink term calculation of the species. On the other hand, tabulated chemistry-based solvers deliver the same calculation time independently on the size of the mechanism with which the table was generated.

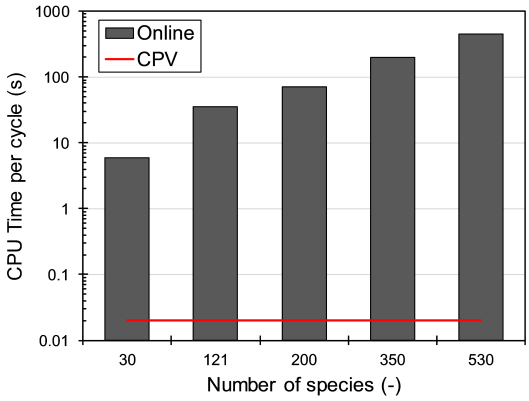


**Figure 5.14.** Number of species in the mechanism versus computational cost; comparison between online and tabulated chemistry solver for a fixed Diesel engine simulation having 100 particles and 1.0 CAD time-step.

With respect to the present engine simulation campaigns, a summary of the CPU times obtained with both solvers and the mentioned model settings (see Table 5.6 and Table 5.10) are reported in Table 5.12.

**Table 5.12.** Computational performance summary assuming SRM settings listed in Table 5.6 and Table 5.10, on an Intel Xeon E5-2687W v4 @ 3.00GHz CPU from the year 2016.

| **Simulation setup** | **Online chemistry on 24 parallel cores (seconds/cycle)** | **Tabulated chemistry on 1 core (seconds/cycle)** |
|---|---|---|
| SI engine simulation | 1136.5 | 4.1 |
| CI engine simulation | 631.7 | 1.6 |

Considering that the SRM solver with CPV solver can be easily run on a single core, as opposed to the online solver that requires multiple cores per run, one can conclude that the present solver delivers a speed-up of at least three orders of magnitude. The size of the auto-ignition table covering the full engine map including EGR variations (between 0 and 40 %) requires approximately 1.5 GB of RAM memory. This size allows the SRM with CPV to be a tool that can be used for engineering applications (e.g., engine performance mapping) even on a regular laptop and not only on a high-performance workstation. Moreover, given the high degree of physical and chemistry models included in its formulation, engine parameter optimization campaigns can be performed within feasible engineering times.

To put the computational results shown in Table 5.12 in a broader prospective, in Figure 5.15 are shown the extrapolated computational costs of two relevant engine development simulation campaigns: an engine performance mapping and a WLTP cycle. Both results have been extrapolated considering only the CPU time needed by in-cylinder combustion model. Additional system components (i.e., intake and exhaust air paths, aftertreatment systems), and their contribution to the total simulation time are not considered. Nevertheless, it can be stated that the tabulated chemistry allows

to include detailed chemistry effects in several applications that are, in most cases, unfeasible for the online chemistry solver.

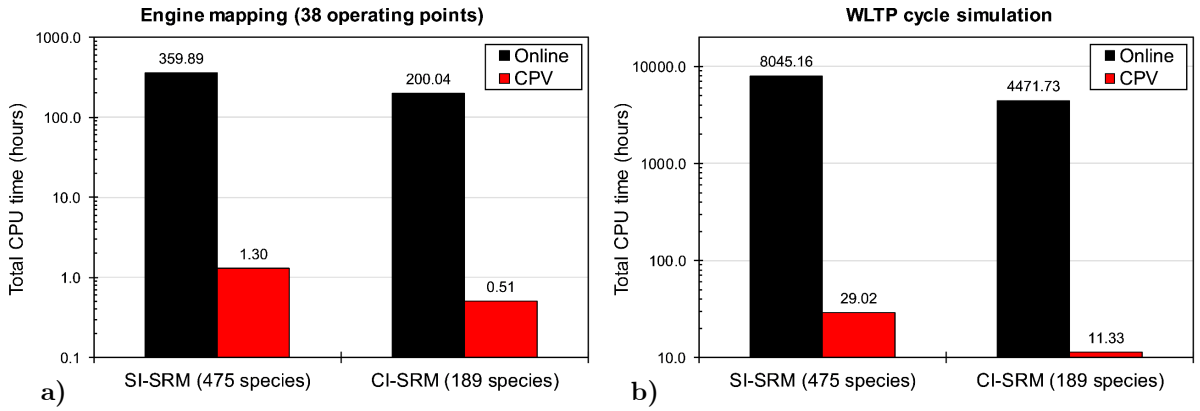


**Figure 5.15.** Comparison between online and tabulated chemistry solver computational performances for: **a)** a full engine performance mapping simulation campaign comprising a total of 38 operating conditions; **b)** the simulation of the full WLTP cycle (30 minutes) in terms of combustion and emission simulations only.

The developed CPV solver is recently applied in two publications for the engine and fuel optimization of Diesel and gasoline engines. In the work of Franken et al. [13] a heavy-duty Diesel engine is optimized to find the best set of engine parameters to reduce fuel consumption and $NO_x$ emissions. The optimization is performed for 10 operating points at different speed and torque. The authors reported optimization times of 20h to 40h for one operating point.

For a single-cylinder research gasoline engine optimization results are published by Franken et al. [19]. The authors used a dual fuel tabulated chemistry approach to find the best set of engine parameters and water/fuel-ratios to reduce the knock tendency at a high load operating point and improve the engine efficiency. The optimization times reported in [13, 19] are within 10h for one operating point using only 4 cores, while an equivalent run with the online chemistry solver would take several days.

# Chapter 6

# CPV Validation in 3-D CFD RANS

This chapter covers the results of a 3-D CFD simulation campaign for Diesel engine sector cases in RANS framework. Firstly, a brief description of the experimental data and computational setups is presented. Secondly, results comparison between online and tabulated chemistry solvers (see paragraph 4.2) in terms of engine performance parameters and engine-out emissions. Lastly, a summary of the recorded CPU times is presented together with remarks of potential applications of the present solver. All the simulation results in this chapter have been obtained using the software CONVERGE v. 2.4 [20] and LOGEapi [52]. Convergence Science Inc. is thanked for providing the licenses and Renault SA is kindly acknowledged for providing the experimental data.

## 6.1. Diesel Engine Sector Simulations

All presented simulation results refer to the experimental data from a passenger car direct injected Diesel engine. More details on the experimental campaign can be found in [139]. Engine specifications are given in Table 6.1 and the analyzed operating conditions in Table 6.2. Depending on the operating point the fuel is injected using a single or double (pilot and main) injection strategy as shown in Figure 6.1.

**Table 6.1.** Engine geometry specification [139].

| Parameter | Value |
|---|---|
| Bore (mm) | 80.0 |
| Stroke (mm) | 80.0 |
| Connecting rod (mm) | 148.4 |
| Compression ratio (-) | 15.5:1 |
| Swirl number (-) | 2.5 |
| Injection pressure (mm) | 1600.0 |

For the 3-D CFD simulations a sector mesh with a maximum cell size of 1.4 mm is used. Based on the velocity field and the local temperatures the mesh is refined down to 350 μm using the adaptive mesh refinement strategy [20]. The cells in the spray area

are fixed to 350 µm. This results in approximately 27 000 cells at bottom dead center and 60 000 cells during injection and combustion.

**Table 6.2.** Operating conditions [139].

| Case name | Speed (rpm) | IMEP (bar) | EGR (%) | Equivalence Ratio (-) |
|---|---|---|---|---|
| Case 01 | 1500 | 20.0 | 3.0 | 0.85 |
| Case 02 | 2500 | 11.5 | 22.0 | 0.80 |
| Case 03 | 4000 | 20.3 | 4.0 | 0.75 |

The $k$-$\varepsilon$ Re-Normalization Group (RNG) is applied using the standard coefficients for engine simulations [20]. For the spray breakup the modified Kelvin-Helmholtz Rayleigh-Taylor breakup model [20, 140, 141] was applied. The heat transfer is modelled using O'Rourke's model [20].

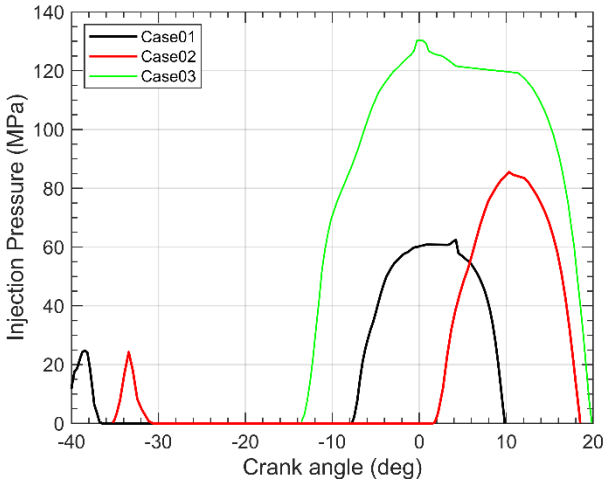


**Figure 6.1.** Injection rates shapes for the simulated cases as noted in Table 6.2.

For the comparison to an online chemistry solver the SAGE detailed chemistry model is used [131]. It is chosen since it employs, as the tabulated CPV approach presented in this work, the well stirred reactor concept. In both approaches a computational cell is assumed to behave as an adiabatic constant pressure rector, which makes the models comparable. For the online chemistry calculation with the SAGE model, a clustering strategy on similar cells is applied based on cell temperature and equivalence ratio to speed up the simulation time [134]. Within the CPV model such approach is not needed, hence this aspect must be kept in mind when comparing the simulation results.

For the soot results comparison, the Particle Mimic (PM) [20] soot model built-in CONVERGE 2.4 has been used in coupled mode with SAGE. Soot moments $M_0$ and $M_1$ have been employed while keeping fractal dimension and fraction of active sites equal to 2.25 and 0.3, respectively. For the NO calculation the Extended Zeldovich model built-in CONVERGE 2.4 has been used in coupled mode with SAGE.

Given the scope of the present work only simulation results from the online (SAGE) and tabulated chemistry solvers are presented. Experimental data as well as online chemistry solver results for both combustion and emissions have been extensively discussed in [139]. In Figure 6.2 in-cylinder pressure trace and rate of heat release for both chemistry solvers are compared for case 01. Despite a slight under-prediction of the peak pressure value, the agreement between the solutions of the two solvers is very close. In fact, the difference in predicted IMEP between online and tabulated chemistry solvers differs only by 1.56 % (19.43 bar for SAGE and 19.13 bar for CPV). Similarly, small discrepancies can be noted in the heat release rate histories. Both the pilot and main start of combustion are in very close agreement as well as the overall evolution of the combustion process. In Figure 6.3 the crank-angle resolved soot moment $M_1$ and $NO$ mass profiles are compared for the SAGE and CPV simulations.

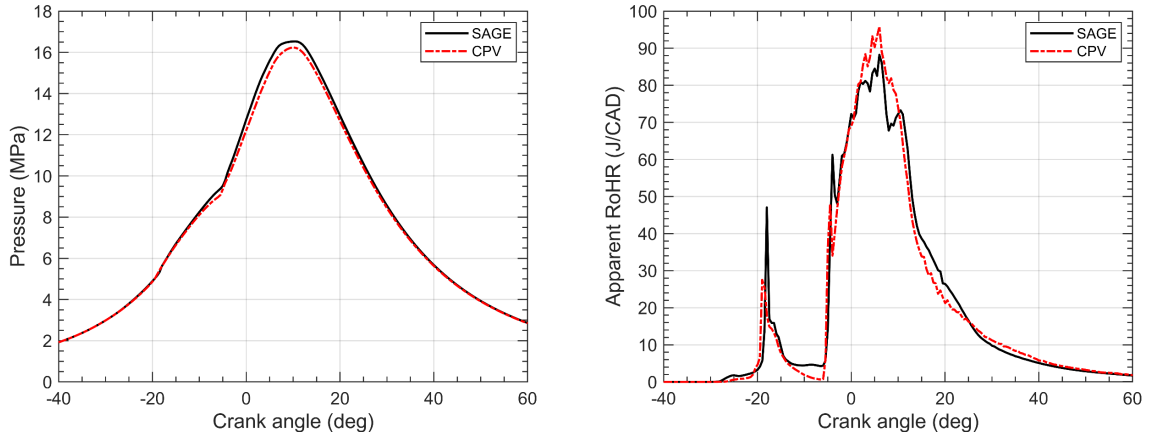


**Figure 6.2.** Online (SAGE) and tabulated (CPV) chemistry solver in-cylinder pressure (left) and apparent rate of heat release (right) histories for Case 01 as noted in Table 6.2.

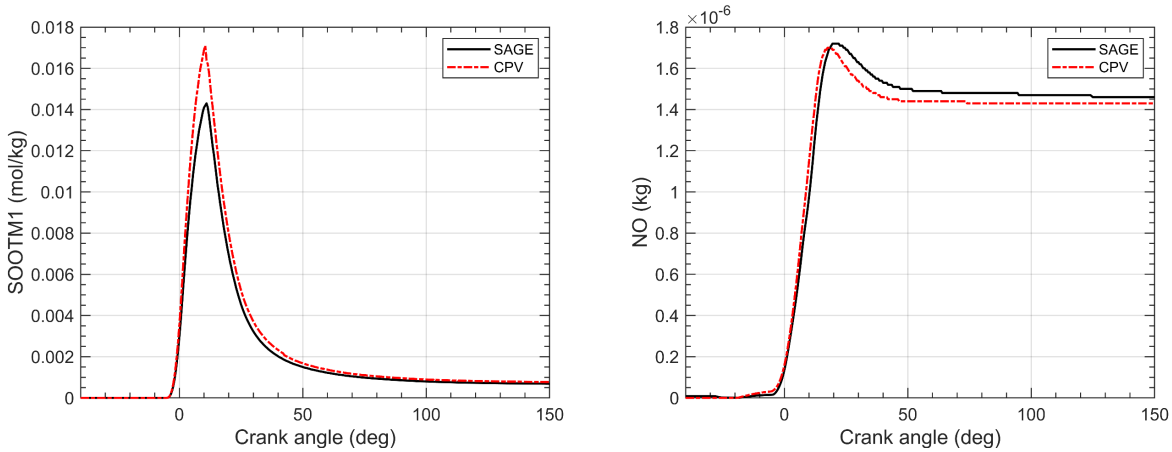


**Figure 6.3.** Online (SAGE) and tabulated (CPV) chemistry solver Soot moment 1 (left) and nitrogen monoxide (right) predictions for Case 01 as noted in Table 6.2.

For both emissions profiles, very good agreement was found during the major emission formation phase as well as at exhaust valve opening, which was set as end of the simulation. The tabulated chemistry-based soot model slightly over predicts the peak soot during the particle inception and dominant surface growth phases (between CAD 0-25). However, the final soot yield at EVO shows to be very close to the value predicted by the online PM soot model. A slight under prediction of the final nitrogen oxide is noted for the tabulated chemistry solver.

To better assess the quality of the tabulated chemistry solver on a cell local basis, contour plots of temperature and parcel representation of the spray are presented in Figure 6.4. The section contours are compared at 10, 50 and 90 percent of the combustion process, noted as CA10, CA50 and CA90, respectively. In the early and mid-position of the combustion phasing, the two solvers present a very close distribution of temperature levels throughout the computational domain. It is important to remind at this point that, although the exact same models and model constants have been used for both runs, sources of discrepancies may still be caused by: (1) the automatic mesh refinement (AMR) algorithm, which by definition adapts the mesh to the evolving combustion process; (2) the adaptive zoning algorithm.

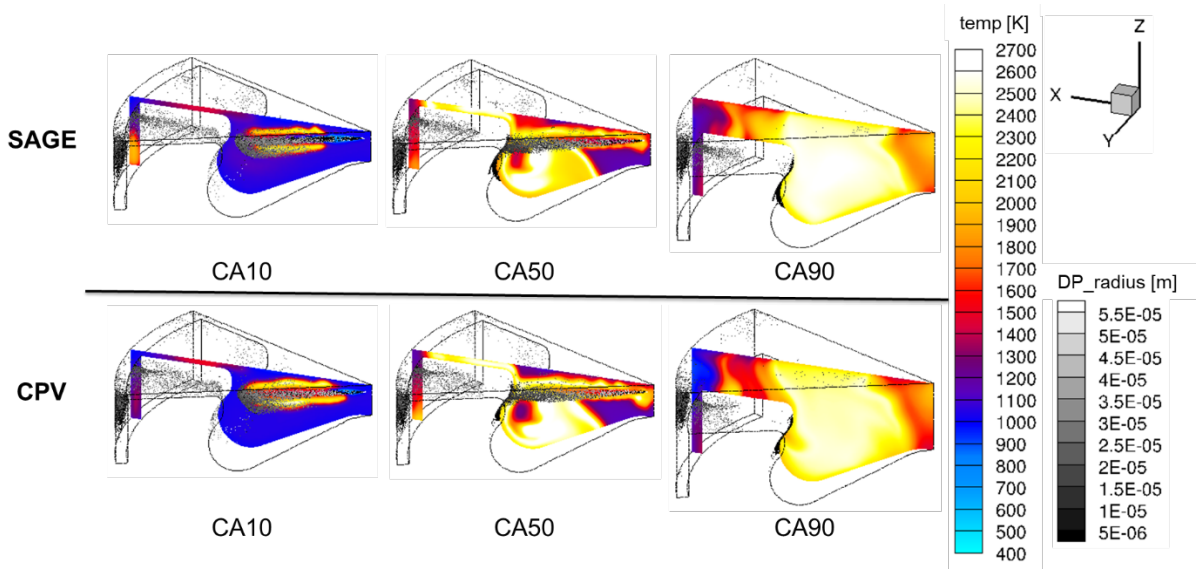


**Figure 6.4.** Comparison of temperature contours and droplet distribution for online (SAGE) and tabulated (CPV) chemistry solver for Case 01 at 10%, 50% and 90% position of the combustion process.

While in the CPV run the chemistry update step is performed in every cell, in the SAGE calculation reactions are solved only for a given number of zones which are computed based on similar values of temperature, equivalence ratio and heat release. Although being very accurate, clustering methods such as the mentioned adaptive zoning algorithm can sometime smear out some auto-ignition events especially during pilot injection heat release, as well as during the premixed peak of the combustion. A fully consistent comparison of such solvers would require a SAGE calculation without the mentioned adaptive zoning algorithm which would in turn cause a noticeable CPU

time increase compared to the present SAGE calculation. In the present thesis, such result is not presented but it will be considered for further validation studies.

In Figure 6.5 and Figure 6.6 in cylinder pressure trace and rate of heat release comparisons between SAGE and CPV are presented for the mid-load high EGR (Case 02) and the high speed, high load (Case 03) operating points. Especially in Case 02 (Figure 6.5) a bigger discrepancy between the predicted rate of heat releases can be noted. Such differences were considered to be acceptable since: 1) the online chemistry has been computed using the adaptive zoning algorithm, 2) the interpolation inaccuracy within the CPV model which is implicitly present in the tabulated chemistry approach. Nevertheless, the presented differences (within 1.5 CAD in ignition onset) are still within an acceptable accuracy range for engineering application and/or design of experiments studies.

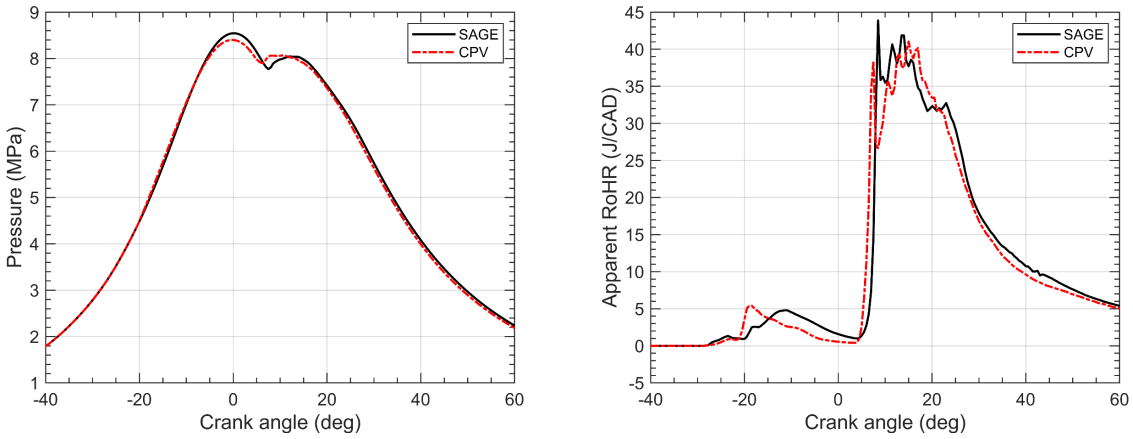


**Figure 6.5.** Online (SAGE) and tabulated (CPV) chemistry solver in-cylinder pressure (left) and apparent rate of heat release (right) histories for Case 02 as noted in Table 6.2.

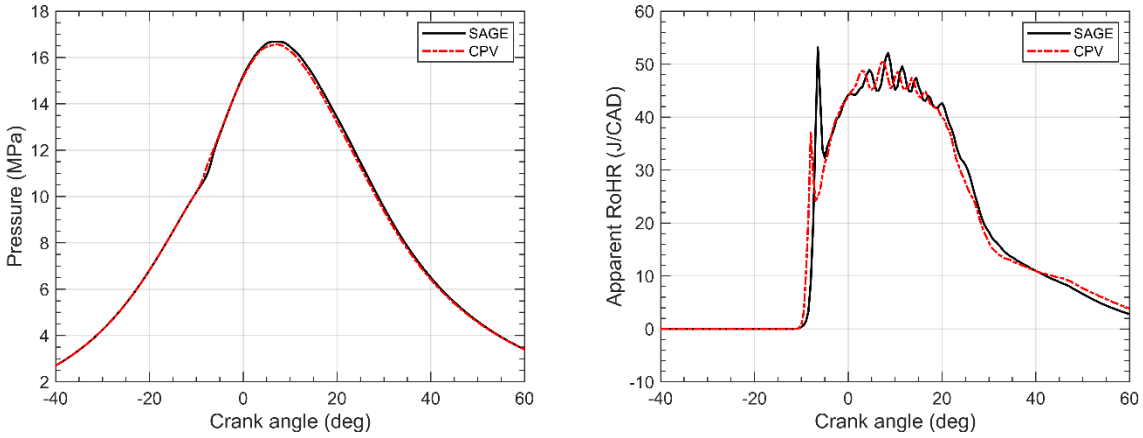


**Figure 6.6.** Online (SAGE) and tabulated (CPV) chemistry solver in-cylinder pressure (left) and apparent rate of heat release (right) histories for Case 02 as noted in Table 6.2.

## 6.2. Computational Performance of CPV in 3-D CFD

Employing a 189 species reaction mechanism and carrying out calculations using the online chemistry solver in parallel on 24 cores (Intel Xeon E5-2687W v4 @ 3.00GHz, from 2016) the SAGE calculation requires a considerably higher number of hours in comparison to the CPV solution. Detailed benchmarks are shown in Table 6.3.

**Table 6.3.** Computational performance of CPV and SAGE solvers in CONVERGE 2.4 on 24 cores, (Intel Xeon E5-2687W v4 @ 3.00GHz, from 2016)

| Case name | SAGE (hours) | CPV (hours) | Speed-up Factor |
|---|---|---|---|
| Case 01 | 12.40 | 1.56 | 7.9 |
| Case 02 | 12.70 | 1.65 | 7.7 |
| Case 03 | 9.52 | 1.25 | 7.6 |

To better understand which process of the simulation is responsible for the reported speed-ups, a CPU-time brake-down has been computed and is shown in Figure 6.7.

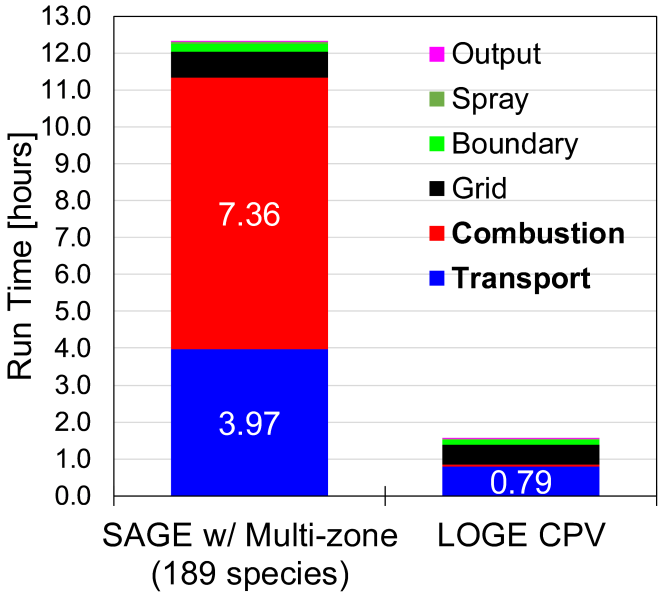


**Figure 6.7.** CPU time brake-down for each sub process of the Case 01 simulation.

It can be noted that the employment of the tabulated chemistry solver reduced the computational time needed for the combustion by almost 99%. Furthermore, given the much lower number of scalars to be transported in the computational domain (189 in SAGE, 15 in CPV), an almost 80% reduction in CPU time needed for the transport step is also noted. The remaining computational costs, such as load balancing, spray, output writing etc. remain completely unchanged as expected. As mentioned in the previous paragraph, the CPV solution resolve the chemistry step in each computational cell, while the SAGE solution uses an adaptive zoning algorithm. The benchmarks

summarized in Table 6.3 do not account for the additional speed-ups that could potentially be obtained by running SAGE without the multi-zone algorithm.

## Chapter 7

# Summary and Outlook

This thesis reported on the formulation and assessment of two methodologies aimed at reducing computational cost of reactive flow simulations using detailed chemistry. The first method, concisely described in Chapter 2 and discussed in paper I, belongs to the mechanism reduction type of methods and focuses on chemical lumping of isomers. The second method, introduced in Chapter 3 and extensively validated in chapters Chapter 5 and Chapter 6, as well as in papers II-V, belongs to a solution mapping-retrieval type of methods. The vast majority of the development and validation efforts were dedicated to the tabulated chemistry solver, hence broader attention has been given to tabulation in the present manuscript in comparison to the lumping method.

In the first part of the PhD studies, a chemical lumping method based on *a priori* thermodynamic data analysis has been proposed. It was applied to the reduction of a large three component reaction mechanism where each isomer group was replaced with one single representative lumped pseudo species. The choice of isomers based on their Gibbs free energy levels, and the hypothesis of equal repartition of rate coefficient within the lumped group, reviled to be acceptable assumptions for such reduction purpose in terms of accuracy loss. The lumped reaction mechanism was extensively tested and compared to the detailed mechanism for a variety of 0-D and 1-D combustion simulations. Even in the very sensitive NTC region, typical of low temperature ignition of large alkane and oxygenated fuel molecules, the lumped mechanism showed to be overall never beyond 12% of the accuracy of detailed mechanism predictions. Furthermore, the resulting lumped mechanism gives an advantageous starting point for additional model reduction steps by species removal techniques, since the main oxidation pathways are mainly kept, while being much more compact. With respect to isomers belonging to class 12, (see [31] for class definition) an additional assumption based on the ring structure has been imposed to improve mechanism accuracy under low temperature combustion regimes. Such assumption was considered necessary since the Gibbs free energy-based assessment resulted in lumping too many species and hence dramatically change the major low temperature pathways.

On the one hand side a ring size-based lumping method, similarly to the Gibbs free energy assessment, can be easily implemented in reduction codes if the molecule structure is known. On the other hand, in many published mechanisms it is not straight forward to derive molecule structure and functional group just based on the species

naming. Hence, this aspect hinders the applicability of the method as a stand-alone tool. Nevertheless, considering that the present methodology aimed to be implemented as a sequential step to be done right after the detailed mechanism generation step, where information on the molecule structures is implicitly known, it was considered acceptable. Furthermore, the most crucial aspect of such methodology remains the quality of the mechanism thermo-data used for each isomer. Potentially, a more accurate set of thermo-data may make the additional ring size-based assumption not necessary and hence remove the dependency of the method on the molecule structure information.

In the second part of the PhD thesis, a progress variable-based method (named CPV, as per combustion progress variable) has been formulated and applied in multiple engine simulation frameworks. Under the assumption of well-stirred reactor, an online chemistry solver, where chemical reactions are computed on-the-fly, was compared to the proposed tabulated chemistry method using different simulation frameworks. Latent enthalpy is chosen as variable for the parametrization of the reaction progress while a dedicated source term based methods are applied to thermal NO formation as well as to soot formation. Initial mixture unburned temperature, pressure, equivalence ratio and EGR are the input variables of the look-up table. Table grid points were chosen to cover the widest possible range of thermodynamic conditions that can be expected to be found in conventional direct injected engines.

Performances of the newly introduced CPV solver were first assessed under homogeneous constant pressure reactor conditions (see Chapter 3). On the one hand side, this analysis was performed to isolate and quantify potential solution accuracy losses due to interpolation. On the other hand, this analysis was instrumental to find the best trade-off between table size vs solution accuracy. A tighter tabulation grid results in a larger file size on disk, which in turn affects the random access memory requirement for the reactive flow simulation during run-time. For the proposed grid resolution, the solution retrieved from the table never exceeded a 6% discrepancy on a single point basis in the initial conditions space (see paragraph 3.4), while the overall error resulted to be approximately 1.5%. The interpolation errors were shown to be higher in the NTC region which is the most challenging area to parametrize [76, 62]. Overall, the presented levels of accuracy were considered an acceptable trade-off and provided good confidence for the subsequent engine simulation campaigns.

In Chapter 5, a stochastic reactor model was used to describe the interaction of chemistry and flow during the engine combustion process. The CPV solver was implemented within the SRM code and compared against the existing online chemistry solver. Model performance, with respect to experimental data and the two chemistry solvers were assessed under passenger car and heavy-duty Diesel engine as well as passenger-car SI engine conditions. The SRM was shown to be capable of mimicking the turbulent mixing controlled combustion as well as flame propagation processes using both chemistry solver. It was found that the main engine performance parameters as well as the main species profiles (CO, $CO_2$, NO and uHC) agree well with the online chemistry runs where chemical reactions are solved during run-time. Minor differences were noticed in terms of start of combustion timing and CO emissions formation between online and CPV solvers. Although still limited to a magnitude of 2.0 CAD,

more noticeable discrepancies between the two solvers were seen in terms of combustion onset at low-load low-speed in both the Diesel and gasoline engine simulation campaigns. This finding was explained by the fact that under these conditions the interpolation error becomes more evident due to fixed point distribution in temperature space. Moreover, depending on how fast or slow the low temperature combustion of the given mechanism is used, the CPV solver accuracy may be hindered by the presence of partially reacted states which are compressed/expanded due to piston motion. This creates a particularly challenging scenario for any progress variable-based method where the initial state is rapidly shifting from one manifold to another. Nevertheless, given the accuracy level shown in the present work, it was concluded that discrepancies between the online and CPV solvers do not affect the predictive capabilities of the 0-D SRM when employed across a vast range of engine operating conditions.

With regard to computational performance, the CPV model was found to be four orders of magnitude faster than the online chemistry solution in the 0-D SRM framework while keeping the same order of chemical and physical models. The proposed approach proved to be a competitive tool, from the computational performance standpoint, with respect to lower order methods (i.e., multizone Vibe models) widely used in 0-D/1-D engine performance studies. Generally, current industrial system simulation practices, as well as driving cycle simulation frameworks, do not include detailed chemistry effects due to their high computational cost. The CPV solver, in conjunction with the SRM framework extended in this work, may allow to include higher order chemical and physical models while keeping a feasible CPU-time.

In Chapter 6 the CPV solver was coupled to a commercial CFD code via user-defined functions and compared against the built-in online solver (referred as SAGE) under 3-D Diesel engine sector simulations. Performance of the newly introduced tabulation methodology was assessed under passenger car Diesel engine conditions using a RANS-based turbulence modeling framework. The comparison against the detailed online chemistry solution was performed not only in terms of major combustion indicators such as pressure and rate of heat release, but also in terms of exhaust emissions like soot and $NO_x$. The CPV solver was shown to be capable of predicting combustion behavior as well emission formation in close agreement with the solution predicted by the SAGE solver. Minor differences (within 1.5 CAD difference in combustion onset) were noted for the mid-load high EGR case in terms of pilot and premixed peak heat release. Such discrepancies may be caused by the fact that the two chemistry solvers are not compared under the exact same conditions. More in detail, the SAGE solution was obtained using the adaptive zoning algorithm, while the CPV simulation computed chemistry in every cell. Such difference may cause a set of error propagation/compensation effects resulting in ignition timing differences within few crank angle degrees, especially under sensitive conditions (i.e., high EGR). Such comparison was still preferred to have the SAGE calculation performed in every cell in order to limit the computational efforts and to compare results with typical setup configurations used in engineering applications.

Although a slight inaccuracy in the computed combustion and emission solution, the CPV solver showed remarkable speed-ups on the same number/type of cores used for the SAGE calculation. While the SAGE calculation required approximately 12 hours

for a single run on 24 cores, the CPV calculation could be performed in about 1.5 hours. As expected by such modelling practices, the tabulated chemistry solver, allowed for much faster evaluation which could lead to consistent reductions in engine development costs, while keeping a good level of confidence on the accuracy of the combustion and emission solution.

Generally, CPU time is one of the main burdens when deployment of detailed chemical mechanisms in 0-D and 3-D CFD simulations is concerned. In particular, if simulations aim to an accurate prediction of exhaust emissions, it often comes a point where a trade-off must be made between computational performances and size of the chemical mechanisms. Employing a tabulated chemistry solver has the potential to break this tread-off, by using the large mechanism only during table generation (a one-time process) while keeping the high fidelity combustion and emission predictive capability. The tabulation strategy presented in this thesis, proved to be a promising solution in both simulation frameworks. However, under low-load, low-speed and high EGR conditions, the CPV solver showed the most noticeable discrepancies in comparison to the detailed online solutions. While interpolation errors are certainly higher under low temperature combustion regimes, the CPV solution accuracy is also limited by the intrinsic high complexity of parametrizing a rapidly changing system due to compression and expansion.

In future works, it is advised to investigate possible automated scaling strategies so that the table look-up retrieval across shifting manifold solutions may be corrected under low temperature combustion regimes. Another area worth to further investigate is the treatment of mixture parametrization under rich conditions ($\phi > 3.0$). The method presented in this thesis, given its latent enthalpy-based formulation, considers as last point in progress variable space the maximum heat release state so to maintain strict monotonicity of the progress variable. Under fuel rich conditions, a rather visible discrepancy may be noted between the last tabulated point and the equilibrium value of latent enthalpy. This effect impacts the accuracy of the retrieved solution in rich cells as well as the soot formation, which mostly occurs under rich conditions. An additional sub-model may be sufficient to compensate for the neglected change in the retrieved progress variable source term. Alternatively, a double progress variable-based method may also be considered for future studies.

# References


[1] L. Meyer, S. Brinkman, L. Van Kesteren, N. Leprince-Ringuet and F. Van Boxmeer, "Climate Change 2014, synthesis report.," IPCC, Geneva, 2014.

[2] N. Hoofman, M. Massagie, J. Van Mierlo and T. Coosemans, "A review of the European passenger car regulations – Real driving emissions vs local air quality," *Renewable and Sustainable Energy Reviews,* no. 86, pp. 1-21, 2018.

[3] J. Jung and S. Alison Park, "Case Study: Volkswagen's Diesel Emissions Scandal," *Thunderbird International Business Review,* vol. 59, pp. 127-137, 2017.

[4] Continental Automotive GmbH, "Worldwide Emissions Standard and Regulations," May 2019. [Online]. Available: https://www.continental-automotive.com/getattachment/8f2dedad-b510-4672-a005-3156f77d1f85/EMISSIONBOOKLET%202019.pdf. [Accessed 15 March 2021].

[5] Polestar, "Polestar.com," September 2020. [Online]. Available: https://www.polestar.com/uk/sustainability/transparency/#:~:text=Being%20transparent%20about%20sustainability&text=That's%20why%20Polestar%20is%20spearheading,transparency%20throughout%20the%20automotive%20industry.&text=And%20communicating%20openly%20abo. [Accessed 20 March 2021].

[6] U. Framer, F. Ortloff, S. Stollenwerk and R. Thee, "Defossilizing the transportation sector," Forschungsvereinigung Verbrennungskraftmaschinen e.V., Frankfurt, 2018.

[7] R. D. Reitz, H. Ogawa, R. Payri and T. Fansler, "IJER editorial: The future of the internal combustion engine," *International Journal of Engine Research,* vol. 21, no. 1, pp. 3-10, 2019.

[8] H. Winner, J. Wiewdemann, F. Gauterin, H. Rottengruber, L. Eckstein, S. Pischinger, R. Baar, P. Elits , K.-L. Krieger, C. Beidl and K. Boulouchos, "WKM. The future of the internal combustion engine / assessment of the Diesel engine situation," Wissenschaftliche Gesellschaft für Kraftfahrzeug- und Motorentechnik e.V. (WKM), 2017. [Online]. Available: https://www.fvv-net.de/fileadmin/user˙upload/medien/aktuelles/WKM˙Position˙The˙Future˙of˙the˙Combustion˙Engine˙2017-09-13.pdf.

[9] P. Senecal and F. Leach, "Diversity in transportation: Why a mix of propulsion technologies is the way forward for the future fleet," *Results in Engineering,* vol. 4, p. 100060, 2019.

[10] European Environment Agency, "New registrations of electric vehicles in Europe," 03 December 2020. [Online]. Available: https://www.eea.europa.eu/data-and-maps/indicators/proportion-of-vehicle-fleet-meeting-5/assessment. [Accessed 10 April 2021].

[11] European automobile manufacturers assosiation, "Average age of the EU vehicle fleet," February 2021. [Online]. Available: https://www.acea.be/statistics/article/average-vehicle-age#:˜:text=EU%20cars%20are%20now%20on,the%20EU%20is%2011.6%20years.. [Accessed 10 April 2021].

[12] M. Pasternak, A. Matrisciano, L. Seidel, C. Klauer and F. Mauss, "Simulation of Diesel surrogate fuels performance under engine conditions using 0D engine – fuel test bench," in *Proceedings of COMODIA, MS2-1*, Fukuoka, 2012.

[13] T. Franken, A. Duggan, A. Matrisciano, H. Lehtiniemi, A. Borg and F. Mauss, "Multi-Objective Optimization of Fuel Consumption and NOx Emissions with Reliability Analysis Using a Stochastic Reactor Model," in *SAE Technical Paper 2019-01-1173*, Detroit, 2019.

[14] T. Lu and C. K. Law, "Toward accommodating realistic fuel chemistry in large-scale computations," *Progress in Energy and Combustion Science,* vol. 35, no. 2, p. 192–215, 2009.

[15] L. Seidel, C. Netzer, A. Matrisciano , M. Hilbig, C. Klauer, M. Pasternak and F. Mauss, "Systematic Reduction of Detailed Chemical Reaction Mechanisms for Engine Applications," *ASME Journal of Engineering for Gas Turbines and Power,* vol. 139, no. 9, p. 091701–9, 2017.

[16] "ECCO-MATE - Experimental and Computational Tools for Combustion Optimization in Marine and Automortive Engines," FP7-PEOPLE-2013-ITN, 2014. [Online]. Available: http://ecco-mate.eu/. [Accessed 02 December 2020].

[17] Energimyndigheten, "Swecris," 01 2020. [Online]. Available: https://www.swecris.se/betasearch/details/project/P393682Energi?lang=en . [Accessed 10 April 2021].

[18] Lund Combustion Engineering - LOGE AB, "LOGEsoft Products," Lund Combustion Engineering - LOGE AB, 2020. [Online]. Available: https://logesoft.com/home/products/. [Accessed 03 December 2020].

[19] T. Franken, L. Seidel, A. Matrisciano, M. S. Gern, M. Kauf and A. C. Kulzer, "Gasoline engine performance simulation of water injection and low-pressure exhaust gas recirculation using tabulated chemistry," *International Journal of Engine Research,* vol. 21, no. 10, pp. 1857-1877, 2020.

[20] K. Richards, P. Senecal and E. Pomraning, *CONVERGE (v2.4), Convergent Science, Inc, Madison, WI,* 2018.

[21] T. Poinsot and D. Veynante, Theoretical and numerical combustion, R.T. Edwards Inc. , 2005.

[22] M. P. Halstead, L. J. Kirsch and C. P. Quinn, "The autoignition of hydrocarbon fuels at high temperatures and pressures," *Combustion and Flame,* vol. 30, pp. 45-60, 1977.

[23] S. S. Sazhin, E. M. Sazhina, M. R. Heikal, C. Marooney and S. V. Mikhalovsky, "The shell autoignition model: a new mathematical formulation," *Combustion and Flame,* vol. 117, no. 3, pp. 529-540, 1999.

[24] E. M. Sazhina, S. S. Sazhin, M. R. Heikal and C. J. Marooney, "The Shell autoignition model: applications to gasoline and diesel fuels," *Fuel,* vol. 78, no. 4, pp. 389-401, 1999.

[25] C. K. Law, Combustion Physics, Cambridge University Press, 2006.

[26] W. Yuan , Y. Li and F. Qi, "Challenges and Perspectives of Combustion Chemistry Research," *Science China Chemistry,* vol. 60, no. 11, pp. 1391-1401, 2017.

[27] H. Wang and D. A. Sheen, "Combustion kinetic model uncertainty quantification, propagation," *Progress in Energy and Combustion Science,* vol. 47, pp. 1-31, 2014.

[28] S. J. Klippenstein, "From Theoretical Reaction Dynamics to Chemical Modeling of Combustion," *Proceedings of the Combustion Institute,* vol. 36, no. 1, pp. 77-111, 2017.

[29] A. Konnov, "Yet another kinetic mechanism for hydrogen combustion," *Combustion and Flame,* vol. 203, pp. 14-22, 2019.

[30] C. Netzer, L. Seidel, F. Ravet and F. Mauss, "Impact of the Surrogate Fromulation on 3D CFD Egnien Knock Prediction Using Detailed Chemistry," *Fuel,* vol. 254, p. 115678, 2019.

[31] H. Curran, P. Gaffuri, W. J. Pitz and C. K. Westbrook, "A Comprehensive Modeling Study of n-Heptane Oxidation," *Combustion and Flame,* vol. 114, no. 1-2, pp. 149-177, 1998.

[32] H. Curran, P. Gaffuri, W. J. Pitz and C. K. Westbrook, "A Comprehensive Modeling Study of iso-Octane Oxidation," *Combustion and Flame,* vol. 129, no. 3, pp. 253-280, 2002.

[33] M. Hilbig, L. Seidel, X. Wang, F. Mauss and T. Zeuch , "Computer Aided Detailed Mechanism Generation for large Hydrocarbons: n-decane," in *23rd ICDERS 2011:24-27*, Irvine, 2011.

[34] M. Hilbig, Z. Malliotakis, L. Seidel , G. Vourliotakis, G. Keramiotis, F. Mauss and M. Founti, "The Effect of Base Chemistry choice in a generated n-hexane Oxidation Model using an Automated Mechanism Generator," *International Journal of Chemical Kinetics,* vol. 51, no. 10, pp. 786-798, 2019.

[35] R. van de Vijver, N. M. Vandewiele, P. L. Bhoorasingh, B. L. Slakman, F. S. Khanshan and H. H. Carstensen, "Automatic Mechanism and Kinetic Model Generation for Gas- and Solution-Phase Processes: A Perspective on Best Practices, Recent Advances, and Future Challenge," *International Journal of Chemical Kinetics,* vol. 47, no. 4, pp. 199-231, 2015.

[36] U. Maas and S. B. Pope, "Simplifying chemical kinetics: Intrinsic low-dimensional manifolds in composition space," *Combustion and Flame,* vol. 88, no. 3-4, pp. 239-264, 1992.

[37] S. H. Lam and D. A. Goussis, "The CSP method for simplifying kinetics," *International Journal of Chemical Kinetics,* vol. 26, no. 4, pp. 461-486, 1994.

[38] P. Pepiot-Desjardins and H. Pitsch, "An automatic chemical lumping method for the reduction of large chemical kinetic mechanisms," *Combustion Theory and Modelling,* vol. 12, no. 6, pp. 1089-1108, 2008.

[39] A. Tomlin, L. Genyuan, H. Rabitz and J. Toth, "The Effect of Lumping and Expanding on Kinetic Differential Equations," *SIAM Journal on Applied Mathematics,* vol. 57, no. 6, pp. 1531-1556, 1997.

[40] H. Huang, M. Fairweather, J. F. Griffiths, A. S. Tomlin and R. B. Brad, "A systematic lumping approach for the reduction of comprehensive kinetic models," *Proceedings of the Combustion Institute,* vol. 30, no. 1, pp. 1309-1316, 2005.

[41] S. P. Zeppieri, S. D. Klotz and F. L. Dryer, "Modeling concepts for larger carbon number alkanes: A partially reduced skeletal mechanism for n-decane oxidation and pyrolysis," *Proceedings of the Combustion Institute,* vol. 28, no. 2, pp. 1587-1595, 2000.

[42] M. Chaos, A. Kazakov, Z. Zhao and F. L. Dryer, "A high-temperature chemical kinetic model for primary reference fuels," *International Journal of Chemical Kinetics,* vol. 39, no. 7, pp. 399-414, 2007.

[43] E. Ranzi , M. Dente, A. Goldaniga, G. Bozzano and T. Faravelli, "Lumping procedures in detailed kinetic modeling of gasification, pyrolysis, partial oxidation and combustion of hydrocarbon mixtures," *Progress in Energy and Combustion Science,* vol. 27, no. 1, pp. 99-139, 2001.

[44] M. Frenklach, "Computer modeling of infinite reaction sequences: A chemical lumping," *Chemical Engineering Science,* vol. 40, no. 10, pp. 1843-1849, 1985.

[45] S. S. Ahmed, F. Mauss, G. Moreac and T. Zeuch, "A comprehensive and compact n-heptane oxidation model derived using chemical lumping," *Physical Chemistry Chemical Physics,* vol. 9, no. 9, pp. 1107-1126, 2007.

[46] W. Hentschel, K. Schindler and O. Haanhtela, "European Diesel Research IDEA-Experimental Results from DI Diesel Engine Investigations," in *SAE Technical Paper 941954*, Detroit, 1994.

[47] X. Wang, "Kinetic mechanism of surrogates for biodiesel," PhD thesis, Brandenburg Technical University Cottbus-Senftenberg, Cottbus, 2017.

[48] A. Matrisciano, M. Pasternak, X. Wang, O. Antoshkiv, P. Berg and F. Mauss, "On the Performance of Biodiesel Blends - Experimental Data and Simulations Using a Stochastic Fuel Test Bench," in *SAE Technical Paper 2014-01-1115*, Detroit, 2014.

[49] C. K. Westbrook, W. J. Pitz, O. Herbinet, H. J. Curran and E. J. Silke, "A comprehensive detailed chemical kinetic reaction mechanism for combustion of n-alkane hydrocarbons from n-octane to n-hexadecane," *Combustion and Flame,* vol. 156, no. 1, pp. 181-199, 2009.

[50] O. Herbinet, W. J. Pitz and C. K. Westbrook, "Detailed chemical kinetic mechanism for the oxidation of biodiesel fuels blend surrogate," *Combustion and Flame,* vol. 154, no. 5, pp. 893-908, 2010.

[51] L. Seidel, "Development and Reduction of a Multicomponent Reference Fuel for Gasoline," PhD thesis, Brandenburg University of Technology Cottbus-Senftenberg, Cottbus, 2017.

[52] LOGE AB - Lund Combustion Engineering, "LOGE Products," 2020. [Online]. Available: www.logesoft.com/loge-software/. [Accessed 02 December 2020].

[53] S. Pope, "Small scales, many species and the manifold challenges of turbulent combustion," *Proceedings of the Combustion Institute,* vol. 34, no. 1, pp. 1-31, 2013.

[54] B. Fiorina, D. Veynante and S. Candel, "Modeling Combustion Chemistry in Large Eddy," *Flow Turbulence and Combustion,* vol. 94, no. 1, pp. 3-42, 2015.

[55] O. Giquel, N. Darabiha and D. Thevenin, "Laminar premixed hydrogen/air counterflow flame simulations using flame prolongation of ILDM with differential diffusion," *Proceedings of the Combustion Institute,* vol. 28, no. 2, pp. 1901-1908, 2000.

[56] N. Peters, "Laminar diffusion flamelet models in non-premixed turbulent combustion," *Progress in Energy an Combustion Science,* vol. 10, no. 3, pp. 319-339, 1984.

[57] D. Bradley, P. Gaskell and X. Gu, "The modeling of aerodynamic strain rate and flame curvature effects in premixed turbulent combustion," *Symposium (International) on Combustion,* vol. 27, no. 1, pp. 849-856, 1998.

[58] H. Lehtiniemi, F. Mauss, M. Balthasar and I. Magnusson, "Modeling diesel spray ignition using detailed chemistry with a progress variable approach," *Combust Science and Technology,* vol. 178, no. 10-11, pp. 1977-1997, 2006.

[59] H. Lehtiniemi, Y. Zhang, R. Rawat and F. Mauss, "Efficient 3-D CFD Combustion Modeling with Transient Flamelet Models," in *SAE Technical Paper 2008-01-0957*, Detroit, 2008.

[60] C. Pierce and P. Moin, "Progress-variable approach for large-eddy simulation of non-premixed turbulent combustion," *Journal of Fluid Mechanics,* vol. 504, pp. 73-97, 2004.

[61] B. Fiorina, O. Giquel, L. Vervisch, S. Carpentier and N. Darabiha, "Premixed turbulent combustion modeling using tabulated detailed chemistry and PDF," *Proceedings of the Combustion Institute,* vol. 30, no. 1, pp. 867-874, 2005.

[62] C. Bekdemir, L. Somers, L. de Goey, J. Tillou and C. Angelberger, "Predicting diesel combustion characteristics with Large-Eddy Simulations including tabulated chemical kinetics," *Proceedings of the Combustion Institute,* vol. 34, no. 2, pp. 3067-3074, 2013.

[63] C. Bekdemir, L. Somers and L. de Goey, "Modeling diesel engine combustion using pressure dependent flamelet generated manifolds," *Proceedings of the Combustion Institute,* vol. 33, no. 22, pp. 2887 - 2894, 2011.

[64] B. Franzelli, B. Fiorina and N. Darabiha, "A tabulated chemistry method for spray combustion," *Proceedings of the Combustion Instiute,* vol. 34, no. 1, pp. 1659-1666, 2013.

[65] A. Karlsson, I. Magnusson, M. Balthasar and F. Mauss, "Simulation of Soot Formation Under Diesel Engine Conditions Using a Detailed Kinetic Soot Model," in *SAE Technical Paper 981022*, Detroit, 1998.

[66] G. Nakov, F. Mauss, P. Wenzel, R. Steiner, C. Krueger, Y. Zhang, R. Rawat, A. Borg, C. Perlman, K. Froejd and H. Lehtiniemi, "Soot Simulation under Diesel Engine Conditions Using a Flamelet Approach," *SAE International Journal of Engines,* vol. 2, no. 2, pp. 89-104, 2010.

[67] G. Nakov, F. Mauss, P. Wenzel and C. Krueger, "Application of a stationary flamelet library based CFD soot model for low-NOx diesel combustion," in *Proceedings of THIESEL Conference on Thermo- and Fluid Dynamic Processes in Diesel Engines*, Valencia, 2010.

[68] P. Wenzel, S. Rudiger, C. Krueger, R. Schiessl, C. Hofrath and U. Maas, "3D-CFD Simulation of DI-Diesel Combustion Applying a Progress Variable

Approach accounting for Detailed Chemistry," in *SAE Technical Paper 2007-01-4137*, Detroit, 2007.

[69] A. Chatzopoulos and S. Rigopoulos, "A chemistry tabulation approach via Rate-Controlled Constrained Equilibrium (RCCE) and Artificial Neural Networks (ANNs), with application to turbulent non-premixed CH4/H2/N2 flames," *Proceedings of the Combustion Institute,* vol. 34, no. 1, pp. 1465-1473, 2013.

[70] S. Weise, S. Popp, D. Messig and C. Hasse, "A Computationally Efficient Implementation of Tabulated Combustion Chemistry based on Polynomials and Automatic Source Code Generation," *Flow, Turbulence and Combustion,* vol. 100, no. 1, pp. 119-146, 2018.

[71] S. Breda, A. D'Adamo, S. Fontanesi, N. Giovannoni, F. Testa, A. Irimescu, S. Merola, C. Tornatore and G. Valentino, "CFD Analysis of Combustion and Knock in an Optically Accessible GDI Engine," *SAE Int. J. Engines,* vol. 9, no. 1, pp. 641-656, 2016.

[72] J. Lingenwood and P. Wu, "Correlation of Autoignition Phenomena in Internal Comustion Engines and Rapid Compression Machines," *Symposium (International) on Combustion,* vol. 5, no. 1, pp. 347-356, 1955.

[73] F.-A. Lafossas, M. Castagne, J. Dumas and S. Henriot, "Development and Validation of a Knock Model in Spark Ignition Engines Using a CFD code," in *SAE Technical Paper 2002-01-2701*, Detroit, 2002.

[74] A. Pires da Cruz, "Three-Dimensional Modeling of Self-Ignition in HCCI and conventional Diesel Engines," *Combustion Science and Technology,* vol. 176, no. 5-6, pp. 867-887, 2004.

[75] O. Colin, A. Pires da Cruz and S. Jay, "Detailed chemistry-based auto-ignition model including low temperature phenomena applied to 3-D engine calculations," *Proceedings of the Combustion Institute,* vol. 30, no. 2, pp. 2649-2656, 2005.

[76] V. Knop, J.-B. Michel and O. Colin, "On the use of a tabulation approach to model auto-ignition during flame propagation in SI engines," *Applied Energy,* vol. 88, no. 12, pp. 4968-4979, 2011.

[77] S. Bougrine, S. Richard, J.-B. Michel and D. Veynante, "Simulation of CO and NO emissions in a SI engine using a 0D coherent flame model coupled with a tabulated chemistry approach," *Applied Energy,* vol. 113, pp. 1199-1215, 2014.

[78] S. Mosbach, A. Aldawood and M. Kraft, "Real-Time Evaluation of a Detailed Chemistry HCCI Engine Model Using a Tabulation Technique," *Combustion Science and Technology,* vol. 180, no. 7, pp. 1263-1277, 2008.

[79] J. Leicher, S. Wirtz and V. Scherer, "Evaluation of an Entropy-Based Combustion Model using Stochastic Reactors," *Chemical Engineering Technology,* vol. 31, no. 7, pp. 935-1071, 2008.

[80] A. Dulbecco, F. Lafossas, G. Mauviot and T. Poinsot, "A New 0D Diesel HCCI Combustion Model Derived from a 3D CFD Approach with Detailed Tabulated Chemistry," *Oil and Gas Science and Technology,* vol. 64, no. 3, pp. 259-284, 2009.

[81] F. Bozza, V. De Bellis and L. Teodosio, "A Tabulated-Chemistry Approach Applied to a Quasi-Dimensional Combustion Model for a Fast and Accurate Knock Prediction in Spark-Ignition Engines," *SAE Technical Paper 2019-01-0471,* 2019.

[82] M. Ihme, L. Shuun and J. Zhang, "Regularization of reaction progress variable for application," *Journal of Computational Physics,* vol. 231, no. 1, pp. 7715-7721, 2012.

[83] Y.-S. Niu, L. Vervisch and P. D. Tao, "An Optimization-based Approach to Detailed Chemistry Tabulation: Automated Progress Variable Definition," *Combustion and Flame,* vol. 160, no. 4, pp. 776-758, 2013.

[84] U. Pruefert, F. Hunger, D. Messig, M. Eiermann and C. Hasse, "A Constrained Control Approach for the Automated Choice of an Optimal Progress Variable for Chemistry Tabulation," *Flow, Turbulence and Combustion,* vol. 94, no. 3, pp. 593-617, 2015.

[85] G. Mauviot, A. Albrecht and T. J. Poinsot, "A New 0D Approach for Diesel Combustion Modeling Coupling Probability Density Function with Complex Chemistry," in *SAE Technical Paper 2006-01-3332*, Detroit, 2006.

[86] J. A. van Oijen, A. Donini, R. M. Bastiaans, J. ten Thieje Boonkkamp and L. de Goey, "State-of-the-art in premixed combustion modeling using flamelet generated manifolds," *Progress in Energy and Combustion Science,* vol. 57, pp. 30-74, 2016.

[87] M. Ihme and H. Pitsch, "Prediction of extinction and reignition in nonpremixed turbulent flames using a flamelet/progress variable model: 1. A priori study and presumed PDF closure," *Combustion and Flame,* vol. 155, no. 1-2, pp. 70-89, 2008.

[88] J. van Oijen, R. Bastiaans and L. de Goey, "Modeling Preferential Diffusion effects in Premixed Methane-Hydrogen-Air flames by using Flemelet-Generated Manifolds," in *ECCOMAS CFD 2010*, Lisbon, 2010.

[89] T. Zeuch, G. Moreac, S. S. Ahmes and F. Mauss, "A comprehensive skeletal mechanism for the oxidation of n-heptane generated by chemistry-guided reduction," *Combustion and Flame,* vol. 155, no. 4, pp. 651-674, 2008.

[90] F. Mauss, Entwicklung eines kinetischen Modells der Rußbildung mit schneller Polymerisation, PhD thesis, Rheinisch-Westfälische Technische Hochschule Aachen, Germany, 1998.

[91] T. Zeuch, G. Moreac, S. Ahmed and F. Mauss, "A comprehensive skeletal mechanism for the oxidation of n-heptane generated by chemistry-guided reduction," *Combustion and Flame,* vol. 155, no. 4, p. 651 – 674, 2008.

[92] A. Matrisciano, T. Franken, C. Perlman, A. Borg, H. Lehtiniemi and F. Mauss, "Development of a Computationally Efficient Progress Variable Approach for a Direct Injection Stochastic Reactor Model," in *SAE Technical Paper 2017-01-0512*, Detroit, 2017.

[93] H. Lehtiniemi, K. Netzell and F. Mauss, "Aspects of Modeling Soot Formation in Turbulent Diffusion Flames," *Combust Science and Technology,* vol. 178, no. 10-11, p. 1871–1885, 2006.

[94] M. Pasternak, F. Mauss, C. Perlman and H. Lehtiniemi, "Aspects of 0D and 3D Modeling of Soot Formation for Diesel Engines," *Combust Science and Technology,* vol. 186, no. 10-11, pp. 1517-1535, 2014.

[95] A. Matrisciano, A. Borg, C. Perlman, H. Lehtiniemi and F. Mauss, "Soot Source Term Tabulation Strategy for Diesel Engine Simulations with SRM," in *SAE Technical Paper 2015-24-2400*, Naples, 2015.

[96] M. Frenklach and H. Wang, "Detailed Modeling of Soot Particle Nucleation and Growth," *Proceedings of the Combustion Institute,* vol. 23, no. 1, pp. 1559-1566, 1991.

[97] M. Frenklach, "Method of moments with interpolative closure," *Chemical Engineering Science,* vol. 57, no. 12, pp. 2229-2239, 2002.

[98] C. Schuetz and M. Frenklach, "Nucleation of soot: molecular dynamics simulations of pyrene dimerization," *Proceedings of the Combustion Institute,* vol. 29, no. 2, pp. 2307-2314, 2002.

[99] M. Balthasar, F. Mauss, A. Knobel and M. Kraft, Soot Formation in Turbulent Reacting Flows - a PDF Based Approach Applied to Carbon Black Production, Technical Report 1,c4e-Preprint Series, Cambridge, 2000.

[100] A. Kazakov and M. Frenklach, "Dynamic modeling of soot particle coagulation and aggregation: Implementation with the method of moments and application to high-pressure laminar premixed flames," *Combustion and Flame,* vol. 114, no. 3-4, pp. 481-501, 1998.

[101] H. Wang, "Formation of nascent soot and other condensed-phase materials in flames," *Proceedings of the Combustion Institute,* vol. 33, no. 1, pp. 41-67, 2011.

[102] Y. Zel'dovich, "The Oxidation of Nitrogen in Combustion Explosions," *Acta Physicochimica U.S.S.R. ,* vol. 21, p. 577–628, 1946.

[103] Y. Zeldovich, D. Frank-Kamenetskii and P. Sadovniko, Oxidation of nitrogen in combustion, Publishing House of the Academy of Sciences of USSR, 1947.

[104] M. Kraft, "Stochastic Modelling of Turbulent Reacting Flow in Chemical Engineering," PhD thesis, VDI Verlag, Fortschrittsberichte des VDI, Dusseldorf, 1998.

[105] M. Tuner, "Stochastic Reactor Models for Engine Simulations," PhD thesis, Lund University, Lund, 2008.

[106] J. Heywood, Internal Combustion Engine Fundamentals, New York: McGraw-Hill, 1988.

[107] A. Bhave and M. Kraft, "Partially stirred reactor model: Analytical solutions and numerical convergence study of a PDF MonteCarlo method," *SIAM Journal on Scientific Computing,* vol. 25, no. 5, pp. 1798-1823, 2004.

[108] K. Samuelsson, A. Gogan, K. Netzell, H. Lehtiniemi and F. Mauss , "Modeling Diesel Engine Combustion and Pollutant Formation Using a Stochastic Reactor Model Approach," in *International Conference on Clean Diesel Combustion*, Lund, 2005.

[109] S. B. Pope, "PDF methods for turbulent reactive flows," *Progress in Energy and Combustion Science,* vol. 11, no. 2, pp. 119-192, 1985.

[110] P. Maigaard, F. Mauss and M. Kraft, "Homogenous charge compression ignition engine: A simulation study on the effect of in-homogeneities," *ASME Journal of Engineering and Gas Turbines,* vol. 125, no. 2, pp. 466-471, 2003.

[111] LOGE AB, LOGEsoft v.1.10 - Manual book 3 - Engine models, Lund, 2018.

[112] N. Peters, Turbulent Combustion, Cambridge: Cambridge University Press, 2000.

[113] H. Kolla, J. Rogerson, N. Chakraborty and N. Swaminathan, "Scalar Dissipation Rate Modeling and its Validation," *Combustion Science and Technology,* vol. 181, no. 3, pp. 518-535, 2009.

[114] S. Bjerkborn, K. Frojd, C. Perlman and F. Mauss, "A Monte Carlo Based Turbulent Flame Propagation Model for Predictive SI In-Cylinder Engine Simulations Employing Detailed Chemistry for Accurate Knock Prediction," *SAE International Journal of Engines,* vol. 5, no. 4, pp. 1637-1647, 2012.

[115] M. Pasternak, F. Mauss, M. Sens, M. Riess, A. Benz and K. G. Stapf, "Gasoline engine simulations using zero-dimensional spark ignition stochastic reactor model and three-dimensional computational fluid dynamics engine

model," *International Journal of Engine Research,* vol. 17, no. 1, pp. 76-85, 2015.

[116] T. Franken , C. Netzer, A. Matrisciano, M. Pasternak, L. Seidel, F. Mauss, A. Borg, H. Lehtiniemi and A. Kulzer, "Multi-objective optimization of water injection in spark-ignition engines using the stochastic reactor model with tabulated chemistry," *International Journal of Engine Research,* vol. 20, no. 10, pp. 1089-1100, 2019.

[117] M. Pasternak, F. Mauss, C. Klauer and A. Matrisciano, "Diesel engine performance mapping using a parametrized mixing time model," *International Journal of Engine Research,* vol. 19, no. 2, pp. 202-2013, 2017.

[118] P. Kozuch, "Phenomenological model for a combined nitric oxide and soot emission calculation in di diesel engines," PhD thesis, University of Stuttgart, Stuttgart, 2004.

[119] A. Dulbecco, S. Richard, O. Laget and P. Aubret, "Development of a Quasi-Dimensional K-k Turbulence Model for Direct Injection Spark Ignition (DISI) Engines Based on the Formal Reduction of a 3D CFD Approach," in *SAE Technical Paper 2016-01-2229*, Detroit, 2016.

[120] M. Pasternak, "Simulation of the Diesel Engine Combustion Process Using the Stochastic Reactor Model," PhD thesis, Brandenburg University of Technology Cottbus-Senftenberg, Cottbus, 2015.

[121] T. Franken and F. Mauss, "Development of a Methodology for Predictive Diesel Combustion Simulation using a 0D Stochastic Reactor Model," in *SAE Technical Paper 2016-01-0566*, Detroit, 2016.

[122] T. Franken, A. Sommerhoff, W. Willems, A. Matrisciano, H. Lehtiniemi, A. Borg, C. Netzer and F. Mauss, "Advanced Predictive Diesel Combustion Simulation Using Turbulence Model and Stochastic Reactor Model," in *SAE Technical Paper 2017-01-0516*, Detroit, 2017.

[123] R. L. Curl, "Dispersed Phase Mixing: 1.Theory and Effects in Simple Reactors," *AIChE Journal,* vol. 9, no. 2, pp. 175-181, 1963.

[124] S. Subramaniam and S. B. Pope, "A mixing model for turbulent reactive flows based on Euclidean minimum spanning trees," *Combustion and Flame,* vol. 115, no. 1, pp. 487-514, 1998.

[125] A. Bhave, M. Balthasar, M. Kraft and F. Mauss, "Analysis of a natural gas fuelled homogeneous charge compression ignition engine with exhaust gas recirculation using a stochastic reactor model," *International Journal of Engine Research,* vol. 5, no. 1, pp. 93-103, 2004.

[126] T. Franken, A. Matrisciano, C. Klauer, M. Kienberg and F. Mauss, "Prediction of thermal stratification in an engine-like geometry using a zero-dimensional stochastic reactor model," *International Journal of Engine Research,* vol. 21, no. 9, pp. 1750-1763, 2019.

[127] G. Woschni, "A Universally Applicable Equation for the Instantaneous Heat Transfer Coefficient in the Internal Combustion Engine," in *SAE Technical Paper 670931*, Detroit, 1967.

[128] T. Echekki and E. Mastorakos, Turbulent Combustion Modeling - Advances, new trends and perspectives. Fluid Mechanics and Its Applications, Springer-Verlag, 2011.

[129] N. Peters, "Multiscale combustion and turbulence," *Proceedings of the Combustion Institute,* vol. 32, no. 1, pp. 1-25, 2009.

[130] D. C. Haworth, "Progress in probability density function methods for turbulent reacting flows," *Progress in Energy and Combustion Science,* vol. 36, no. 2, pp. 168-256, 2010.

[131] P. Senecal, E. Pomraning and K. Richards, "Multi-Dimensional Modeling of Direct-Injection Diesel Spray Liquid Length and Flame Lift-off Length using CFD and Parallel Detailed Chemistry," in *SAE Technical Paper 2003-01-1043*, Detroit, 2003.

[132] Lawrence Livermore National Laboratory, "SUNDIALS," [Online]. Available: https://computation.llnl.gov/casc/sundials/main.html. [Accessed April 2020].

[133] Lawrence Livermore National Laboratory, "SuperLU Users' Guide," [Online]. Available: http://crd.lbl.gov/~xiaoye/SuperLU/. [Accessed April 2020].

[134] A. Babajimopoulos, D. Assanis, D. Flowers, S. Aceves and R. Hessel, "A Fully Coupled Computational Fluid Dynamics and Multi-Zone Model with Detailed Chemical Kinetics for the Simulation of Premixed Charge Compression Ignition Engines," *International Journal of Engine Research,* vol. 6, no. 5, pp. 497-512, 2005.

[135] Sandia National Laboratories, "Engine combustion network fuels.," [Online]. Available: https://ecn.sandia.gov/diesel-spray-combustion/sandia-cv/fuels/. [Accessed 20 April 2020].

[136] M. Kauf, M. Gern and S. Seefeldt, "Evaluation of Water Injection Strategies for NOx Reduction and Charge Cooling in SI Engines," in *SAE Technical Paper 2019-01-2164*, Detroit, 2019.

[137] C. Netzer, T. Franken, L. Seidel, H. Lehtiniemi and F. Mauss, "Numerical Analysis of the Impact of Water Injection on Combustion and Thermodynamics in a Gasoline Engine Using Detailed Chemistry," *SAE International Journal of Engines,* vol. 11, no. 6, pp. 1151-1166, 2018.

[138] T. Franken, L. Seidel, A. Matrisciano, F. Mauss, A. C. Kulzer and F. Schuerg, "Analysis of the Water Addition Efficiency on Knock Suppression for Different Octane Ratings," in *SAE Technical Paper 2020-01-0551*, Detroit, 2020.

[139] F. Ravet, L. Dutofoy, B. Rathinam, H. Lehtiniemi, L. Seidel, C. Netzer and F. Mauss, "Soot modeling with Particle sectional model (PSM) in diesel engine. Results and discussion.," in *Proceedings of THIESEL 2016: conference on thermo-and fluid dynamic processes in direct injection engines*, Velencia, 2016.

[140] R. Reitz and F. Bracco, "Mechanisms of Breakup of Round Liquid Jets," *The Encyclopedia of Fluid Mechanics,* vol. 3, pp. 223-249, 1986.

[141] P. Senecal, K. Richards, E. Pomraning, T. Yang, M. Dai, R. McDavid, M. Patterson, S. Hou and T. Shethaji, "A New Parallel Cut-Cell Cartesian CFD Code for Rapid Grid Generation Applied to In-Cylinder Diesel Engine Simulations," in *SAE Technical Paper 2007-01-0159*, Detroit, 2007.

# Summary of Papers and Author Contribution

**Paper I: An *a priori* Thermodynamic Data Analysis based Chemical Lumping Method for the Reduction of Large and Multi-component Chemical Kinetic Mechanisms.**

**Matrisciano A.**, Seidel L., Mauss F.
Submitted to International Journal of Chemical Kinetics journal

**Summary.** This paper reports on the development and application of a lumping technique developed for the reduction of large multi-component reaction mechanisms. The lumping strategy was based on an a priori analysis of the Gibbs free energy of the isomers of a detailed mechanism having oxidation paths for three main fuel molecules (*n*-decane, alpha-methylnaphthalene and methyl decanoate) and comprising 807 species and 7807 reactions. A total of 74 isomer groups were identified within the oxidation of *n*-decane and methyl decanoate. The lumping procedure led to a mechanism of 463 species and 7600 reactions, whose performances were compared against the detailed version over several reactor conditions and over a broad range of temperature, pressure and equivalence ratio. In all cases, very good agreement between the predictions obtained using the lumped and the detailed mechanism were observed with an overall absolute error below 12%.

**Author contribution.** I investigated different lumping techniques and eventually developed the Gibbs free energy-based analysis. I then implemented a series of bash scripts to automate the lumping process and apply it to the mentioned reaction mechanism, which was developed prior to my work by Wang X., Seidel L. and Mauss F. Once the lumping technique was in place, I ran all necessary calculations to validate the reduction methodology and post-processed the results. I wrote the vast majority of the paper to which Seidel L. and Mauss F. contributed with edits and fruitful comments. I presented the results at 5$^{th}$ International Workshop on Model Reduction in Reactive Flow (IWMRRF) as well as at the 3$^{rd}$ topical workshop: Testing combustion models with experimental data, prior the 7$^{th}$ European Combustion Meeting (ECM) in 2015.

**Paper II: Soot Source Term Tabulation Strategy for Diesel Engine Simulations with SRM**

**Matrisciano A.**, Borg A., Perlman C., Lehtiniemi H., Pasternak M., Mauss F.
SAE Technical Paper 2015-24-2400, 2015, doi:10.4271/2015-24-2400.

**Summary.** A flamelet-based tabulation method for soot source terms was coupled to the stochastic reactor model and tested against a well stirred reactor-based approach under Diesel engine conditions. The main purpose was to assess the benefits of tabulation within the 0-D SRM framework with respect to soot formation only. A pre-existing soot source term table, obtained using an *n*-heptane kinetic scheme of 121 species and 974 reactions, was used and a look-up strategy was implemented in the SRM framework to reconstruct the contributions of the different soot formation and oxidation processes. As a validation test case, a heavy-duty Diesel engine case was used, and the tabulated chemistry-based soot predictions were compared against the regular on-the-fly (WSR-based) chemistry solver.

**Author contribution.** The flamelet-based soot source terms tabulation strategy was developed prior to my work by Borg A., Lehtiniemi H. and Mauss F. for 3-D CFD applications. I implemented the mentioned methodology within the 0-D SRM code and run all the presented simulations as well as post-processing. I wrote the main parts of the paper to which Lehtiniemi H. and Mauss F. contributed with edits and useful comments. I presented the paper at the 12$^{th}$ international SAE-NA conference on engines and vehicles in 2015.

**Paper III. Development of a Computationally Efficient Progress Variable Approach for a Direct Injection Stochastic Reactor Model.**

**Matrisciano A.**, Franken T., Perlman C., Borg A., Lehtiniemi H., Mauss F.
SAE Technical Paper 2017-01-0512, 2017, doi:10.4271/2017-01-0512.

**Summary.** This paper discusses the theory and application of the tabulated chemistry solver (CPV) developed during my PhD studies and applied to the 0-D SRM. After various iterations, a latent enthalpy-based progress variable definition was assumed for the tabulation phase and implemented. Different structures and tabulation grid resolutions were tested so that both accuracy and table size are in line with typical mid-range workstation computer specifications. All sub-models of the SRM (such as fuel injection, heat transfer and mixing) were updated to comply with the new tabulated chemistry solver. One heavy-duty conditions as well as ten passenger car Diesel engine conditions were used as validation cases to assess accuracy and computational performance of the CPV solver against the on-the-fly chemistry solution. Reasonably good agreement was found between the two solvers. Further, the methodology proved to be an attractive solution to facilitates the usage of the SRM in the engine development process.

**Author contribution.** The basic solver routines for tabulation and the subsequent interpolation were developed by Perlman C., Borg A., Lehtiniemi H. and others prior the beginning of my work. I contributed to small developments of some updates/features needed to account for the new CPV table structure. With respect to the 0-D SRM engine code, I implemented the new coding infrastructure necessary to couple a tabulated chemistry-based solver with the SRM code which, previously, had always relied on an online chemistry-based solver. I worked on each of the sub-models present in the SRM code for online chemistry and ensured their correct functionality with the CPV solver. I also coupled the SRM with the EMST mixing model (starting from the code developed by Pope and co-workers) and implemented the mixture fraction constrain on the spanning tree construction. I then ran all simulations presented in the paper and postprocessed the results. I wrote the paper and Lehtiniemi H., Perlman C. and Mauss F. contributed with edits and comments. I presented the work at the 2017 SAE world congress in Detroit.

**Paper IV. A Computationally Efficient Progress Variable Approach for In-Cylinder Combustion and Emissions Simulations.**

**Matrisciano A.**, Netzer C., Werner A., Borg A., Seidel L., Mauss F.
SAE Technical Paper 2019-24-0011, 2019, doi:10.4271/2019-24-0011.

**Summary.** The CPV solver described in Paper III was coupled to CONVERGE 2.4 via user defined functions designed to override the built-in detail chemistry model (SAGE). In this work three passenger car Diesel engine conditions were used as validation cases under the RANS sector mesh assumptions. The CPV solver was then compared against the SAGE solver predictions for combustion, soot and $NO_x$ as well as for run-time performances. A two component (70% *n*-decane, 30% alpha-methylnaphthalene, by mass) Diesel surrogate, comprising 189 species was used for both the online and tabulated chemistry solver tests. Remarkable speed-ups were noted while keeping a low loss of accuracy across all the investigated conditions.

**Author contribution.** The main implementation work of the CONVERGE User Defined Functions was performed by my colleagues Lehtiniemi H. and Borg A. I contributed to some marginal parts of the debugging process of the mentioned UDFs and implemented some minor improvements in the look-up methodology. I then ran all the presented simulations in CONVERGE 2.4 and post-processed the results. Werner A. contributed to the generation of the 3-D contour plots while Netzer C. and Seidel L. contributed to the writing of parts of the introduction and case setup description paragraphs. I wrote the results and conclusions sections and took care of all necessary edits and refinements during the rebuttal phase. Although the work was accepted for public presentation at the 2019 SAE-NA conference, I did not have the chance to publicly present the work due to an un-expected business trip cancelation.

**Paper V. Development of a Computationally Efficient Tabulated Chemistry Solver for Internal Combustion Engines Optimization using Stochastic Reactor Models.**

**Matrisciano A.**, Franken T., Gonzales Mestre L.C., Borg A., Mauss F.
Applied Sciences, 10 (24) 8979, 2020, doi:10.3390/app10248979.

**Summary.** Following numerous code improvements on both the tabulation and the solver coupling in 0-D, this paper discusses theory and application of the CPV solver in the 0-D SRM framework. Compared to paper III, this work presents a broader set of validation cases as well as a dedicated paragraph to SI engine applications. Tabulation grid resolutions were further tested so to improve the trade-off between RAM requirements at run-time and accuracy of the interpolation method. Refinements and improvements were implemented across all sub-models of the SRM (such as fuel injection, heat transfer and mixing) so to make the CPV solver even faster. A heavy-duty Diesel engine campaign, as well as a passenger car SI engine were performed.

In total, 18 engine operating points are presented so to comprehensively assess performance of the CPV solver against the detailed on-the-fly chemistry solutions. Reasonably good agreement was found between the two solvers for both combustion phasing and engine-out emission predictions. Based on the reported CPU times (which were recorded using 1 core of a mid-spec laptop) it was concluded that the method is particularly suitable for engine optimization campaigns.

**Author contribution.** I analyzed and debugged several aspects of the SRM-CPV and SRM-Online solver source codes. This led to several performance and accuracy improvements. I implemented a refined methodology for the assessment of the interpolation strategy as well as a procedure to visualize the large results datasets. On the tabulation procedure itself, several improvements were implemented by Seidel L., Borg A. and Kienberg M. The SRM simulations with CPV have been initially setup and calibrated by Franken T. and Gonzales Mestre L.C. in previous studies where I have been involved as co-author. In this paper, I have re-calibrated the SRM model parameters for the Diesel engine campaign and run the whole set of simulations with for both engine settings. I have performed the data post processing as well as written the paper. Franken T. and Gonzales Mestre L.C. have provided fruitful feedback during the simulation campaign as well as during manuscript preparation. Mauss F. contributed with edits and comments.